Droplet Microfluidics Coupled to Capillary Electrophoresis and Mass Spectrometry for Pharmacological Applications

by

Cara I. D'Amico

A dissertation submitted in partial fulfillment
of the requirements for the degree of
Doctor of Philosophy
(Pharmacology)
in the University of Michigan
2022

Doctoral Committee:

Professor Robert T. Kennedy, Chair
Professor Yoichi Osawa
Professor Brandon T. Ruotolo
Professor Shaomeng Wang

Cara I. D'Amico

cidamico@umich.edu

ORCID iD: 0000-0002-0669-7916

Dedication

To my mother,

who taught me kindness and perseverance.

Acknowledgements

There are many people who I have to thank for contributing to the success of my PhD. First and foremost, I would like to thank my advisors Professor Robert Kennedy and Professor Brandon Ruotolo. I was fortunate enough to have not one but two incredible mentors who have shaped me as a scientist. I am most thankful for their support, resources, and encouragement in allowing me to pursue the projects I did. Without this license for creativity, droplet-CIU would have never come to be.

I must also thank Professors Yoichi Osawa and Shoameng Wang, my committee members. I value their insight on all of the work I have been a part of. I would also like to thank Professor Yoichi Osawa for all of his feedback through the years in the Pharmacology Seminar Series. Your input was instrumental in the development of my scientific communication. I would like to thank my collaborators in the Lomabard and Neamati Groups. Without them the Sirtuin-5 research I conducted would have not been possible. Additionally, I want to thank my collaborators at Bristol Myers Squibb for the opportunity to work with therapeutic antibodies. It was truly a joy to be a part of that project. I would like to thank my undergraduate mentor, Dr. Richard Vachet, for sparking my passion for analytical chemistry and mass spectrometry.

Some of my greatest friendships are from my time in the Kennedy and Ruotolo Groups. While I learned something from each person in the lab, I would especially like to thank my mentors Dr. Claire Ouimet, Dr. Daniel Polasky, and Dr. Daniel Steyer. It was from Claire that I learned all of the joys and heartaches of capillary electrophoresis. Not only did she teach me instrumentation, but she set an example of what an innovative and dedicated scientist should be. I would like to

thank Dan Polasky for showing me my way around native mass spectrometry and for suffering through my lack of computational skills. Thank you to Dan Steyer for all of the guidance in droplet microfluidics. My work would not have been possible without your knowledge and patience, and quite possibly our coffee runs. I would also like to thank Dr. Sugyan Dixit for fielding any data analysis questions I had and introducing me to the wonders of Nepali Cuisine. Thank you to Emory Payne for all of the microfluidic ideas and for the countless hours reminiscing about Central Mass. To Dr. Brian Shay, Dr. Daniel Holland-Moritz, Megan Connolly, Dr. Shane Wells, Dr. Matthew Sorensen, Kelcie Zegalia, Brady Anderson, Dr. Varun Gadkari, Dr. Sarah Fantin, Kristine Parson, and Brock Juliano: thank you for making the lab a brilliant place to be.

I need to thank all of my amazing friends who have supported me along this journey, especially Kristen Sikora who has been by biggest cheerleader from 700 miles away. Thank you to the forever roommates from 903 S. Main Street; graduate school would not have been the same without you.

A special thanks to my parents for supporting me and encouraging my love for all things science. Thank you to my siblings for never failing to make me laugh. I would also like to thank the Valenta family for standing in, when Massachusetts was a little too far away.

Finally, I would like to thank Alec Valenta for being my greatest supporter throughout graduate school. You were always a spot of brightness, even on the rainiest of Ann Arbor days. I could not ask for a better lab or life partner.

Table of Contents

List of Figures

List of Tables

List of Abbreviations

Abl	Abelson Protein Tyrosine Kinase
AC	Alternating Current
ACN	Acetonitrile
AMC	7-amino-4-methylcoumarin
AMI	Acoustic Mist Ionization
AS-MS	Affinity Selection-Mass Spectrometry
BLI	Biolayer Inferometry
CCS	Collisional Cross Section
CE	Capillary Electrophoresis
CHO	Chinese Hampster Ovary
CIU	Collision Induced Unfolding
CPS1	Carbamoyl Phosphate Synthetase 1
CRM	Charged Residue Model
CV	Collision Voltage
DC	Direct Current
DESI	Desorption Electrospray Ionization
DSC	Differential Scanning Calorimetry
DSF	Differential Scanning Fluorimetry
DTPA	diethylenetriamiepentaacetic acid

EOF	Electroosmotic Flow
ESI	Electrospray Ionization
FITC	Fluorescein
FRET	Fluorescence resonance Energy Transfer
HMGSCS2	Methylglytaryl-CoA Synthase 2
HOS	Higher Order Structure
HTS	High-Throughput Screening
IC50	Half Maximal Inhibitory Concentration
IgG	Immunoglobulin G
IM-MS	Ion Mobility-Mass Spectrometry
ITC	Isothermal Titration Calorimetry
K_D	Dissociation Constant
LC	Liquid Chromatography
LIF	Laser Induceed Fluorescence
LoD	Limit of Detection
LoQ	Limit of Quantitation
mAb	Monoclonal Antibody
MCE	Microchip Capillary Electrophoresis
MS	Mass Spectrometry
MST	Microscale Thermophoresis
NAD+	Nicotinamide Adenine Dinucleotide
nESI	Nano-Electrospray Ionization
NMR	Nuclear Magnetic Resonance

PDC	Pyruvate Dehydrogenase Complex
PDMS	Polydimethylsiloxane
PFD	Perfluorodecalin
PFO	Perfluorooctanol
PTM	Post-Translational Modification
RF	Radio Frequency
RF-MS	RapidFire Mass Spectrometry
RMSD	Root-Mean-Square Deviation
RSD	Relative Standard Deviation
RWG	Resonant Waveguide
SDH	Succinate Dehydrogenase
SIRT5	Silent Mating Type Information Regulation 2 Homolog 5
SOD1	Superoxide Dismutase
SPR	Surface Plasmon Resonance
TIC	Total Ion Chromatogram
ToF	Time-of-Flight
TWIMS	Traveling Wave Ion Mobility

Abstract

Modern drug discovery relies on high-throughput screening for lead generation and protein target evaluation. There is a critical need to develop assays that not only have large-scale screening capabilities but provide insight of greater physiological relevance. It is in this space that biophysical methods are used to extract high information content datasets; however, throughput is often limited by sample introduction to the instrument. Droplet microfluidics represents an attractive approach for coupling high-throughput sampling with analytical and biophysical approaches. The aim of this thesis is to improve high-throughput workflows coupled to to capillary electrophoresis and ion mobility-mass spectrometry for the analysis of enzymatic activity and intact protein analysis.

Optical assays are a fast and simple approach for screening small molecule activity against enzymatic reactions but can be prone to high false discovery rates. A capillary electrophoresis method was developed to screen against Sirtiuin-5 activity, where substrate and product peptides were separated and detected. Using a commercial capillary electrophoresis system, eight novel Sirtuin-5 inhibitors were confirmed through dose-response analysis. This assay was then coupled to a microchip capillary electrophoresis platform coupled to droplet sample introduction via an density-based oil drain. A sampling rate of 0.1 Hz, using only 4 nL sample volumes. This was applied to screen over 160 Sirtuin-5 samples. Future work is focused on developing a label-free mass spectrometry assay with on-line reagent addition.

Native mass spectrometry coupled to ion mobility (IM-MS) has become an important tool for the investigation of protein structure and dynamics upon ligand binding. Additionally,

collisional activation or collision induced unfolding (CIU) can further probe conformational changes induced by ligand binding. In this work we explore the high-throughput capabilities of CIU fingerprinting. Fingerprint collection times were reduced 10-fold over traditional data collections through the use of improved smoothing and interpolation algorithms. Fast-CIU was then coupled to a droplet sample introduction approach and applied to a 96-compound screen against Sirtuin-5. Over 20 novel Sirtuin-5 binders were identified, and it was found that Sirtuin-5 inhibitors will stabilize specific Sirtuin-5 gas-phase conformations. This work demonstrates that droplet-CIU can be implemented as a high-throughput biophysical characterization approach. Future work will focus on improving the throughput of this workflow and on automating data acquisition and analysis.

Monoclonal antibodies (mAbs) are an important class of biotherapeutics, but the diversity and structural complexity of mAbs create an analytical challenge. Moreover, mAbs are produced through recombinant DNA technology and grown in mammalian cells, giving rise to complex background matrices and possible post-translational modification (PTM). A miniaturized MS-friendly mAb purification is developed and couped to droplet-MS. In-droplet calibrations were performed and an ultimate LOD of 0.15 mg/mL and LOQ of 2.6 mg/mL were achieved. This method was then applied to screen mAb production in 48 cell expression conditions with a rate of 0.04 Hz, identifying the most productive media conditions. This work was complemented by high resolution MS for PTM profiling, identifying a range of glycoforms on the intact mAb species. Future goals are aimed at coupling on-line sample preparation and droplet sample introduction to high resolution MS for high-throughput glycoform characterization.

Chapter 1: Introduction

1.1 Motivation

High-throughput screening (HTS) plays an integral role in the modern drug discovery process. With advances in combinatorial and multiparallel chemical synthesis, as well as the availability of isolated natural products, chemical libraries have grown to contain hundreds of thousands up to millions of unique compounds.[1] Concurrently, progress in the fields of genomics and proteomics has led to a dramatic increase in potential therapeutic targets.[2] Because of the diversity in chemical space and the resulting vast experimental possibilities, HTS is often a crucial first step in lead discovery.

Historically, large-scale screens have been based off optical assay approaches.[3] These assays rely on a change in spectroscopic properties that indicates binding or a reaction. Optical-based assays are high throughput (subsecond/sample), compatible with modern robotic technologies, and require minimal data analysis; however, they have several drawbacks including the need for a chemical label, limited applications in the biochemical space (primarily enzymatic reactions), and a propensity for high false discovery rates.[4–6] Recent trends in HTS have been

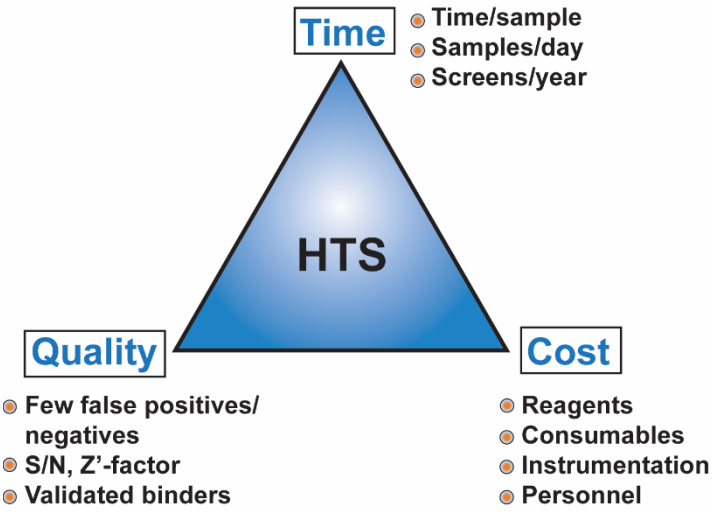

Figure 1-1. The "Magic Triangle of HTS". The triangle represents the three key factors of success for HTS: time, cost, and data quality. Optimization of an HTS assay requires balancing all three factors. Adapted from Mayr, 2008.

towards the development of label-free assays that can provide complimentary, information-rich data about candidate-target interactions, while maintaining high-throughput and minimizing the use of precious reagents (**Figure 1-1**).[7] Ideally these assays would provide more biologically relevant lead compounds earlier on in the drug discovery pipeline. Beyond small molecule screening, the rise of biotherapeutics has also necessitated the use of more sophisticated, high-throughput measurement tools.[8]

The need for alternative screening approaches has led to the development of many analytical/biophysical HTS technologies (**Table 1-1**).[9] These binding assays provide complementary insight to typical activity assays, such as confirmation of binding and binding strength, stoichiometry, and thermodynamic information. Approaches like NMR and ITC can provide detailed affinity data and information about binding modes, but at the cost of throughput and larger sample requirements.[10,11] Similarly, other calorimetric-based methods supply in-depth thermodynamic data at the sacrifice of throughput.[9] Recent advances in SPR and RWG (resonance-based techniques) have led to increases in throughput and the rise of their use in drug discovery efforts; however, the protein target must first be immobilized and is not amenable to every protein system.[12,13] Of the technologies listed, AS-MS detects binding events with the highest throughput but provides little information about binding dynamics or stoichiometry.[14] Nonetheless, AS-MS has been successfully employed in several screening campaigns to identify lead compounds.[14] With such biodiversity in protein targets as alluded to above, there is no "one size fits all" approach for HTS characterization of protein-ligand interactions and there is a continuous need to develop new strategies for protein analysis with respect to drug development.

Detection Readout	Target Conditions	Data Content	Protein Requirement (Per Data Point)	Buffer Requirements	Data Points/ Day
Nuclear Magnetic Resonance (NMR)	In Solution	Binding; K_D; Dynamics	10-500 µg	NMR Compatible	<75
Isothermal Titration Calorimetry (ITC)	In Solution	Binding; K_D; Stoichiometry; ΔH; ΔS	200-5000 µg	Matching Reference Cell	<10
Differential Scanning Calorimetry (DSC)	In Solution	ΔT; ΔH; ΔS	100-500 µg	Matching Reference Cell	<75
Differential Scanning Fluorimetry (DSF)	In Solution, with Tracer Dye	ΔT_m	0.2-1 µg	Matching Reference Cell	<10K
Surface Plasmon Resonance (SPR)	Immobilized	Binding; K_D; k_{off}; $k_{on;}$ stoichiometry; ΔH; ΔS	0.001-0.2 µg	Low Refractive Index	<5K
Resonant Waveguide (RWG)	Immobilized	Binding; K_D	0.5-2 µg	Low Refractive Index	<10K
Biolayer Interferometry (BLI)	Immobilized	Binding; K_D; k_{off}; $k_{on;}$	0.2- 1 µg	Low Refractive Index	<5K
Affinity Selection-Mass Spectrometry (AS-MS)	In Solution	Binding	1-5 µg	MS Compatible	<1K
Microscale Thermophoresis (MST)	In Solution	Binding; K_D; ΔH; ΔS	0.4-4 µg	All	<50

Table 1-1. Commonly used biophysical techniques for protein-ligand binding in drug discovery. The list includes information output, sample requirements, and typical throughput. Adapted from Genick, 2014.

1.2 Ion Mobility Mass-Spectrometry

Ion mobility-mass spectrometry (IM-MS) coupled with soft ionization is a powerful tool for biomolecular analysis of proteins.[15] In the past decade, IM-MS has expanded into applications

for protein-ligand interactions and drug discovery.[16,17] To fully utilize IM-MS technology for lead discovery, it is necessary to understand the instrumentation fundamentals. Most of the work presented in this dissertation was performed on a Waters Synapt G2 instrument with a traveling

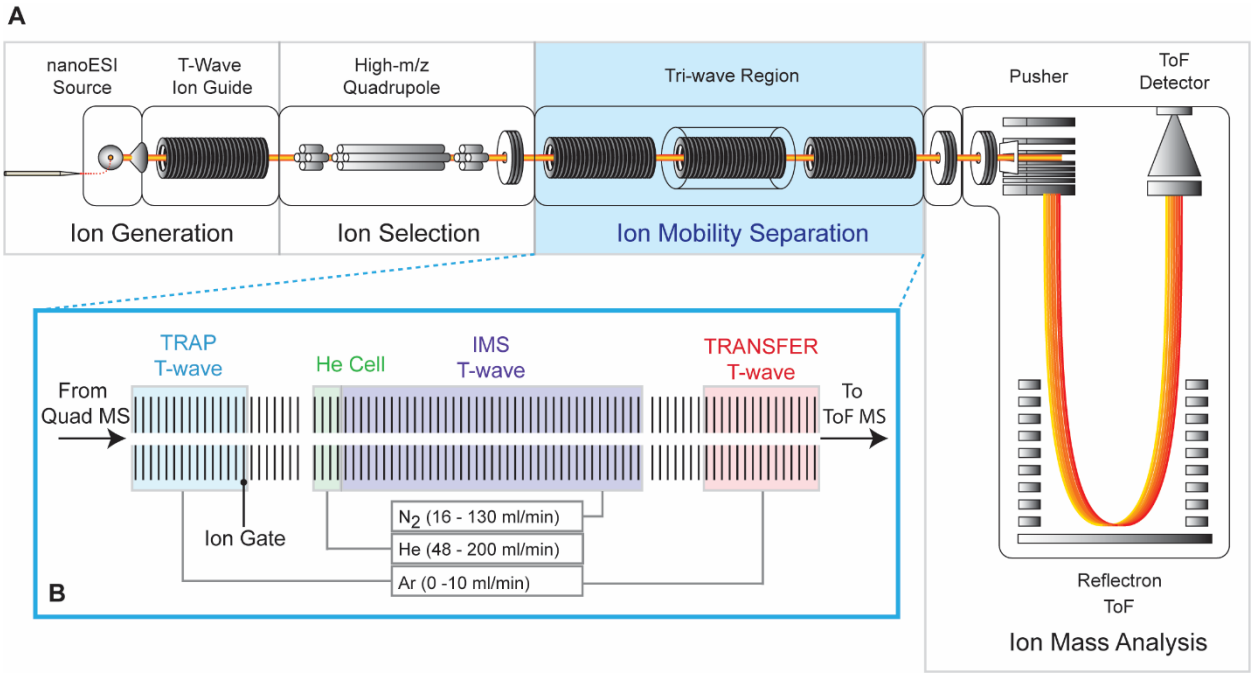

Figure 1-2. Instrument schematic of the Waters Synapt G2 IM-MS. The instrument is separated into four main regions: a nanoESI source where ions are generated, a modified quadrupole for high-mass transition and selection, the IM region for separation and a time-of-flight (ToF) mass analyzer (A). A detailed view of the separation region illustrating the trap and transfer T-wave ion guides, the T-wave IM separator, and the helium cell buffer region between the high pressure IMS region and the low pressure transfer region (B). Gas flows are indicated for each region.

wave IM separator (TWIMS) (**Figure 1-2**), although there many IM-MS platforms.[18]

1.2.1 Ion Generation of Native Like Protein Structures

For any MS experiment, analytes of interest must first be converted into ions in the gas phase. The introduction of electrospray ionization (ESI), a gentle form of ionization can transfer large, intact molecules into the gas phase directly from solution, has enhanced the use of MS for the study of biomolecules.[19] ESI is particularly suitable for MS analysis of large proteins because it generates multiply charged ions, enabling easier detection of these biomolecules at a lower mass-to-charge (m/z) range.[20,21] Additionally, ionization by ESI preserves noncovalent interactions

allowing for the study of intact protein-ligand interactions by MS.[20,21] The mechanism for ESI is illustrated in **Figure 1-3**.

During ESI, an aqueous phase is flowed through a conductive emitter held at a high voltage. For protein analysis positive ion mode is typically used, where an applied positive voltage generates cations at the emitter tip. Due to the strong electric field, the solution becomes polarized and forms a Taylor cone that disperses into a fine spray of charged droplets.[22] The micrometer diameter droplets from the initial spray further shrink due to solvent evaporation, often assisted by heat or gas flow. Jet fission will then produce smaller droplets when the charge density on the shrinking droplets reaches the Rayleigh limit.[23] This repeated cycle of evaporation/fission eventually results in desolvated, multiply charged analytes.

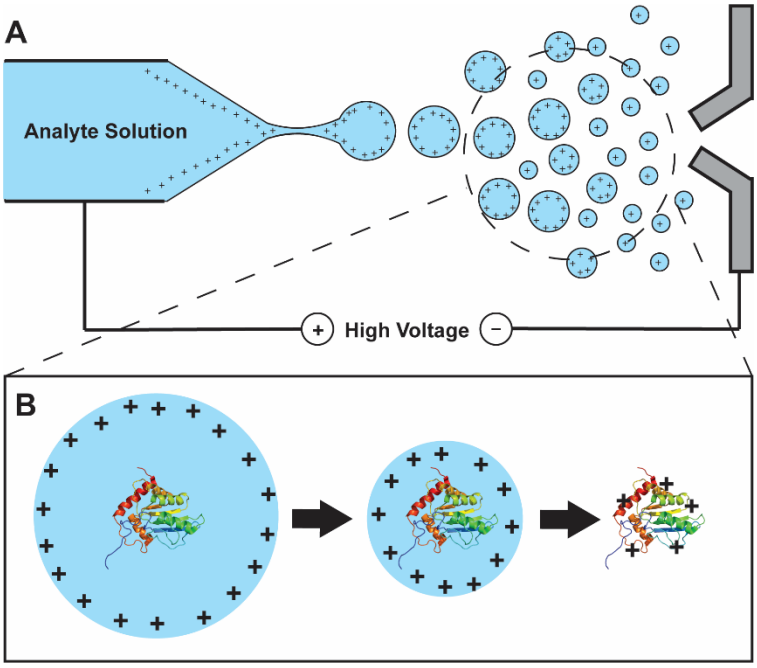

Figure 1-3. Electrospray ionization in positive ion mode. Stream of aqueous analyte solution is shown on the left with the instrument source on the right (A). Depiction of droplet fission and evaporation, as described by the charge residue model (B).

Although several models have been proposed to explain the mechanism of how analyte ions are formed in the last stages of ESI, the charged residue model (CRM) is the most widely accepted model for large macromolecules.[24] In the CRM model, Coulombic fission occurs until a droplet containing a single analyte molecule remains. A "naked" analyte ion, or charged residue, remains once complete evaporation of the solvent occurs, where the overall charge state of the ion

is proportional to the protein surface area in solution.[24] Because the evaporation/fission cycle is a relatively slow ionization process, with limited energy transfer, proteins remain folded with a native-like structure upon entering the gas phase.[25] To preserve protein function and structure, ammonium acetate salts are commonly utilized. These salts are used to control pH and ionic strength but are volatile enough to be MS compatible.[26] To enhance the sensitivity of native MS experiments, nano-ESI (nESI) is often employed. Reduced emitter diameters and nL/min flow rates reduce initial ESI droplet sizes resulting in greater ionization efficiency and tolerance of the ion source for the salts present in biologically relevant matrices.[27,28]

1.2.2 Transmission, Selection, and Detection of High Mass Protein Ions

The Synapt G2 is a hybrid mass spectrometer that orthogonally combines a quadrupole mass analyzer with a time-of-flight mass analyzer. A ToF determines the m/z of an ion by measuring their flight time within a drift-tube free of electric fields. The ions are introduced into the mass analyzer with a set amount of kinetic energy, where the velocity (and therefore flight time) of the ion is dependent on its m/z.[29] The implementation of the reflectron ToF has greatly improved the resolving power of this class of mass analyzers, due to their elongated flight paths and energy spread correction capabailites.[30] ToFs are well suited for large biomolecule analysis because of the high resolution that can be achieved over a broad m/z range.[31] Quadrupole mass analyzers consist of four conductive rods set in a parallel quadrilateral configuration. The rods are paired, and paired rods are held at the same direct current (DC) and alternating current (AC) radio frequency (RF) potentials, whereas there is a DC offset between rod pairs. Only ions with a particular m/z can traverse the mass analyzer at a given combination of RF and DC voltages.[32] In combination with a ToF mass analyzer, the quadrupole serves as a mass filter for the selection of specific ions.

1.2.3 Ion Mobility Separation

IM separates protein ions on the millisecond timescale based on their charge and shape. Ions are introduced as packets into an ion guide pressurized with a neutral gas in the presence of a weak electric field. As ions traverse the IM separator, elongated ions experience more collisions with the natural gas molecules, resulting in longer arrival times as compared to smaller, more compact ions (**Figure 1-4**).[33,34] This information is represented as an arrival time distribution (ATD). While there are a number of IMS platforms, the IM separations presented in this dissertation take place in the presence of a dynamic electric field, known as traveling waves (TW), and thus the IM technology is typically known as traveling wave ion mobility (TWIM)

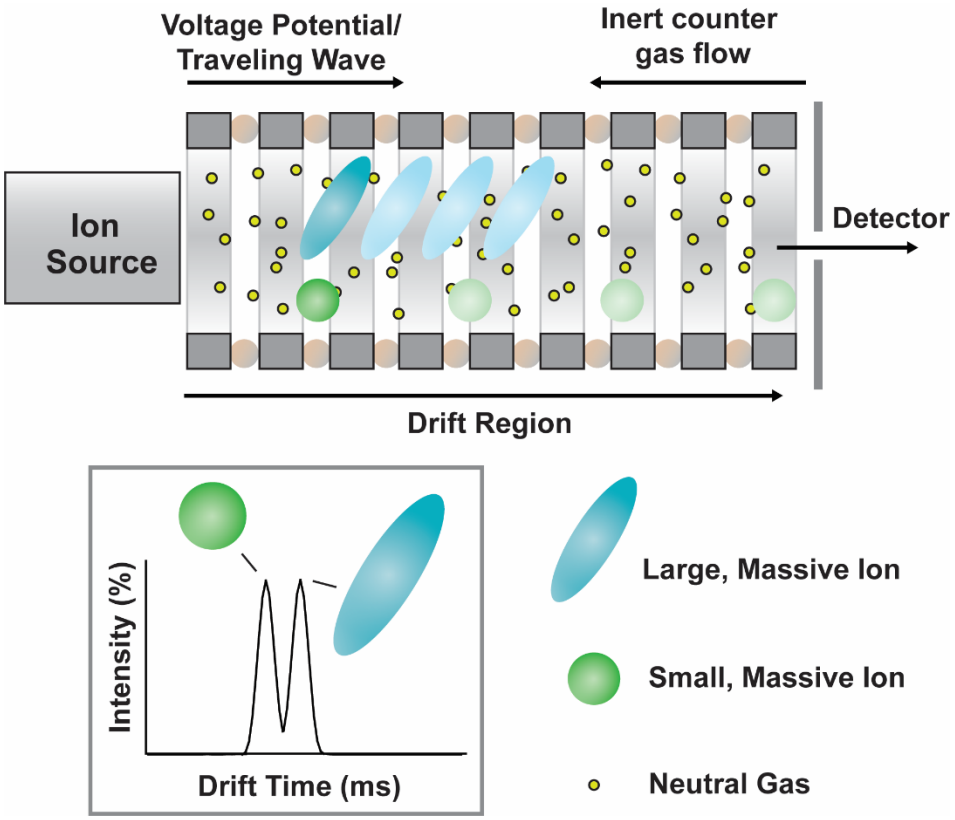

Figure 1- 4. IM separation of ions based on charge and apparent surface area. Ions are guided through a gas-filled drift tube by an electric field. Larger ions experience more collisions and take longer to pass through the drift tube as compared to smaller ions. This data is recorded as an arrival time distribution.

spectrometry. Through careful calibration, TWIM ATDs can be used to calculate the orientationally-averaged collisional cross section (CCS) of the analyte ions.[35] CCS values have been correlated with protein structure models and have been used to validate protein structures derived from NMR or X-ray crystallography.[36,37] Furthermore, IM-MS has been used for the analysis of protein-ligand interactions in addition to structural analysis of biotherapeutics, by monitoring changes in CCS upon ligand binding.[16,38]

1.3 Collision Induced Unfolding

Collisional activation, in tandem with IM-MS, can provide further insight into the structure and stability of proteins in the gas phase. Collisional induced unfolding (CIU) is often viewed as the gas-phase counterpart to differential scanning calorimetry.[39] During a CIU experiment, selected protein ions are activated through energetic collisions with an inert background gas. Energy is increased in the system by ramping the applied voltage, causing unfolding of the protein without breaking covalent bonds (**Figure 1-5**).[39] The unfolding is monitored by IM-MS and the changing

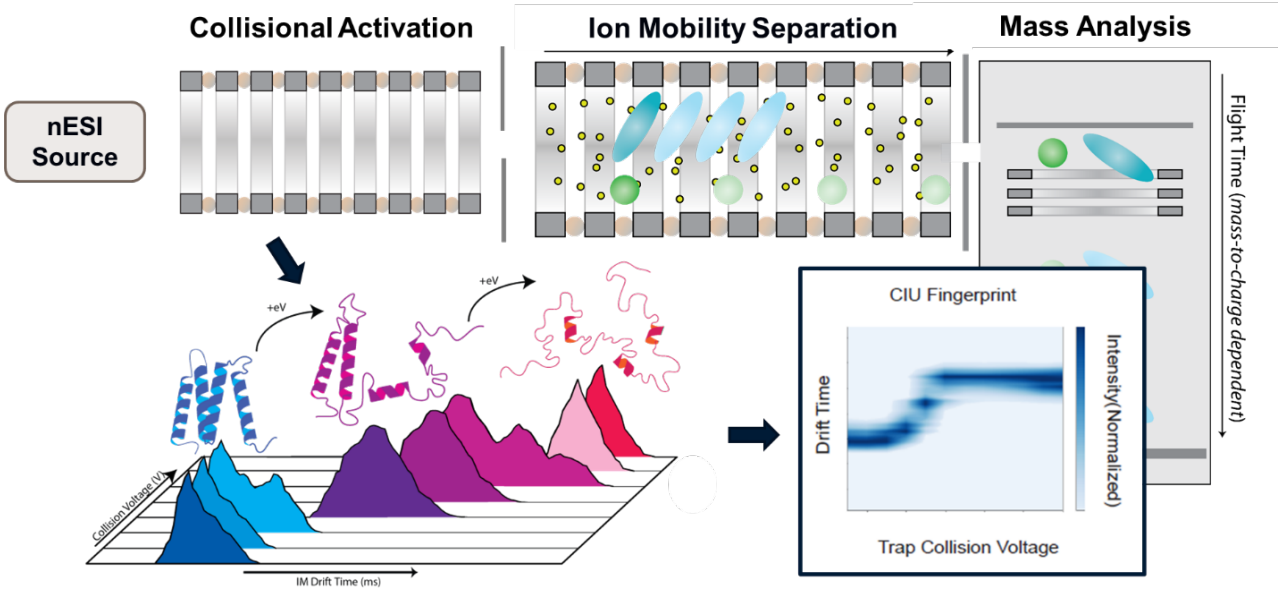

Figure 1-5. Schematic of collision induced unfolding. Proteins unfold as collisional energy is increased in a stepwise fashion. This unfolding is monitored through IM-MS analysis and arrival time distributions. The changes in arrival time are plotted versus the increase in voltage in a three-dimensional contour plot called a CIU fingerprint. Adapted from Dixit, 2018.

arrival time distributions are plotted against the change in voltage yielding a three-dimensional contour plot. The plot is referred to as a CIU fingerprint. CIU has proven to be sensitive to small changes in protein stability upon ligand binding.[40] Additionally, CIU fingerprinting does not require purified samples and is much faster than its solution phase counterparts, making it more amenable to high-throughput biophysical analysis.[16] The utility of CIU for the assessment of inhibitor binding to enzymes has been across several protein-ligand systems, yet the throughput of this workflow is on the minutes/sample timescale, limiting its application in a screening context.[41–43]

1.4 Rapid Sample Introduction for Mass Spectrometry

IM-MS has great potential for implementation as a HTS tool because separation and detection take place on the millisecond scale. Additionally, ESI and nESI are amenable to HTS formats because they are fast, flow-based ionization techniques that allow for continuous sampling. The main bottleneck in the throughput of IM-MS methods lies in sample introduction. ESI-MS is most commonly paired with liquid chromatography (LC), due to flow and solvent compatibility.[44] While LC-MS is a gold standard for many analytical applications, it is limited by large sample volumes (>5 μL) and low throughputs (minutes).[45,46] As a result, there is a demand for high-throughput direct ESI-MS methods that do not rely on a separation prior to sample introduction to the MS.

The interest in developing high-throughput sample introduction has led to an array of both homebuilt and commercial sample introduction systems (**Figure 1-6**).[47] Commercialized systems, such as the Agilent RapidFire (RF-MS), are an attractive option because they are robust and easy to operate.[48] RF-MS also incorporates automated solid phase extraction, allowing for analysis of biomolecules from complex background matrices with improved sensitivity.[48] There have been

reports of throughput up to ~0.14 Hz for small molecule analysis; however, throughput for intact protein analysis has only been reported at ~0.03 Hz when loading and washing steps are included in the total cycle time.[49,50] Although this throughput is orders of magnitude lower than other sample introduction methods, RF-MS has enabled accurate mass determination of intact, therapeutic antibodies from both cell culture media and plasma with bassline resolution of glycoforms.[50]

Beyond, ESI-MS, alternative ambient ionization approaches can be implemented to achieve high throughputs for sample introduction. During desorption electrospray ionization (DESI) a charged solvent plume is directed at the sample surface, where the analytes are then dissolved in the stream and are transferred towards the MS source as secondary droplets.[51] DESI-MS can be achieved at a sampling rate of 2.8 Hz with sample volumes down to 50 nl, but efficient analyte ionization is limited to proteins less than 17 kDa.[52,53] This precludes the use of DESI-MS for many protein targets of interest or antibody-based therapeutics. Another recently developed ambient ionization tool for HTS applications is acoustic mist ionization. Samples are prepared on a well-plate where ultrasonic pulses generate femtoliter droplets directly from the sample surface. The use of a charged ion guide and heated transfer tube then guide the droplets to the MS.[54] With contactless ionization and rapid desolvation, sample introduction rates of 3 Hz can be achieved by acoustic mist ionization.[54] Additionally, the generation of such small droplets compared to ESI improves ionization efficiency. Acoustic mist ionization has yet to be demonstrated for intact protein analysis and it is unclear whether protein ions would be generated with the same efficiency as their small molecule counterparts.

The fastest throughputs for intact protein analysis by MS have been achieved through droplet microfluidics. Sampling rates over 30 Hz have been reported, using a customized QToF with enhanced acquisition speeds.[55] Additionally, sampling rates over 5 Hz were demonstrated across three different instrument platforms. While throughput was over a magnitude greater than the next fastest method (acoustic mist), it came at 20-fold decrease in sensitivity at the highest sampling rates and loss of mass resolution of the intact protein analytes.[55] It is important to note

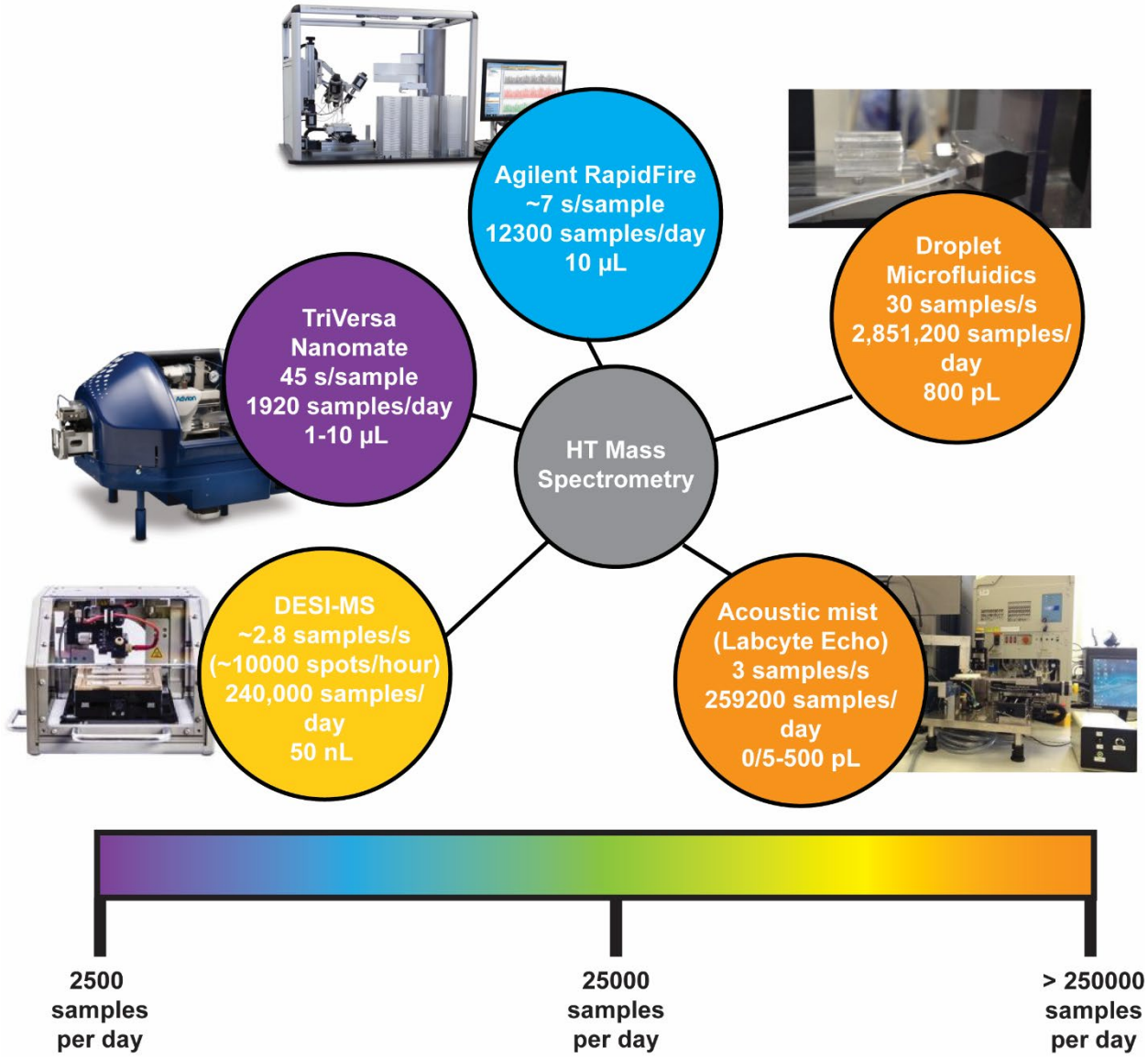

Figure 1-6. Summary of high throughput sample introduction for ESI and other ionization techniques. Figures of merit include throughput and sample volume consumption. Adapted from Kempa, 2019. Figure was modified to include more recent reports of higher sampling rates.

that although analyte signal traces were monitored at 33 Hz, protein spectra were only shown at 1 Hz sampling rates. Nonetheless, Droplet microfluidics is an attractive approach for high-throughput MS analysis because of the achievable throughputs, low sample requirements, adaptable fluid manipulation, and ease of coupling to available ESI and nESI sources.

1.5 Droplet Microfluidics

Microfluidics utilizes fluidic devices with micron-width channels to miniaturize biological and analytical applications.[56] These miniaturized liquid handling systems are advantageous because they allow for the fast manipulation of low volumes (low µL to fL), and are often multiplexed or automated.[57] Microfluidic technologies have been applied in HTS across many fields such as pharmaceutical development, genetic analysis, chemical synthesis, and biomedical diagnostics.[58–60] Droplet microfluidics is a subset of microfluidics in which individual sample plugs are separated by an immiscible carrier phase. The formation of discrete sample plugs in droplet microfluidics offers several advantages over traditional microfluidics, including increased throughput and accessibility to smaller fluid volumes.[61]

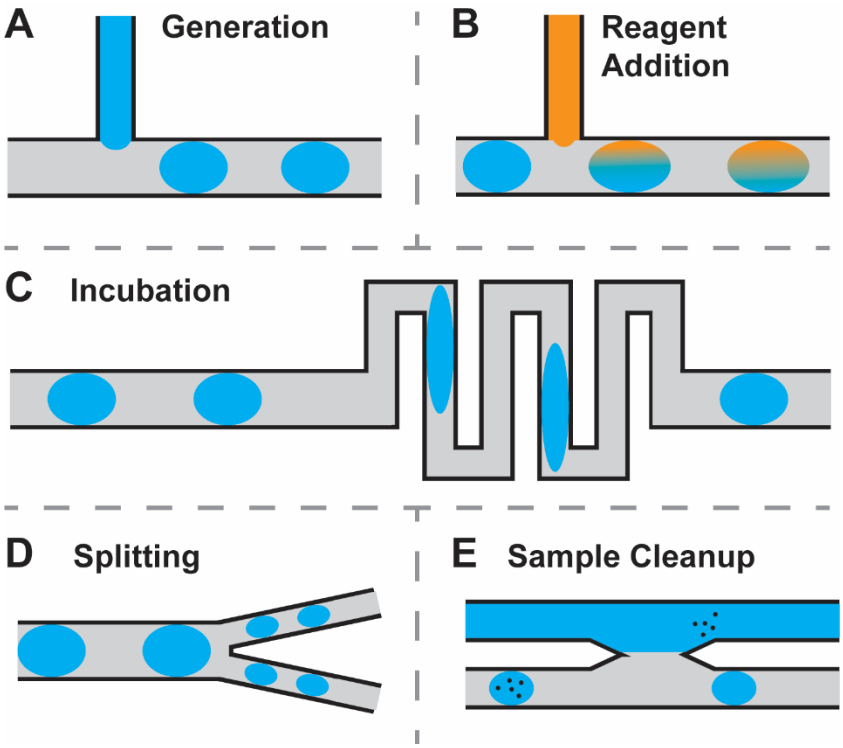

Figure 1-7. Examples of common droplet microfluidic manipulations/operations including: droplet generation (A), adding reagent (B), incubation of droplet samples (C), splitting droplet samples (D), and in-droplet sample cleanup (D). Adapted from Payne, 2020

Sample droplets in a microfluidic system are amenable to many types of operations (**Figure 1-7**).[62] The first step in a droplet microfluidic workflow is the generation of sample droplets. This can be performed on-line/on-chip (**Figure 1-7A**) or off-chip from a multi-well plate. The work presented in this dissertation was exclusively done with droplets generated off-line format from a well plate. While generating droplets on-chip is the higher throughput approach, the well plate format has several distinct advantages: sample plating can be integrated with modern robotic technology, sample reactions can be run in parallel, and sample order can be easily maintained, simplifying the coordination of the chemical readout upon analysis.[63,64] Other operations can be coupled to droplet generation prior to analysis, such as reagent addition, reaction incubation, splitting, and sample cleanup, to further improve automation and throughput of these miniaturized systems.[62] Finally, droplet microfluidic platforms can be paired with an array of analyzers including optical detectors, microscopy, and mass spectrometry.[65]

1.5.1 Droplet-MS

As stated above, MS is a fast, label-free detection method that can provide information rich data sets. With fast acquisition rates, MS can be readily paired with droplet microfluidics for high throughput applications. Droplets are coupled to ESI or nESI by simply connecting a tubing containing a flowing droplet train to the emitter. As aqueous samples reach the emitter tip the samples will ionize through the standard electrospray mechanism, but the carrier fluid will not. Carrier fluids used are non-conductive and will bead and fall off of the emitter instead of ionizing (**Figure 1-8A,B**). Because there is no signal observed when carrier phase passes through the emitter, each incoming droplet produces a discrete MS signal for the analytes of interest.[66]

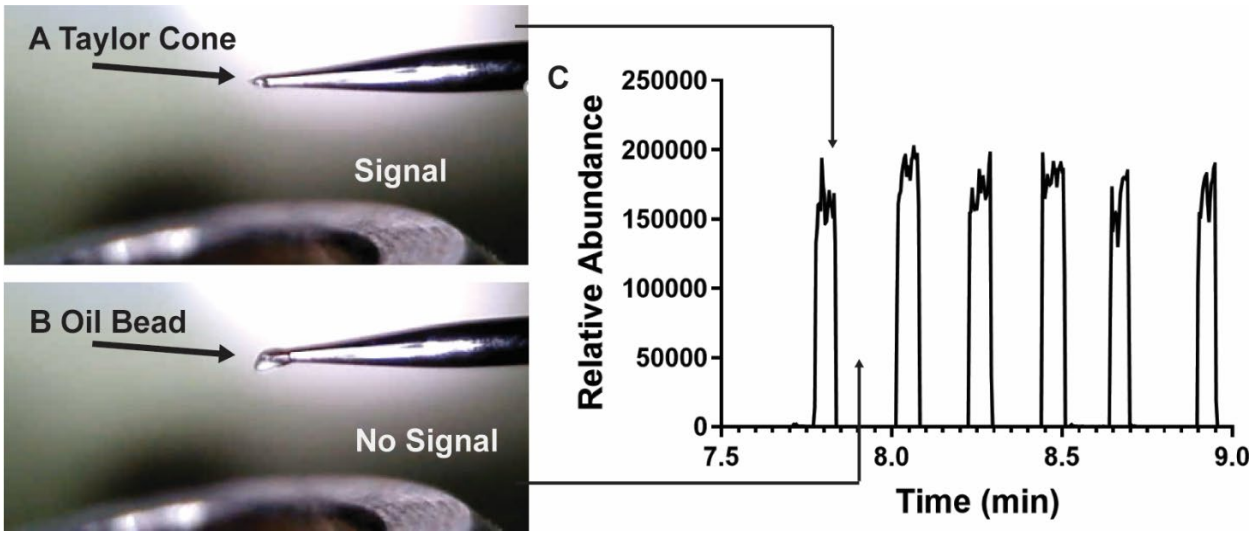

Figure 1-8. MS data corresponding to droplet droplet infusion of 1 uM SDH peptide. Image of aqueous sample at emitter tip, where Taylor cone formation can be observed. nESI plume is was too faint to capture in this image (A). Image of carrier phase at emitter tip, where the oil beading can be observed (B). Corresponding signal trace with alternating sample and oil plugs (C).

The first reports of droplet microfluidics demonstrated on-chip droplet generation coupled to sample extraction in a continuous stream for peptide analysis. While the content from individual droplets was able to be distinguished, the use of an aqueous carrier stream limited throughput and detection limits (0.1 Hz and 500 μM bradykinin respectively).[67] The first report describing the direct interfacing of droplets with ESI utilized air segmentation to reach analysis rates of 0.8 Hz. Furthermore, detection limits of 1 nM were achieved for leucine-enkephalin from 13 nL sample volumes.[66] Since these initial reports, continuous improvements have been made in the interfacing of droplet microfluidics including the reduction of droplet volumes, improvements in sensitivity, analysis of complex samples, and increases in throughput.[68,69] There have been reports of droplet sizes as low as 60 pL in volume and throughputs of up to 30 Hz.[55,70] This has enabled the use of droplet-MS for several HTS workflows including enzyme evolution and inhibitor screening.[71,72]

1.5.2 Droplet-MS for Intact Protein Analysis

Although there has been a diverse group of analytes monitored by droplet-MS over the past decade, there are only two reports of droplet-MS for intact protein analysis. In the first example, four populations of droplets containing either cytochrome C, α-chymotrypsin, carbonic anhydrase, or chicken lysozyme were generated off-chip and reintroduced to a ToF MS at a sampling rate of 2.6 Hz.[73] Ion traces and accurate masses were observed for all four proteins from ~650 pL samples. Detection limits were not reported as protein concentrations were held at 25 μM for all experiments. Seven years later the second example of intact protein analysis by droplet-MS not only pushed the limits of throughput, but demonstrated the versatility of droplet-MS across three different instrument platforms.[55] Sample volumes ranged from 0.8 nL to 2.1 nL and throughputs ranged from 5 Hz to 33 Hz. While this throughput was an order of magnitude greater than the previous example, the decreased time in data acquisition necessitated the use of high protein concentrations (60-100 μM). For experiments performed on the Orbitrap MS, isotopic resolution was lost at these throughputs. Overall, both the platforms establish droplet-MS as a viable approach for high throughput protein analysis; however, more sophisticated analyses have yet to be attempted such as evaluation of protein stability, monitoring of non-covalent interactions, and quantitation in complex samples.

1.6 Target Proteins

Droplet sample introduction coupled to mass spectrometry should have wide use across different proteins and protein-ligand interactions. In this work we target two different proteins to test our methods.

1.6.1 Sirtuin-5

Sirtuins are a family of nicotinamide adenine dinucleotide (NAD+)–dependent histone deacylases, with seven human homologs (sirt1-7).[74] The general structure is conserved among sirtuins and consists of a zinc binding domain and a catalytic domain (or Rossman Fold domain).[75] The pocket between the two domains is critical for NAD+ and substrate binding.[76] The biological roles of sirtuin proteins have been studied for decades, revealing catalytic functions such as deacylation, deglutarylation, demalonylation, decrotonylation, and desuccinylation, as well as a vast array of protein targets.[77–80] More recent work has shown that silent mating type information regulation 2 homolog 5 (Sirtuin 5, or SIRT5) has weaker deacetylase activity than its other sirtuin counterparts, and instead has strong catalytic efficiency for desuccinylase, deglutarylase, and demalonylase activity.[81]

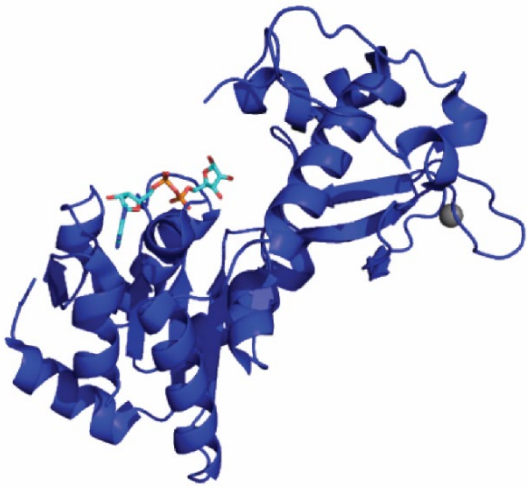

Figure 1-9. Crystal structure of SIRT5 with NAD+ bound in the catalytic site. A zinc ion can be observed in the zinc binding domain. From Zhao, X. et al. (2013).

SIRT5 is primarily localized to the mitochondria and is involved in the regulation of cellular respiration and metabolism through its many substrates, including pyruvate dehydrogenase complex (PDC), succinate dehydrogenase (SDH), superoxide dismutase (SOD1), carbamoyl phosphate synthetase 1 (CPS1), methylglutaryl-CoA synthase 2 (HMGSCS2), and others.[82,83] Because of its role in cellular metabolism, SIRT5 has been identified as a potential target for the treatment of unregulated cell growth and mitochondrial-dysfunction related diseases. Specifically, genomic analyses and over-expression models have demonstrated that SIR5 may drive proliferation in melanomas, breast cancers, and non-small cell lung cancers.[84–86] Inhibiting

SIRT5 activity represents a novel approach for the treatment of these cancers, many of which develop resistance to currently available therapies.[87] As such, there is a need for assays that can identify small molecule inhibitors that target SIRT in a specific and efficacious manner.

1.6.2 Monoclonal Antibody Therapeutics

Biopharmaceuticals, notably monoclonal antibodies (mAbs), are an important class of therapeutic molecules.[88] The success of mAbs can be attributed to higher specificity and affinity for target molecules as compared to their small-molecule counter parts, increasing the therapeutic window and reducing potential side effects.[89,90,91] Immunoglobulin Gs, or IgGs, are the dominant subclass of antibody therapeutics and are typically ~150 kDa[92]. These multi-domain proteins have two heavy chains (50 kDa) and two light chains (25 kDa). The variable domains of each, V_H and V_L respectively, form the region that is responsible for highly specific antigen-binding. Together with the first constant domains from the heavy (C_H1) and light chains (C_L) they from the antigen-binding fragment (Fab)[93]. The C_H2 and C_H3 domains makeup the crystallizable (Fc) region and contains a conserved N-linked glycosylation site[94]. The Fab region is connected to the Fc region through a hinge region. A representation of the overall structure is depicted in **Figure 1-10**.

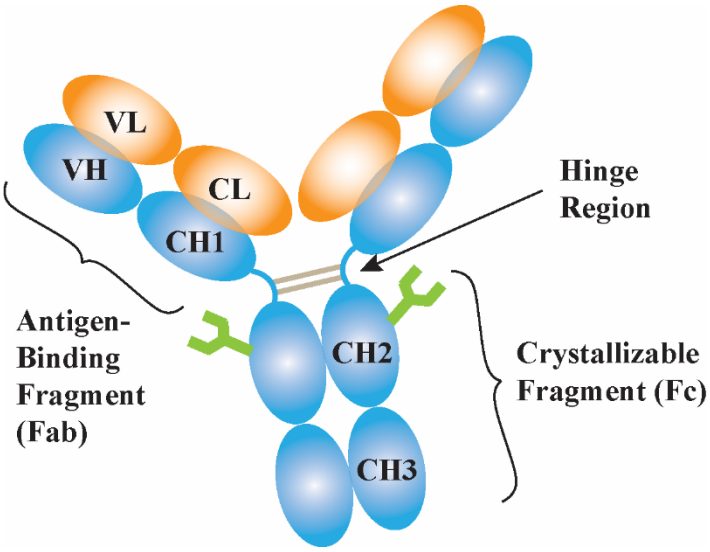

Figure 1-10. Cartoon representation of an IgG antibody. The light chain is colored orange and the heavy chain is blue. Glycosylation sites are depicted in green.

IgGs are generally produced through recombinant DNA technology. Most are humanized or fully human and produced mammalian cells[95]. As such, they are susceptible to typical cellular

processes, including post-translational modification. Glycosylation is the most prominent PTM in the literature, however, oxidation, disulfide shuffling, truncations, site-specific isomerization, and deamidation have all been reported. These modifications can impact protein function and efficacy, as well as formulation and storage requirements[94,96,97,98]. It is important to note that the presence and extent of PTMs can be affected by the growth conditions used during IgG production. This includes cell type, culture media components, temperature, and pH[99]. Tools for antibody analysis must be able to handle the heterogeneity present in mAb populations and complex background matrices.

1.7 Dissertation Overview

The aim of this work is to improve upon previously developed droplet microfluidic methods for the rapid analysis of protein-ligand interactions with applications in drug discovery. Work was also done towards the development of droplet-MS for the analysis of biotherapeutics from complex background matrices.

In **Chapter 2** improvements were made to existing capillary electrophoresis assays for the analysis of SIRT5 enzymatic activity and identification of SIRT5 inhibitors. A commercial capillary electrophoresis method was developed to validate results from other platforms and was used to confirm 8 novel SIRT5 inhibitors through dose-response analysis. Further improvements in throughput were made on previous microchip capillary electrophoresis separations for monitoring SIRT5 reaction progress and coupled to droplet sample introduction via an density-based oil drain. Finally, steps were taken towards the development of a label-free, droplet-MS SIRT5 assay coupled to online reagent addition.

The aim of **Chapter 3** was to combine droplet microfluidics with rapid CIU data acquisition for the high-throughput analysis biophysical analysis of protein ligand interactions.

CIU fingerprint acquisition times were reduced by an order of magnitude as compared to traditional fingerprint collection. Additionally, droplet methods compatible with native mass spectrometry were developed and coupled to an IM-MS instrument. Droplet-CIU was then used to screen 96 small-molecule compounds against SIRT5, where over 20 binders of SIRT5 were identified. Comparisons to activity assays revealed that inhibitors stabilize certain gas-phase conformations of SIRT5, providing more insight into the mechanism of SIRT5 inhibition.

In **Chapter 4** a droplet-MS method was developed to rapidly quantify monoclonal antibodies from cell expression media. This work started with the miniaturization and modification of a protein A-based cleanup protocol to ensure compatibility with droplet-MS. The sample cleanup was coupled to droplet generation and MS analysis to screen a panel of IgGs expressed in 48 different media conditions. Good correlation with existing LC-MS assays was determined and the most productive media conditions were identified. This work was also supplemented with the use of high-resolution MS for glycan profiling.

1.8 References

(1) Volochnyuk, D. M.; Ryabukhin, S. V.; Moroz, Y. S.; Savych, O.; Chuprina, A.; Horvath, D.; Zabolotna, Y.; Varnek, A.; Judd, D. B. Evolution of Commercially Available Compounds for HTS. *Drug Discov. Today* **2019**, *24* (2), 390–402. https://doi.org/10.1016/J.DRUDIS.2018.10.016.

(2) Guo, S.; Zou, J.; Wang, G. Drug Design, Development and Therapy Dovepress Advances in the Proteomic Discovery of Novel Therapeutic Targets in Cancer. *Drug Des. Devel. Ther.* **2013**. https://doi.org/10.2147/DDDT.S52216.

(3) Hertzberg, R. P.; Pope, A. J. High-Throughput Screening: New Technology for the 21st Century. *Curr. Opin. Chem. Biol.* **2000**, *4* (4), 445–451. https://doi.org/10.1016/S1367-5931(00)00110-1.

(4) Caraus, I.; Alsuwailem, A. A.; Nadon, R.; Makarenkov, V. Detecting and Overcoming Systematic Bias in High-Throughput Screening Technologies: A Comprehensive Review of Practical Issues and Methodological Solutions. *Brief. Bioinform.* **2015**, *16* (6), 974–986. https://doi.org/10.1093/BIB/BBV004.

(5) Blay, V.; Tolani, B.; Ho, S. P.; Arkin, M. R. High-Throughput Screening: Today's Biochemical and Cell-Based Approaches. *Drug Discov. Today* **2020**, *25* (10), 1807–1821. https://doi.org/10.1016/J.DRUDIS.2020.07.024.

(6) Stoddart, L. A.; White, C. W.; Nguyen, K.; Hill, S. J.; Pfleger, K. D. G. Fluorescence- and Bioluminescence-Based Approaches to Study GPCR Ligand Binding. *Br. J. Pharmacol.* **2016**, *173* (20), 3028–3037. https://doi.org/10.1111/BPH.13316.

(7) Mayr, L. M.; Fuerst, P. The Future of High-Throughput Screening. **2008**. https://doi.org/10.1177/1087057108319644.

(8) Samra, H. S.; He, F. Advancements in High Throughput Biophysical Technologies: Applications for Characterization and Screening during Early Formulation Development of Monoclonal Antibodies. **2012**. https://doi.org/10.1021/mp200404c.

(9) Genick, C. C.; Barlier, D.; Monna, D.; Brunner, R.; Bé, C.; Scheufler, C.; Ottl, J. Applications of Biophysics in High- Throughput Screening Hit Validation. *J. Biomol. Screen.* **2014**, *19* (5), 707–714. https://doi.org/10.1177/1087057114529462.

(10) D. Shortridge, M.; S. Hage, D.; S. Harbison, G.; Powers, R. Estimating Protein−Ligand Binding Affinity Using High-Throughput Screening by NMR. *J. Comb. Chem.* **2008**, *10* (6), 948–958. https://doi.org/10.1021/cc800122m.

(11) Damian, L. Chapter 4 Isothermal Titration Calorimetry for Studying Protein-Ligand Interactions. https://doi.org/10.1007/978-1-62703-398-5_4.

(12) Halai, R.; Cooper, M. A. Using Label-Free Screening Technology to Improve Efficiency in Drug Discovery. *http://dx.doi.org/10.1517/17460441.2012.651121* **2012**, *7* (2), 123–131. https://doi.org/10.1517/17460441.2012.651121.

(13) Cooper, M. A. Optical Biosensors in Drug Discovery. *Nat. Rev. Drug Discov. 2002 17* **2002**, *1* (7), 515–528. https://doi.org/10.1038/nrd838.

(14) Prudent, R.; Annis, D. A.; Dandliker, P. J.; Ortholand, J. Y.; Roche, D. Exploring New Targets and Chemical Space with Affinity Selection-Mass Spectrometry. *Nat. Rev. Chem. 2020 51* **2020**, *5* (1), 62–71. https://doi.org/10.1038/s41570-020-00229-2.

(15) Lanucara, F.; Holman, S. W.; Gray, C. J.; Eyers, C. E. The Power of Ion Mobility-Mass Spectrometry for Structural Characterization and the Study of Conformational Dynamics. *Nat. Chem. 2014 64* **2014**, *6* (4), 281–294. https://doi.org/10.1038/nchem.1889.

(16) Niu, S.; Rabuck, J. N.; Ruotolo, B. T. Ion Mobility-Mass Spectrometry of Intact Protein–Ligand Complexes for Pharmaceutical Drug Discovery and Development. *Curr. Opin. Chem. Biol.* **2013**, *17* (5), 809–817. https://doi.org/10.1016/J.CBPA.2013.06.019.

(17) Skeene, K.; Khatri, K.; Soloviev, Z.; Lapthorn, C. Current Status and Future Prospects for Ion-Mobility Mass Spectrometry in the Biopharmaceutical Industry. *Biochim. Biophys. Acta - Proteins Proteomics* **2021**, *1869* (12), 140697. https://doi.org/10.1016/J.BBAPAP.2021.140697.

(18) Cumeras, R.; Figueras, E.; Davis, C. E.; Baumbach, J. I.; Gràcia, I. Review on Ion Mobility Spectrometry. Part 1: Current Instrumentation. *Analyst* **2015**, *140* (5), 1376–1390.

https://doi.org/10.1039/C4AN01100G.

(19) Fenn, J. B.; Mann, M.; Meng, C. K.; Wong, S. F.; Whitehouse, C. M. Electrospray Ionization for Mass Spectrometry of Large Biomolecules. *Science* **1989**, *246* (4926), 64–71. https://doi.org/10.1126/SCIENCE.2675315.

(20) Loo, J. A. *STUDYING NONCOVALENT PROTEIN COMPLEXES BY ELECTROSPRAY IONIZATION MASS SPECTROMETRY*; 1996.

(21) Loo, J. A. Electrospray Ionization Mass Spectrometry: A Technology for Studying Noncovalent Macromolecular Complexes. *Int. J. Mass Spectrom.* **2000**, *200* (1–3), 175–186. https://doi.org/10.1016/S1387-3806(00)00298-0.

(22) Taylor, G. Disintegration of Water Drops in an Electric Field. *Proc. R. Soc. London. Ser. A. Math. Phys. Sci.* **1964**, *280* (1382), 383–397. https://doi.org/10.1098/RSPA.1964.0151.

(23) Rayleigh, Lord. XX. On the Equilibrium of Liquid Conducting Masses Charged with Electricity. *London, Edinburgh, Dublin Philos. Mag. J. Sci.* **1882**, *14* (87), 184–186. https://doi.org/10.1080/14786448208628425.

(24) Dole, M.; L. Hines, R.; L. Mack, L.; C. Mobley, R.; D. Ferguson, L.; B. Alice, M. Gas Phase Macroions. *Macromolecules* **2002**, *1* (1), 96–97. https://doi.org/10.1021/ma60001a017.

(25) Breuker, K.; Mclafferty, F. W. *Stepwise Evolution of Protein Native Structure with Electrospray into the Gas Phase, 10 12 to 10 2 S*; 2008.

(26) Heck, A. J. R. Native Mass Spectrometry: A Bridge between Interactomics and Structural Biology. **2008**. https://doi.org/10.1038/NMEtH.1265.

(27) El-Faramawy, A.; Siu, K. W. M.; Thomson, B. A. Efficiency of Nano-Electrospray Ionization. *J. Am. Soc. Mass Spectrom.* **2005**, *16* (10), 1702–1707. https://doi.org/10.1016/J.JASMS.2005.06.011.

(28) Wilm, M.; Mann, M. Analytical Properties of the Nanoelectrospray Ion Source. *Anal. Chem.* **1996**, *68* (1), 1–8. https://doi.org/10.1021/ac9509519.

(29) Chernushevich, I. V; Loboda, A. V; Thomson, B. A. An Introduction to Quadrupole-Time-of-Flight Mass Spectrometry. *J. MASS Spectrom. J. Mass Spectrom* **2001**, *36*, 849–865. https://doi.org/10.1002/jms.207.

(30) Mamyrin, B. A.; Karataev, V. I.; Shmikk, D. V.; Zagulin, V. A. The Mass-Reflectron. A New Nonmagnetic Time-of-Flight High Resolution Mass-Spectrometer. *Zhurnal Ehksperimental'noj i Teor. Fiz.* **1973**, *64* (1), 82–89.

(31) Radionova, A.; Filippov, I.; Derrick, P. J. In Pursuit of Resolution in Time-of-Flight Mass Spectrometry: A Historical Perspective. *Mass Spectrom. Rev.* **2016**, *35* (6), 738–757. https://doi.org/10.1002/MAS.21470.

(32) de Hoffmann, E.; Stroobant, V. Mass Spectrometry Principles and Applications.

(33) Kanu, A. B.; Dwivedi, P.; Tam, M.; Matz, L.; Hill, H. H. Ion Mobility–Mass Spectrometry. *J. Mass Spectrom.* **2008**, *43* (1), 1–22. https://doi.org/10.1002/JMS.1383.

(34) Mason, E. A. (Edward A.; McDaniel, E. W. Transport Properties of Ions in Gases. **1988**, 560.

(35) Bush, M. F.; Hall, Z.; Giles, K.; Hoyes, J.; Robinson, C. V; Ruotolo, B. T.; Duijn, van; R Chem, A. J. Collision Cross Sections of Proteins and Their Complexes: A Calibration Framework and Database for Gas-Phase Structural Biology. *Proc. Natl. Acad. Sci. U.S.A* **2010**, *39* (2), 9557–9565. https://doi.org/10.1021/ac1022953.

(36) Butler, K. E.; Takinami, Y.; Rainczuk, A.; Baker, E. S.; Roberts, B. R. Utilizing Ion Mobility-Mass Spectrometry to Investigate the Unfolding Pathway of Cu/Zn Superoxide Dismutase. *Front. Chem.* **2021**, *9*, 23. https://doi.org/10.3389/FCHEM.2021.614595/BIBTEX.

(37) Pukala, T. Importance of Collision Cross Section Measurements by Ion Mobility Mass Spectrometry in Structural Biology. **2018**. https://doi.org/10.1002/rcm.8294.

(38) Terral, G.; Beck, A.; Cianférani, S. Insights from Native Mass Spectrometry and Ion Mobility-Mass Spectrometry for Antibody and Antibody-Based Product Characterization. *J. Chromatogr. B* **2016**, *1032*, 79–90. https://doi.org/10.1016/J.JCHROMB.2016.03.044.

(39) Dixit, S. M.; Polasky, D. A.; Ruotolo, B. T. Collision Induced Unfolding of Isolated Proteins in the Gas Phase: Past, Present, and Future. *Curr. Opin. Chem. Biol.* **2018**, *42*, 93–100. https://doi.org/10.1016/J.CBPA.2017.11.010.

(40) Niu, S.; Ruotolo, B. T. Collisional Unfolding of Multiprotein Complexes Reveals Cooperative Stabilization upon Ligand Binding. *Protein Sci.* **2015**, *24* (8), 1272–1281. https://doi.org/10.1002/PRO.2699.

(41) N. Rabuck, J.; Hyung, S.-J.; S. Ko, K.; C. Fox, C.; B. Soellner, M.; T. Ruotolo, B. Activation State-Selective Kinase Inhibitor Assay Based on Ion Mobility-Mass Spectrometry. *Anal. Chem.* **2013**, *85* (15), 6995–7002. https://doi.org/10.1021/ac4012655.

(42) Mehmood, S.; Marcoux, J.; Gault, J.; Quigley, A.; Michaelis, S.; Young, S. G.; Carpenter, E. P.; Robinson, C. V. Mass Spectrometry Captures Off-Target Drug Binding and Provides Mechanistic Insights into the Human Metalloprotease ZMPSTE24. *Nat. Chem.* **2016**, *8* (12), 1152–1158. https://doi.org/10.1038/nchem.2591.

(43) Byrne, D. P.; Vonderach, M.; Ferries, S.; Brownridge, P. J.; Eyers, C. E.; Eyers, P. A. CAMP-Dependent Protein Kinase (PKA) Complexes Probed by Complementary Differential Scanning Fluorimetry and Ion Mobility-Mass Spectrometry. **2016**. https://doi.org/10.1042/BCJ20160648.

(44) Tomer, K. B. Separations Combined with Mass Spectrometry. *Chem. Rev.* **2001**, *101* (2), 297–328. https://doi.org/10.1021/CR990091M.

(45) Pitt, J. J. Principles and Applications of Liquid Chromatography-Mass Spectrometry in Clinical Biochemistry. *Clin. Biochem. Rev.* **2009**, *30* (1), 19.

(46) Dass, C. Hyphenated Separation Techniques. *Fundam. Contemp. Mass Spectrom.* **2007**, 151–194. https://doi.org/10.1002/9780470118498.CH5.

(47) Kempa, E. E.; Hollywood, K. A.; Smith, C. A.; Barran, P. E. High Throughput Screening

of Complex Biological Samples with Mass Spectrometry – from Bulk Measurements to Single Cell Analysis. *Analyst* **2019**, *144* (3), 872–891. https://doi.org/10.1039/C8AN01448E.

(48) Jannetto, P. J.; Langman, L. J. High-Throughput Online Solid-Phase Extraction Tandem Mass Spectrometry: Is It Right for Your Clinical Laboratory? *Clin. Biochem.* **2016**, *49* (13–14), 1032–1034. https://doi.org/10.1016/J.CLINBIOCHEM.2016.04.012.

(49) Zhang, W.; Wu, X.; Wang, J.; Tan, L.; Bui, J.; Gjerstad, E.; Mcmillan, K. In Vitro ADME Profiling Using High-Throughput RapidFire Mass Spectrometry: Cytochrome P450 Inhibition and Metabolic Stability Assays. *J. Biomol. Screen.* **2012**, *17* (6), 761–772. https://doi.org/10.1177/1087057112441013.

(50) Sawyer, W. S.; Srikumar, N.; Carver, J.; Chu, P. Y.; Shen, A.; Xu, A.; Williams, A. J.; Spiess, C.; Wu, C.; Liu, Y.; Tran, J. C. High-Throughput Antibody Screening from Complex Matrices Using Intact Protein Electrospray Mass Spectrometry. *Proc. Natl. Acad. Sci. U. S. A.* **2020**, *117* (18), 9851–9856. https://doi.org/10.1073/pnas.1917383117.

(51) Takáts, Z.; Wiseman, J. M.; Gologan, B.; Cooks, R. G. Mass Spectrometry Sampling under Ambient Conditions with Desorption Electrospray Ionization. *Science* **2004**, *306* (5695), 471–473. https://doi.org/10.1126/SCIENCE.1104404.

(52) Vimer, S.; Ben-Nissan, G.; Sharon, M. Mass Spectrometry Analysis of Intact Proteins fromCrude Samples. *Anal. Chem.* **2020**, *92* (19), 12741. https://doi.org/10.1021/ACS.ANALCHEM.0C02162.

(53) Shin, Y. S.; Drolet, B.; Mayer, R.; Dolence, K.; Basile, F. Desorption Electrospray Ionization-Mass Spectrometry (DESI-MS) of Proteins. *Anal. Chem.* **2007**, *79* (9), 3514. https://doi.org/10.1021/AC062451T.

(54) Sinclair, I.; Stearns, R.; Pringle, S.; Wingfield, J.; Datwani, S.; Hall, E.; Ghislain, L.; Majlof, L.; Bachman, M. Novel Acoustic Loading of a Mass Spectrometer: Toward Next-Generation High-Throughput MS Screening. *J. Lab. Autom.* **2016**, *21* (1), 19–26. https://doi.org/10.1177/2211068215619124.

(55) Kempa, E. E.; Smith, C. A.; Li, X.; Bellina, B.; Richardson, K.; Pringle, S.; Galman, J. L.; Turner, N. J.; Barran, P. E. Coupling Droplet Microfluidics with Mass Spectrometry for Ultrahigh-Throughput Analysis of Complex Mixtures up to and above 30 Hz. *Anal. Chem.* **2020**, *92* (18), 12605–12612. https://doi.org/10.1021/acs.analchem.0c02632.

(56) Stone, H. A.; Kim, S. Microfluidics: Basic Issues, Applications, and Challenges. *AIChE J.* **2001**, *47* (6), 1250–1254. https://doi.org/10.1002/AIC.690470602.

(57) Hou, X.; Zhang, Y. S.; Santiago, G. T. De; Alvarez, M. M.; Ribas, J.; Jonas, S. J.; Weiss, P. S.; Andrews, A. M.; Aizenberg, J.; Khademhosseini, A. Interplay between Materials and Microfluidics. *Nat. Rev. Mater. 2017 25* **2017**, *2* (5), 1–15. https://doi.org/10.1038/natrevmats.2017.16.

(58) Dittrich, P. S.; Manz, A. Lab-on-a-Chip: Microfluidics in Drug Discovery. *Nature Reviews Drug Discovery*. Nature Publishing Group March 2006, pp 210–218. https://doi.org/10.1038/nrd1985.

(59) Rivet, C.; Lee, H.; Hirsch, A.; Hamilton, S.; Lu, H. Microfluidics for Medical Diagnostics and Biosensors. *Chem. Eng. Sci.* **2011**, *66* (7), 1490–1507. https://doi.org/10.1016/J.CES.2010.08.015.

(60) Elvira, K. S.; I Solvas, X. C.; Wootton, R. C. R.; Demello, A. J. The Past, Present and Potential for Microfluidic Reactor Technology in Chemical Synthesis. *Nat. Chem. 2013 511* **2013**, *5* (11), 905–915. https://doi.org/10.1038/nchem.1753.

(61) Ding, Y.; Howes, P. D.; Demello, A. J. Recent Advances in Droplet Microfluidics. **2019**. https://doi.org/10.1021/acs.analchem.9b05047.

(62) Payne, E. M.; Holland-Moritz, D. A.; Sun, S.; Kennedy, R. T. High-Throughput Screening by Droplet Microfluidics: Perspective into Key Challenges and Future Prospects. *Lab Chip* **2020**, *20*, 2247–2262. https://doi.org/10.1039/d0lc00347f.

(63) Al-Hetlani, E.; Amin, M. O. Continuous Magnetic Droplets and Microfluidics: Generation, Manipulation, Synthesis and Detection. *Mikrochim. Acta* **2019**, *186* (2). https://doi.org/10.1007/S00604-018-3118-6.

(64) Shang, L.; Cheng, Y.; Zhao, Y. Emerging Droplet Microfluidics. *Chemical Reviews*. American Chemical Society June 28, 2017, pp 7964–8040. https://doi.org/10.1021/acs.chemrev.6b00848.

(65) Zhu, Y.; Fang, Q. Analytical Detection Techniques for Droplet Microfluidics—A Review. *Anal. Chim. Acta* **2013**, *787*, 24–35. https://doi.org/10.1016/J.ACA.2013.04.064.

(66) Pei, J.; Li, Q.; S. Lee, M.; A. Valaskovic, G.; T. Kennedy, R. Analysis of Samples Stored as Individual Plugs in a Capillary by Electrospray Ionization Mass Spectrometry. *Anal. Chem.* **2009**, *81* (15), 6558–6561. https://doi.org/10.1021/ac901172a.

(67) Fidalgo, L. M.; Whyte, G.; Ruotolo, B. T.; Benesch, J. L. P.; Stengel, F.; Abell, C.; Robinson, C. V.; Huck, W. T. S. Coupling Microdroplet Microreactors with Mass Spectrometry: Reading the Contents of Single Droplets Online. *Angew. Chemie Int. Ed.* **2009**, *48* (20), 3665–3668. https://doi.org/10.1002/ANIE.200806103.

(68) Wang, X.; Yi, L.; Mukhitov, N.; Schrell, A. M.; Dhumpa, R.; Roper, M. G. Microfluidics-to-Mass Spectrometry: A Review of Coupling Methods and Applications. *J. Chromatogr. A* **2015**, *1382*, 98–116. https://doi.org/10.1016/J.CHROMA.2014.10.039.

(69) Ngernsutivorakul, T.; J. Steyer, D.; C. Valenta, A.; T. Kennedy, R. In Vivo Chemical Monitoring at High Spatiotemporal Resolution Using Microfabricated Sampling Probes and Droplet-Based Microfluidics Coupled to Mass Spectrometry. *Anal. Chem.* **2018**, *90* (18), 10943–10950. https://doi.org/10.1021/acs.analchem.8b02468.

(70) Steyer, D. J.; T. Kennedy, R. High-Throughput Nanoelectrospray Ionization-Mass Spectrometry Analysis of Microfluidic Droplet Samples. *Anal. Chem.* **2019**, *91* (10), 6645–6651. https://doi.org/10.1021/acs.analchem.9b00571.

(71) Holland-Moritz, D. A.; Wismer, M. K.; Mann, B. F.; Farasat, I.; Devine, P.; Guetschow, E. D.; Mangion, I.; Welch, C. J.; Moore, J. C.; Sun, S.; Kennedy, R. T. High-Throughput Screening Hot Paper Mass Activated Droplet Sorting (MADS) Enables High-Throughput

Screening of Enzymatic Reactions at Nanoliter Scale. https://doi.org/10.1002/ange.201913203.

(72) Sun, S.; Slaney, T. R.; Kennedy, R. T. Label Free Screening of Enzyme Inhibitors at Femtomole Scale Using Segmented Flow Electrospray Ionization Mass Spectrometry. *Anal. Chem.* **2012**, *84* (13), 5794–5800. https://doi.org/10.1021/ac3011389.

(73) A. Smith, C.; Li, X.; H. Mize, T.; D. Sharpe, T.; I. Graziani, E.; Abell, C.; T. S. Huck, W. Sensitive, High Throughput Detection of Proteins in Individual, Surfactant-Stabilized Picoliter Droplets Using Nanoelectrospray Ionization Mass Spectrometry. *Anal. Chem.* **2013**, *85* (8), 3812–3816. https://doi.org/10.1021/ac400453t.

(74) Sauve, A. A.; Wolberger, C.; Schramm, V. L.; Boeke, J. D. The Biochemistry of Sirtuins. **2006**. https://doi.org/10.1146/annurev.biochem.74.082803.133500.

(75) Zhao, X.; Allison, D.; Condon, B.; Zhang, F.; Gheyi, T.; Zhang, A.; Ashok, S.; Russell, M.; Macewan, I.; Qian, Y.; Jamison, J. A.; Gately Luz, J. The 2.5 Å Crystal Structure of the SIRT1 Catalytic Domain Bound to Nicotinamide Adenine Dinucleotide (NAD +) and an Indole (EX527 Analogue) Reveals a Novel Mechanism of Histone Deacetylase Inhibition. **2013**. https://doi.org/10.1021/jm301431y.

(76) Yang, L.; Ma, X.; He, Y.; Yuan, C.; Chen, Q.; Li, G.; Chen, X. Sirtuin 5. *Sci China Life Sci* **2017**, *60* (3), 249–256. https://doi.org/10.1007/s11427-016-0060-7.

(77) Feldman, J. L.; Baeza, J.; Denu, J. M. Activation of the Protein Deacetylase SIRT6 by Long-Chain Fatty Acids and Widespread Deacylation by Mammalian Sirtuins. *J. Biol. Chem.* **2013**, *288* (43), 31350–31356. https://doi.org/10.1074/JBC.C113.511261.

(78) Du, J.; Zhou, Y.; Su, X.; Yu, J. J.; Khan, S.; Jiang, H.; Kim, J.; Woo, J.; Kim, J. H.; Choi, B. H.; He, B.; Chen, W.; Zhang, S.; Cerione, R. A.; Auwerx, J.; Hao, Q.; Lin, H. Sirt5 Is a NAD-Dependent Protein Lysine Demalonylase and Desuccinylase. *Science (80-.).* **2011**, *334* (6057), 806–809. https://doi.org/10.1126/SCIENCE.1207861.

(79) Peng, C.; Lu, Z.; Xie, Z.; Cheng, Z.; Chen, Y.; Tan, M.; Luo, H.; Zhang, Y.; He, W.; Yang, K.; Zwaans, B. M. M.; Tishkoff, D.; Ho, L.; Lombard, D.; He, T.-C.; Dai, J.; Verdin, E.; Ye, Y.; Zhao, Y. The First Identification of Lysine Malonylation Substrates and Its Regulatory Enzyme* □ S. *Mol. Cell. Proteomics* **2011**, *10*, M111.012658. https://doi.org/10.1074/mcp.M111.012658.

(80) Tan, M.; Peng, C.; Anderson, K. A.; Chhoy, P.; Xie, Z.; Dai, L.; Park, J.; Chen, Y.; Huang, H.; Zhang, Y.; Ro, J.; Wagner, G. R.; Green, M. F.; Madsen, A. S.; Schmiesing, J.; Peterson, B. S.; Xu, G.; Ilkayeva, O. R.; Muehlbauer, M. J.; Braulke, T.; Mühlhausen, C.; Backos, D. S.; Olsen, C. A.; McGuire, P. J.; Pletcher, S. D.; Lombard, D. B.; Hirschey, M. D.; Zhao, Y. Lysine Glutarylation Is a Protein Posttranslational Modification Regulated by SIRT5. *Cell Metab.* **2014**, *19* (4), 605–617. https://doi.org/10.1016/J.CMET.2014.03.014.

(81) Roessler, C.; Tüting, C.; Meleshin, M.; Steegborn, C.; Schutkowski, M. A Novel Continuous Assay for the Deacylase Sirtuin 5 and Other Deacetylases. *J. Med. Chem.* **2015**, *58* (18), 7217–7223. https://doi.org/10.1021/acs.jmedchem.5b00293.

(82) Rardin, M. J.; He, W.; Nishida, Y.; Newman, J. C.; Carrico, C.; Danielson, S. R.; Guo, A.;

Gut, P.; Sahu, A. K.; Li, B.; Uppala, R.; Fitch, M.; Riiff, T.; Zhu, L.; Zhou, J.; Mulhern, D.; Stevens, R. D.; Ilkayeva, O. R.; Newgard, C. B.; Jacobson, M. P.; Hellerstein, M.; Goetzman, E. S.; Gibson, B. W.; Verdin, E. SIRT5 Regulates the Mitochondrial Lysine Succinylome and Metabolic Networks. *Cell Metab.* **2013**, *18* (6), 920–933. https://doi.org/10.1016/J.CMET.2013.11.013.

(83) Nishida, Y.; Rardin, M. J.; Carrico, C.; He, W.; Sahu, A. K.; Gut, P.; Najjar, R.; Fitch, M.; Hellerstein, M.; Gibson, B. W.; Verdin, E. SIRT5 Regulates Both Cytosolic and Mitochondrial Protein Malonylation with Glycolysis as a Major Target. *Mol. Cell* **2015**, *59* (2), 321–332. https://doi.org/10.1016/J.MOLCEL.2015.05.022.

(84) Abril, Y. L. N.; Fernandez, I. R.; Hong, J. Y.; Chiang, Y.-L.; Kutateladze, D. A.; Zhao, Q.; Yang, M.; Hu, J.; Sadhukhan, S.; Li, B.; He, B.; Remick, B.; Bai, J. J.; Mullmann, J.; Wang, F.; Maymi, V.; Dhawan, R.; Auwerx, J.; Southard, T.; Cerione, R. A.; Lin, H.; Weiss, R. S. Pharmacological and Genetic Perturbation Establish SIRT5 as a Promising Target in Breast Cancer. *Oncogene* **2021**, *40* (9), 1644–1658. https://doi.org/10.1038/s41388-020-01637-w.

(85) Lu, W.; Zuo, Y.; Feng, Y.; Zhang, M. SIRT5 Facilitates Cancer Cell Growth and Drug Resistance in Non-Small Cell Lung Cancer. https://doi.org/10.1007/s13277-014-2372-4.

(86) Giblin, W.; Bringman-Rodenbarger, L.; Guo, A. H.; Kumar, S.; Monovich, A. C.; Mostafa, A. M.; Skinner, M. E.; Azar, M.; Mady, A. S. A.; Chung, C. H.; Kadambi, N.; Melong, K. A.; Lee, H. J.; Zhang, L.; Sajjakulnukit, P.; Trefely, S.; Varner, E. L.; Iyer, S.; Wang, M.; Wilmott, J. S.; Peter Soyer, H.; Sturm, R. A.; Pritchard, A. L.; Andea, A. A.; Scolyer, R. A.; Stark, M. S.; Scott, D. A.; Fullen, D. R.; Bosenberg, M. W.; Chandrasekaran, S.; Nikolovska-Coleska, Z.; Verhaegen, M. E.; Snyder, N. W.; Rivera, M. N.; Osterman, A. L.; Lyssiotis, C. A.; Lombard, D. B. The Deacylase SIRT5 Supports Melanoma Viability by Influencing Chromatin Dynamics. *J. Clin. Invest.* **2021**, *131* (12). https://doi.org/10.1172/JCI138926.

(87) Yang, D.-H.; Montopoli, M.; Vergara, D.; Li, Q.; Sun, X.; Wang, S.; Gai, J.; Guan, J.; Li, J.; Li, Y.; Zhao, J.; Zhao, C.; Fu, L. SIRT5 Promotes Cisplatin Resistance in Ovarian Cancer by Suppressing DNA Damage in a ROS-Dependent Manner via Regulation of the Nrf2/HO-1 Pathway. *Front. Oncol.* | *www.frontiersin.org* **2019**, *1*, 754. https://doi.org/10.3389/fonc.2019.00754.

(88) Awwad, S.; Angkawinitwong, U. Pharmaceutics Overview of Antibody Drug Delivery. https://doi.org/10.3390/pharmaceutics10030083.

(89) Weiner, G. J. Building Better Monoclonal Antibody-Based Therapeutics. *Nat. Publ. Gr.* **2015**. https://doi.org/10.1038/nrc3930.

(90) Cruz, E.; Kayser, V. Monoclonal Antibody Therapy of Solid Tumors: Clinical Limitations and Novel Strategies to Enhance Treatment Efficacy. *Biol. Targets Ther.* **2019**, *13*, 33–51. https://doi.org/10.2147/BTT.S166310.

(91) Shefet-Carasso, L.; Benhar, I. Antibody-Targeted Drugs and Drug Resistance—Challenges and Solutions. *Drug Resist. Updat.* **2015**, *18*, 36–46. https://doi.org/10.1016/J.DRUP.2014.11.001.

(92) Ecker, D. M.; Jones, S. D.; Levine, H. L. The Therapeutic Monoclonal Antibody Market. *MAbs* **2015**, *7* (1), 9–14. https://doi.org/10.4161/19420862.2015.989042.

(93) Chiu, M. L.; Goulet, D. R.; Teplyakov, A.; Gilliland, G. L. Antibody Structure and Function: The Basis for Engineering Therapeutics. *Antibodies* **2019**, *8* (4), 55. https://doi.org/10.3390/antib8040055.

(94) Jefferis, R. Glycosylation as a Strategy to Improve Antibody-Based Therapeutics. *Nat. Rev. Drug Discov.* **2009**, *8* (3), 226–234. https://doi.org/10.1038/nrd2804.

(95) Rodrigues, M. E.; Costa, A. R.; Henriques, M.; Azeredo, J.; Oliveira, R. Technological Progresses in Monoclonal Antibody Production Systems. *Biotechnol. Prog.* **2010**, *26* (2), 332–351. https://doi.org/10.1002/btpr.348.

(96) Alam, M. E.; Slaney, T. R.; Wu, L.; Das, T. K.; Kar, S.; Barnett, G. V.; Leone, A.; Tessier, P. M. Unique Impacts of Methionine Oxidation, Tryptophan Oxidation, and Asparagine Deamidation on Antibody Stability and Aggregation. *J. Pharm. Sci.* **2020**, *109* (1), 656–669. https://doi.org/10.1016/J.XPHS.2019.10.051.

(97) Schmid, I.; Bonnington, L.; Gerl, M.; Bomans, K.; Thaller, A. L.; Wagner, K.; Schlothauer, T.; Falkenstein, R.; Zimmermann, B.; Kopitz, J.; Hasmann, M.; Bauss, F.; Haberger, M.; Reusch, D.; Bulau, P. Assessment of Susceptible Chemical Modification Sites of Trastuzumab and Endogenous Human Immunoglobulins at Physiological Conditions. *Commun. Biol.* **2018**, *1* (1). https://doi.org/10.1038/s42003-018-0032-8.

(98) Moritz, B.; Stracke, J. O. Assessment of Disulfide and Hinge Modifications in Monoclonal Antibodies. *Electrophoresis* **2017**, *38*, 769–785. https://doi.org/10.1002/elps.201600425.

(99) Wang, Y.; Li, X.; Liu, Y. H.; Richardson, D.; Li, H.; Shameem, M.; Yang, X. Simultaneous Monitoring of Oxidation, Deamidation, Isomerization, and Glycosylation of Monoclonal Antibodies by Liquid Chromatography-Mass Spectrometry Method with Ultrafast Tryptic Digestion. *MAbs* **2016**, *8* (8), 1477–1486. https://doi.org/10.1080/19420862.2016.1226715.

Chapter 2: Development of Droplet-Based Capillary Electrophoresis and Mass Spectrometry Assays for the Identification of Sirtuin-5 Inhibitors

Reproduced in part from Ouimet, C.O.; D'Amico, C., I.; Kennedy, R. T. Anal. Bioanal. Chem. 2019, 411(23), 6155-6163. Fluorescent images in Figure 2-8 taken by Ouimet. Data presented in Figures 2-9,10 collected by D'Amico and formatted by Ouimet.

2.1 Introduction

Sirtuin proteins, a group of enzymes belonging to the class III histone deacetylase family, have been extensively studied as drug targets due to their role in modulating many biochemical pathways.[1,2] Specifically, sirtuins alter the functions of their target proteins by removing acetyl, succinyl, glutaryl, crotonyl, and malonyl groups from lysine residues in a nicotinamide adenine dinucleotide (NAD)-dependent fashion.[3–5] Many sirtuin protein targets are involved in cellular respiration and metabolism, therefore sirtuin regulation by small molecules has been widely explored for the treatment of cancers, diabetes, cardiovascular diseases, neurodegenerative diseases, and other ageing-affiliated disorders.[6,7] With such great interest in identifying small molecule regulators of sirtuins, there is a need for high-throughput screening (HTS) assays that can rapidly and accurately assess the effects of these drug candidates against sirtuin enzymatic activity.

Many sirtuin activity assays have been developed across a range of analytical platforms, with most research focused optical or fluorescence-based approaches.[8] The most common sirtuin activity assay is the commercially available *Fluor-de-Lys*™ assay, which utilizes a fluorogenic peptide modified with 7-amino-4-methylcoumarin (AMC)[9]. Fluorescent signal increases once the lysine modification is catalytically removed from the substrate peptide by a sirtuin, allowing for

cleavage of the AMC fluorophore via trypsin.[9] This assay has been employed in a HTS format to identify novel activators of Sirtuin-1.[10] The use of fluorescence resonance energy transfer (FRET)-based assays has also been explored for measuring sirtuin enzymatic activity[11]. The FRET-based assay uses a modified, acylated substrate peptide where the fluorescence of the donor dye is quenched by an acceptor dye. Fluorescence increases after deacylation of the peptide by a sirtuin, followed by a trypsin digest that releases the donor dye.[11] While fluorescence-based assays, such as FRET and *Fluor-de-Lys*™, are amenable to HTS and have been used to identify small molecule modulators of sirtuin activity, they require the use of a fluorophores which have been shown to cause false positive hits due to their proximity to the lysine residue and interactions with the sirtuin active site.[12,13]

There are also label-free approaches for screening sirtuin activity, most notably mass spectrometry coupled to liquid chromatography (LC-MS).[8] In this format substrate and product peptides can be separated, analyzed, and directly quantified without the need for a fluorophore or a secondary reaction. LC-MS analyses for sirtuin activity have been shown to be reliable; however, the use of LC-MS is typically reserved for secondary screens and hit confirmation due to longer separation times and difficulties with parallelization.[14,15] There remains an interest in developing new sirtuin activity assays that are both robust and amenable to HTS.

There has been an increasing interest in miniaturizing enzymatic assays and using microfluidic technologies in the drug discovery process to decrease reagent consumption and analysis time.[16,17] Regarding sirtuins, microchip capillary electrophoresis (MCE) has been employed in the identification of novel sirtuin modulators, where fluorescently labeled substrate and product peptides are separated based on electrophoretic mobility and detected on-chip.[18–20] The label can be placed at a remote location from the target lysine residue, reducing the chance of

false positives from non-specific interactions. Droplet-based sample introduction techniques have been coupled to MCE to further enhance the throughput of these sirtuin assays. In one screen, 1280 compounds were tested against the activity of sirtuin-5 (SIRT5) and analyzed in 0.5 Hz in a total of 46 min, resulting in the identification of eight novel SIRT5 inhibitors.[18] Droplet-based sample introduction has also been coupled directly to MS detection for the identification of sirtuin-1 (SIRT1) modulators.[21] In this study, 80 compounds were tested against SIRT1 and analyzed at 0.8 Hz in a label free manner. Overall, microfluidic and droplet microfluidic platforms represent an attractive approach for HTS sirtuin assays.

The focus on this chapter is on improving and developing high throughput assays for the identification of inhibitors of SIRT5 activity, an enzyme that is a potential target for melanomas, breast cancers, and non-small cell lung cancers. In this work we adapt existing SIRT5 assays to run on a commercial CE system and verify potential SIRT5 inhibitors using dose-response analysis. Additionally, we make improvements in throughput and S/N to previously developed SIRT5 MCE assays and couple this to a novel density-based droplet sample introduction device. Finally, we work towards an all-droplet, label-free MS assay for the identification of new SIRT5 inhibitors (**Appendix 1**).

2.2 Methods

Chemicals and Materials

All reagents were purchased from Sigma-Aldrich (St. Louis, MO) unless otherwise noted. SIRT5 was expressed and purified as previously described.[22] SDHA-derived peptides were obtained from GenicBio Limited (Shanghai, China). Test compounds were supplied by the Epigenetics Screening Library (Cayman Chemical, Ann Arbor, MI), the Center of Chemical

Genomics (University of Michigan, Ann Arbor, MI), or synthesized by the Neamati Group (University of Michigan, Ann Arbor, MI).

Peptide-Based SIRT5 Assay

The substrate peptide, GGQSLK[succ]FGKG, was based on the SIRT5 target protein succinate dehydrogenase. The sequence is based on the residues that surround the succinylation site of some SIRT5 target proteins. Dessuccinylation by SIRT5 yields the GGQSLKFGKG product (**Figure 2-1A**). 5-carboxyfluoroscein (an N-terminus label) and ^{13}C labeled forms of the peptide were obtained for CE/MCE and MS experiments respectively. For CE/MCE experiments, reactions were performed in a 10 µL volume containing 45 nM SIRT5, 1 µM substrate, 10 mM Tris, 1 mM 1,4-dithiothreitol, 0.5 mM NAD^+, 4.5% (v/v) glycerol, 30 mM NaCl, and 2 mM sodium phosphate and quenched with 45 µL of electrophoresis buffer (10 mM sodium tetraborate, 0.9 mM 2-hydroxypropyl-β-cyclodextrin). For MS experiments, SIRT5 reactions were carried out in 10 µL of 45 nM SIRT5, 1 µM substrate, and 10 mM ammonium bicarbonate, pH 8 and quenched with 45 µL 80% acetonitrile (ACN), 20% water, and 0.1% formic acid. Reaction yields were calculated by dividing product peak area over total product and substrate peak areas and normalized to positive and negative controls.

Capillary Electrophoresis

CE experiments were performed on a Beckman Coulter P/ACE MDQ instrument (Fullerton, CA). The excitation wavelength filter and emission wavelength filter were 488 nm and 520 nm respectively. Fused silica capillary (Polymicro Technologies, Phoenix, AZ) with a 360 µm outer diameter, 40 µm inner diameter, and 30 cm length was used for all experiments. Length to the detector window was set at 10 cm. 32 Karat software (Beckman Coulter) was used for data

acquisition and electropherograms were analyzed using Cutter 7.0 software.[23] Dose-response analyses were plotted and fit using a non-linear regression in GraphPad Prism 7.

Capillaries were preconditioned by sequentially rinsing with water, 0.1 M hydrochloric acid, water, 1.0 M sodium hydroxide, and filled with running buffer (10 mM sodium tetraborate, 0.9 mM 2-hydroxypropyl-β-cyclodextrin). Capillaries were reconditioned after eight injections, or after a noticeable shift in migration time was observed. Samples were introduced by hydrodynamic injection for 5 s at 0.1 psi. A field of 667 V/cm was applied for separation.

Device Fabrication

Glass MCE devices were fabricated from two etched glass slides (Telic Company, Valencia, CA) using previously established photolithography and wet etching protocols.[24–26] Sample, injection, and separation channels were etched to a depth of 4 μm on a single slide and capillary insertion channels were etched to 80 μm on both slides. A 0.5 mm drill bit was used to make fluidic access holes. The glass slides were washed in piranha solution (75% sulfuric acid, 25% hydrogen peroxide) for 20 min and in heated RCA solution (15% ammonium hydroxide, 15% hydrogen peroxide, 70% water) for 40 min prior to alignment and bonding. The two slides were bonded at 610 °C for 8 h. Finally, reservoirs and fused silica capillary 150 μm o.d. 75 μm i.d. were attached using marine epoxy (Loctite, Düsseldorf, Germany).

Polydimethylsiloxane (PDMS) reagent addition devices were fabricated using standard pour-over soft lithography protocols.[27] Negative masters were formed by spinning SU-8 2050 photoresist to a depth of 100 μM on silicon wafers (University Wafer, Boston, MA) and developed using photolithography. PDMS (Curbell Plastics, Livonia, MI) was then poured over master wafers or blank wafers and cured for at 65 °C for at least 45 min. Patterned PDMS and blank PDMS were exposed to atmospheric plasma for 45 s, bonded, and baked at 65 °C overnight.

Channels in reagent addition devices were derivatized with 2% trichloro (1H, 1H, 2H, 2H-perfluorooctyl)silane in perfluorodecalin (PFD) prior to each experiment.

Droplet Generation

Droplets approximately 4 nL in volume were generated into 360 µm o.d. 150 µm i.d. PFA Teflon tubing (Idex Health & Science, Oak Harbor, WA) from modified 384 well-plates using previously described methods.[28] Briefly, the Teflon tubing was mounted to a computer controlled XYZ- positioner that directed the inlet into corresponding wells. The outlet was connected to a 100 µL syringe mounted in a PHD 200 syringe pump (Harvard Apparatus, Holliston, TX), operated in withdrawal mode. For MCE experiments a silicone oil (10 cST) carrier phase was used and droplets were generated at 0.3 µL/min. For reagent addition and MS experiments the carrier phase was 0.5% perfluroroctanol (PFO) in perfluorodecalin and droplets were generated at 1000 nL/min. In all experiments the tubing was prefilled with carrier phase to remove any air bubbles.

Microchip Capillary Electrophoresis

Prior to MCE experiments, chip reservoirs were filled with the separation buffer described above. Vacuum was applied at the waste reservoir for at least ten minutes to ensure all channels were filled. Chip setup and operation were as previously described.[18]An applied field of 3500 V/cm was used for separations with a 1 mm length to the detector. Samples were electrokinetically injected with 100 ms gated injections every 250 ms. Prior to droplet sample introduction, Rain-X was flushed through the fused silica transfer capillary to facilitate droplet transfer and minimize surface interactions. Droplet trains were introduced on chip by inserting the transfer capillary into theTeflon tubing and sealing the junction with marine epoxy. An Olympus IX71 fluorescence microscope (Tokyo, Japan) was used for imaging droplet transfer and sample injection. An in-

house epiilumination laser induced fluorescence (LIF) detector was used for all other MCE experiments.[18]

Mass Spectrometry

All ESI-MS analysis was carried out on an Agilent 6410 triple quadrupole mass spectrometer (Agilent Technologies, Santa Clara, CA). ESI potential was set to 2200 V, the nebulizer gas to 15 psi and the drying gas was 10 L/min at 325 ºC. Scan settings were set to a mass range of 300 m/z to 1400 m/z with 150 ms scans. Droplets were introduced to the mass spectrometry via a sheath sprayer (Agilent Technologies, Santa Clara, CA). Teflon tubing containing droplet trains was threaded through the sheath sprayer. The sheath liquid was 80% acetonitrile (ACN), 20% water, and 0.1% formic acid. Sheath flows and droplet flows were in a 10:1 ratio and were driven by Fusion 400 syringe pumps for a total flow rate of 10.1μL/min (Chemyx, Stanford, TX).

Reagent Addition

Prior to reagent addition, devices were wetted with PFD to facilitate tubing insertion. Saltwater electrodes were filled with sodium chloride to disrupt surface tension and promote droplet merging with the reagent stream. Incoming ~ 4 nL droplets were spaced with ~12 nL carrier phase and flowed at 800 nL/min. Reagent stream flow was at 200 nL/min and outcoming droplets were 51%± 4% larger in volume. Outgoing droplets were exported directly off chip in Teflon tubing.

2.3 Results and Discussion

Development of CE Assay for Dose-Response Analysis of Potential Sirtuin Inhibitors

Before improving on existing CE methods for screening SIRT5 enzymatic activity, we wanted to our assay to a commercial CE platform to serve as a comparison for other methods, similar to previous work for protein kinase A.[29] This CE assay is based on a fluorescently labeled substrate peptide. Both the substrate and product are detected and are separated based on a difference in charge (**Figure 2-1A,B**). The positively charged product migrates faster towards the capillary outlet, followed by the net-neutral substrate, both driven by the electroosmotic flow (EOF). Enzymatic activity can be measured by taking the ratio of product to substrate signals. An example electropherogram is shown in **Figure 2-1C**.

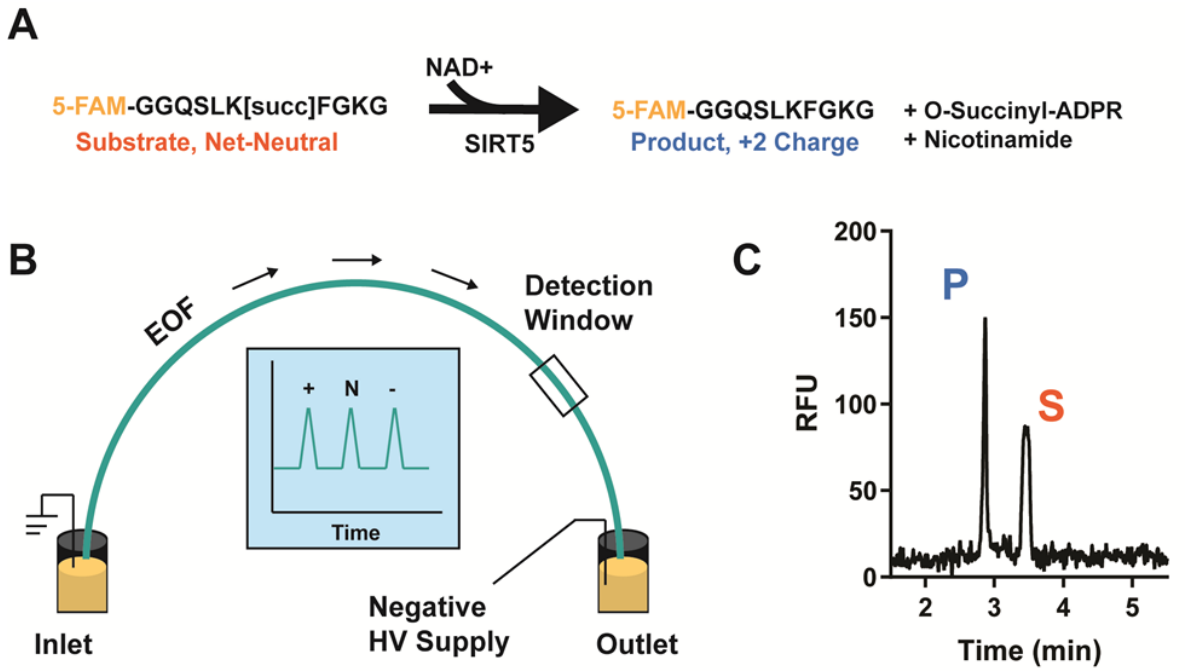

Figure 2-1. Illustration of CE-based SIRT5 peptide assay. Sequence of succinylated and 5-FAM labeled substrate peptide. Removal of the succinyl group, catalyzed by SIRT5 in a NAD+ dependent manner, yields the 5-FAM labeled neutral product peptide (A). A basic CE instrument schematic indicating electrode and detector locations, direction of EOF, and order of analyte migration based on charge (B). Example electropherogram showing both product and substrate analyte peaks (C).

To determine the maximum voltage that could be used with the separation buffer, the voltage was ramped from 0 kV to 22 kV and the corresponding current was plotted in an Ohm's Law Plot. (**Figure 2-2**). Linearity was observed up to 20 kV, indicating that capillary temperatures

were stable below 20 kV. All following CE experiments were performed with an applied voltage of 18 kV to maximize throughput while minimizing the effects of Joule heating.

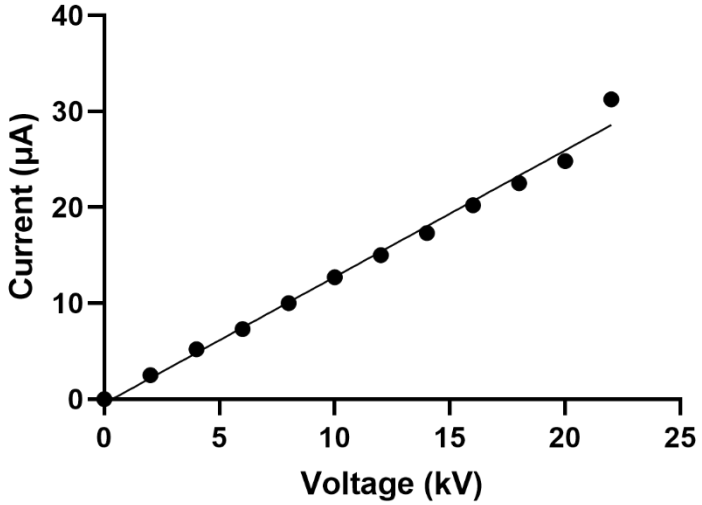

Figure 2-2. Ohm's Law Plot for 10 mM sodium tetraborate, 0.9 mM 2-hydroxypropyl-β-cyclodextrin. Voltages were ramped from 0 kV to 22 kV in increments of 2 kV. A dwell time of 1 min was used for each voltage. The corresponding current was recorded and plotted at each voltage increment (n=3).

In addition to establishing appropriate voltages for the separation, it was necessary to select injection parameters. Hydrodynamic injections were chosen over electrokinetic to reduce injection bias. Injection pressures and durations were varied from 0.1 psi to 0.5 psi in 0.1 psi increments and from 1 s to 10 s in 0.5 s increments respectively. It was found that a 5 s injection at 0.1 psi resulted in the greatest signal to noise ratio, while minimizing peak broadening and avoiding sample overload.

Prior to performing dose-response analyses of potential SIRT5 inhibitors, reaction progress was monitored using 10 nM SIRT5 and 1 μM peptide. These concentrations were chosen based on previously reported Michaelis-Menton kinetics under identical conditions.[18] Reaction progress was tested up to 125 min and was linear up to 20 min (**Figure 2-3**). Additionally quenching with 4.5 volumes of separation buffer completely quenched SIRT5 reactions. For all following experiments, reactions were quenched after 15 min to remain in the linear activity range.[30,31]

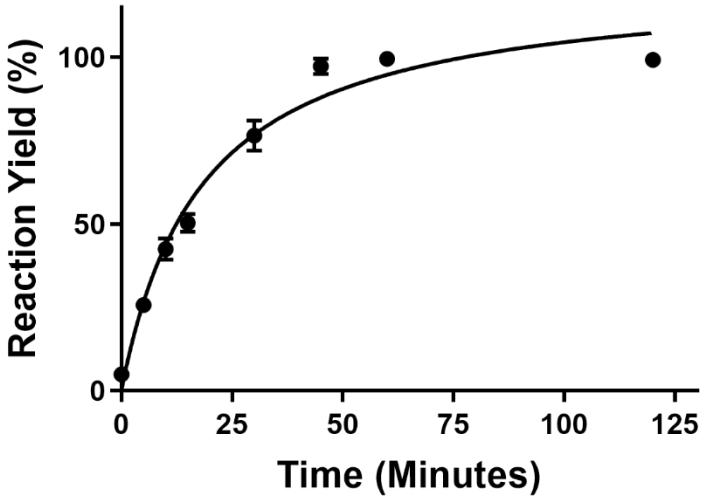

Figure 2-3. Reaction progress for 10 nM SIRT5 and 1 μM substrate. Linearity was demonstrated up to 20 min (n=3).

Selected compounds identified in previous, first-pass screens were evaluated for dose-dependent SIRT5 inhibition to confirm the compounds' activity against SIR5 enzymatic function (unpublished, Neamati Group, University of Michigan). IC_{50} values were calculated from using best fit curves (**Figure 2-4**). To verify the accuracy of this assay, suramin, a previously identified inhibitor, was screened against SIRT5. The IC_{50} value of 8.8 ± 3.2 μM obtained from the dose-response analysis is within error of previously reported literature values that range from 2.6 μM to 22 μM (**Figure 2-4A**).[32] We confirmed eight other compounds as novel SIR5 inhibitors; however, most of these inhibitors were found to lack potency with IC_{50} values in the mid-high micromolar range (**Figure 2-4B-L**). While more research is needed to develop more potent SIRT5 inhibitors, this work demonstrates that our CE-based assay can identify SIRT5 inhibitors with a range of IC_{50} values, and can be adapted to multiple CE platforms, including commercial instrumentation.

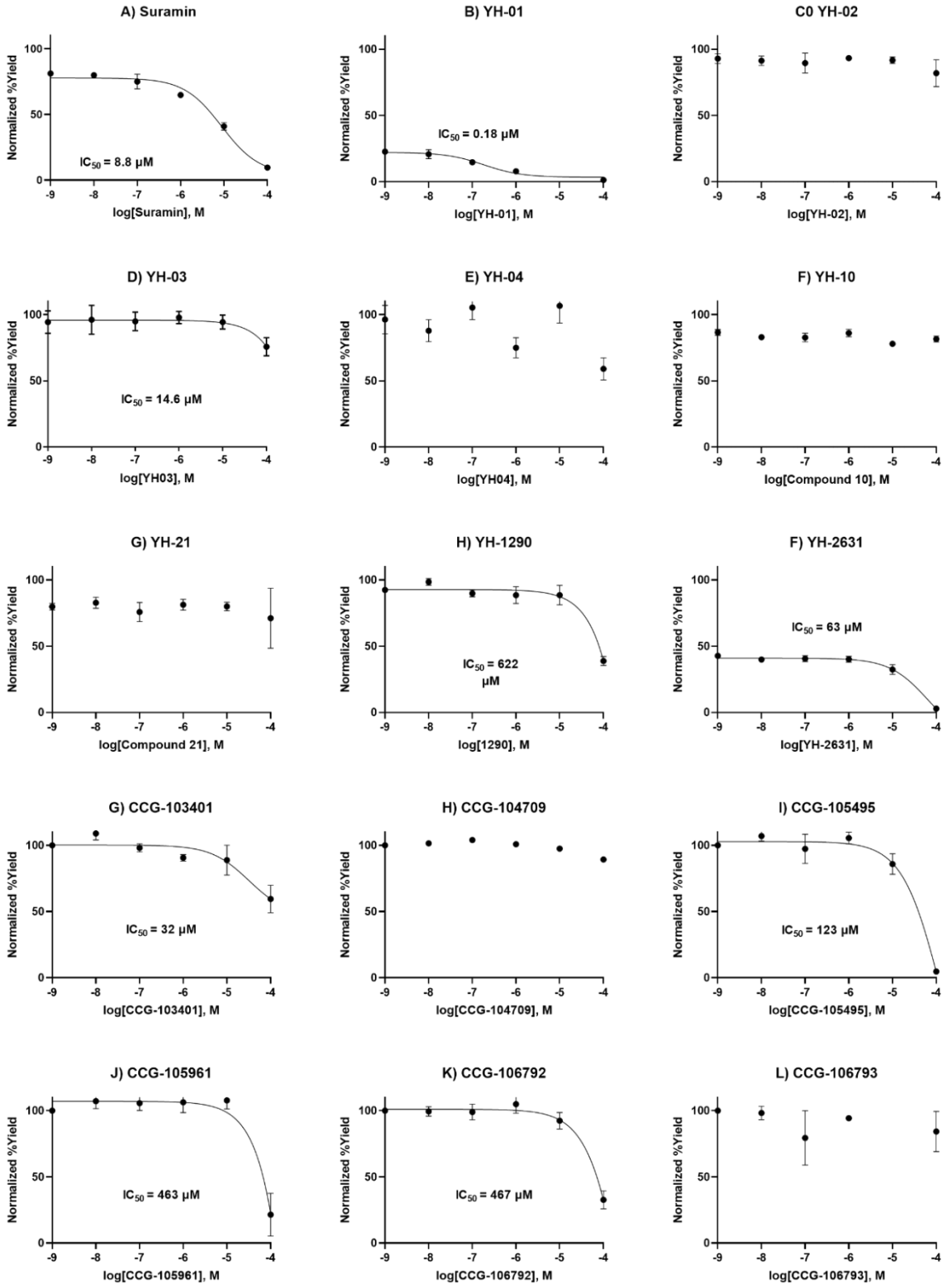

Figure 2-4. Dose-response analysis of potential SIRT5 inhibitors. Percent inhibition was normalized to positive and negative controls. Concentration of inhibitors ranged from 1 nM to 100 µM. IC_{50} values derived from best-fit curves are displayed (n=3).

Improvements in MCE and Density-Based Oil Drain for Injection of Droplet Samples

To further improve the throughput of our SIRT5 assay, we explored the use of MCE to achieve rapid separations of the product and substrate peptides. Higher fields and faster separations can be achieved on chip as compared to commercial CE due to smaller channel diameters (larger surface area to volume ratio) and more efficient heat dissipation. Previous reports demonstrate a separation time of 250 ms at a field of 3000 V/cm and detection at 2 mm on chip.[18] It was found that separation times could be reduced to 150 ms by increasing the field to 3500 V/cm and reducing the detection point to a 1 mm distance, while maintaining good S/N and resolution for both the substrate and product (**Figure 2-5A**). Peak variance and S/N was calculated across a range of injection durations from 10 ms to 50 ms (**Figure 2-5B,C**). Under these conditions, 15 ms injections yielded the minimum peak variance without sacrificing signal intensity. These conditions were used for all further experiments.

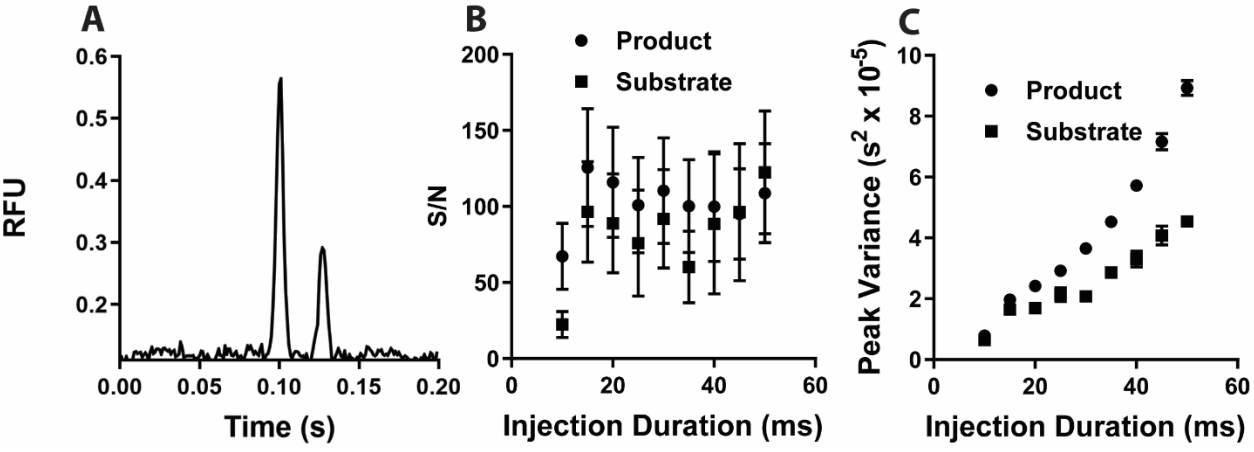

Figure 2-5. On-chip separation of SIRT5 substrate and product peptide. Example trace of a 150 ms separation (A). S/N of substrate and product peaks across injection times ranging from 10 ms to 50 ms (n=50)(B). Variance of substrate and product peaks across injection times ranging from 10 ms to 50 ms (n=50)(C).

Because this chip was developed for HTS purposes, it was important to evaluate electropherogram stability over many injections. Across 750 injections migration time RSD for

both substrate and product remained less than 2%. Additionally, peak areas were stable across all injections and RSD was less than 5%. Traces for all 750 injections are shown in Figure **2-6A**. A zoomed-in view is presented for visualization of separate injections, where substrate and product peaks can be observed (**Figure 2-6B**).

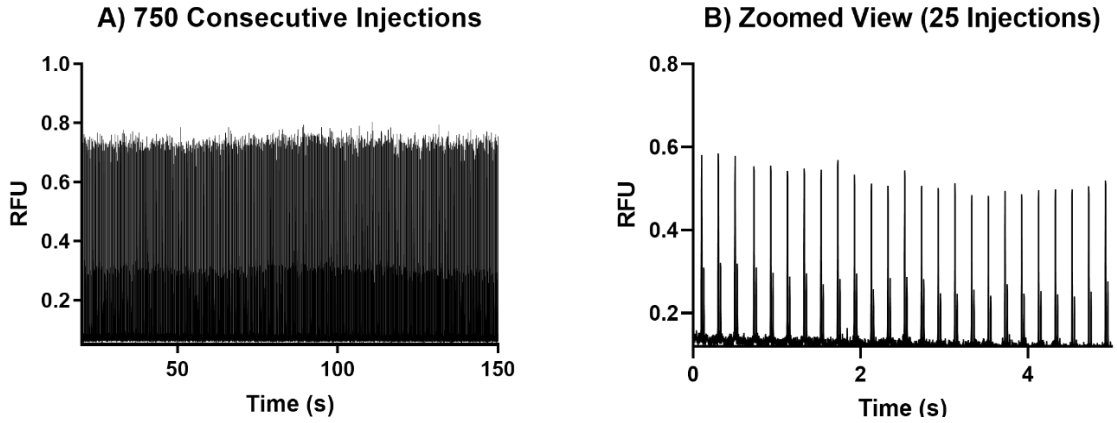

Figure 2-6. Electropherogram stability over many injections. SIRT5 enzymatic reactions were carried out using established protocols for ~60% product yield. Trace of 750 injections containing both substrate and product peptide(A). Zoomed-in view of 25 injections (B).

With such fast separation speeds, the bottleneck in throughput is sample introduction. To achieve rapid, automated sample loading, we coupled MCE to a novel droplet-based introduction method. Droplet microfluidics is an attractive approach for introducing samples on chip due to compatible volumes and ease of fluid manipulation, but there remains a challenge. The inert oil carrier phases typically used in droplet microfluidic experiments will disrupt the EOF and ultimately the analysis if it enters the separation channel. Therefore, the carrier phase must be removed before each sample is loaded onto the MCE device. For these experiments, an oil drain that utilizes the difference in densities between the carrier phase and the background electrolyte was constructed. Droplet samples are introduced on chip via syringe pump into a fused silica capillary and are flowed into a reservoir containing background electrolyte. The less-dense carrier phase floats to the top of the reservoir while the analytes are electrophoresed to the sampling channel. The outlet of the capillary and the inlet of the sampling channel are on the same plane to

reduce analyte diffusion prior to entering the sampling and separation channels. Schematics of the microchip illustrate droplet sample introduction with both side (**Figure 2-7A**).

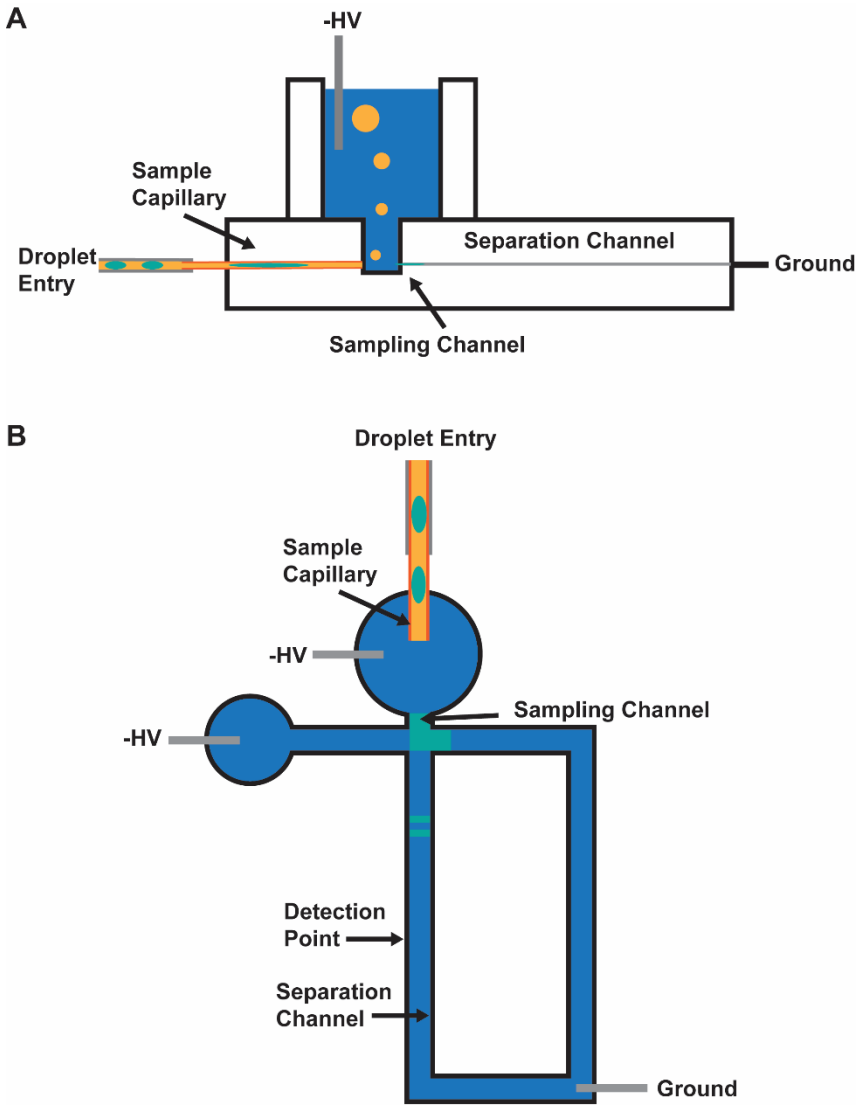

Figure 2-7. Schematic of microchip with density-based oil drain. Droplets (teal) are segmented by the low-density oil carrier phase (yellow). The oil floats to the top of the reservoir filled with denser separation buffer (blue) where the high voltage is applied. Analytes are electrophoresed towards ground. Side (A) and top-down (B) views are illustrated.

Fluorescent imaging of droplets containing FITC was performed to monitor droplet introduction into the sampling channel and (**Figure 2-8A**) and injections from a droplet into the separation channel (**Figure 2-8B**). Negative high voltage is constantly applied at the reservoir, such that droplets enter the sampling channel and are directed towards the grounded waste reservoir. While the microchip was designed to reduce diffusion, some diffusion of the analyte in the oil drain reservoir can be observed in the second panel of **Figure 2-8A.** Once a droplet enters the sampling channel and migrates to the injection cross, gated injections control analyte flow into the electrophoresis channel and towards the detection point. Because of the droplet flow rates and volumes and speed of the separation, multiple discrete injections can be made per droplet sample. This allows for signal averaging across multiple electropherograms per sample.

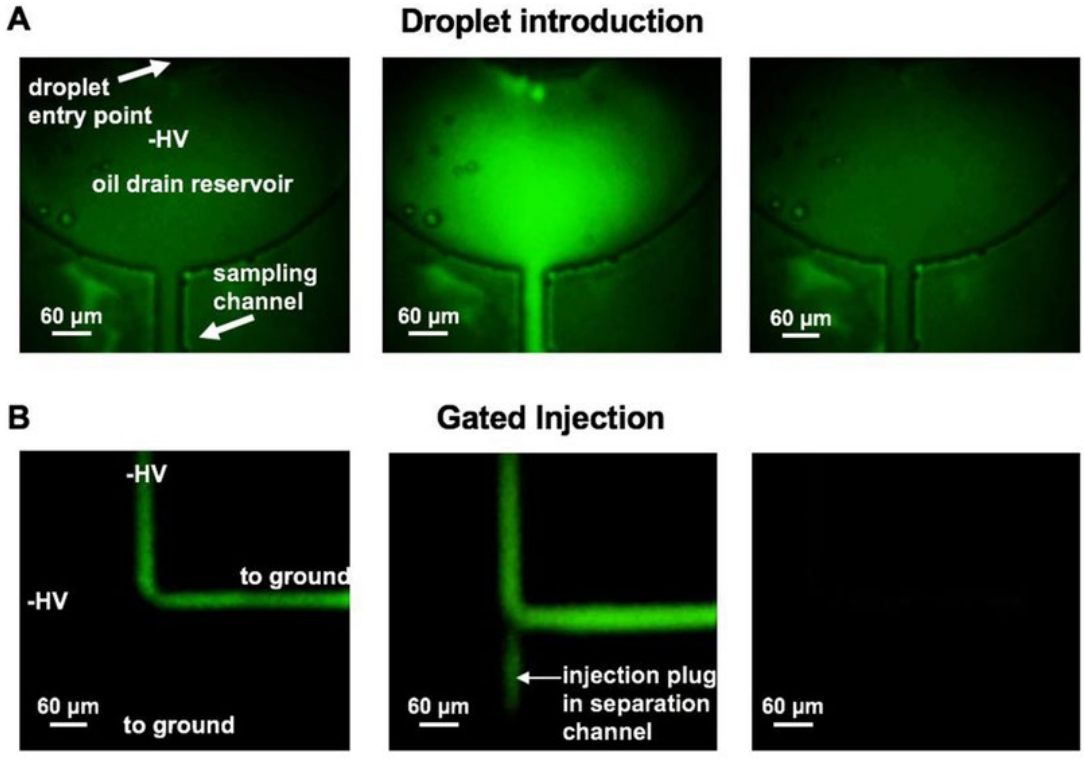

Figure 2-8. Fluorescence imaging of droplet introduction and injection. Pre-droplet introduction onto chip, followed by droplet arrival through the transfer capillary, and clearing as it is electrophoresed into the sampling channel (A). Droplet entering the sample channel and gated towards the grounded waste. A discrete plug is then injected into the separation channel and the droplet is finally washed out (B).

To determine if this density-based oil drain was compatible with SIRT5 assay conditions as described above, over 160 droplet samples were analyzed with a total of 1,250 separations without the need to recondition the microchip (**Figure 2-9A**). Droplets contained alternating sample content: those containing no enzyme and those containing 45 nM enzyme. Reaction yields using peak area could be calculated for each injection and average reaction yield for all enzyme containing droplets was 49 ± 5 % (**Figure 2-9B**).

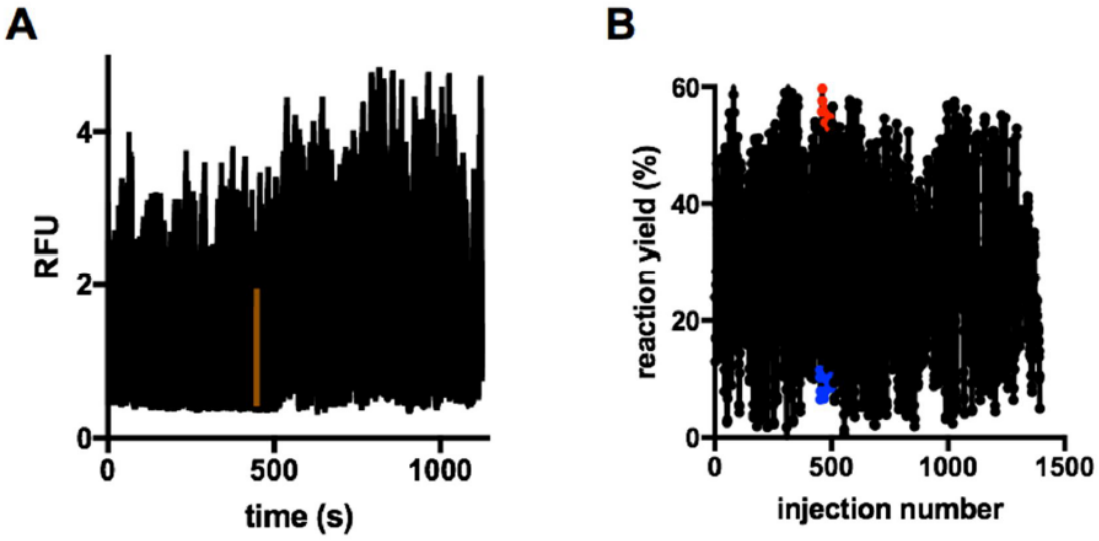

Figure 2-9. Continuous injection of 160 samples containing 1 µM substrate with every other droplet containing 45 nM SIRT5 or no SIRT5. Raw traces for concatenated electropherograms of 1,250 total injections (A). Calculated reaction yield from each electropherogram. Red indicates data from samples with 45 nM SIRT5 and blue indicates samples with no SIRT5 (B). Colored data points correspond to same colored data points in Figure 2-10.

For samples containing no SIRT5 only substrate peak is observed, while both substrate and product peeks are seen in the samples containing 45 nM SIRT5 with a resolution of 1.8. (**Figure 2-10A**). As described above multiple, injections are made per each sample droplet and percent yield is calculated from averaging substrate to product ratios across multiple injections (**Figure 2-10B**). Some data points correspond to intermediate yield values before substrate and product signals stabilized. This is likely due to the discontinuous droplet injection and mixing between

droplets at the sample capillary or sampling channel. Carryover issues could potentially be addressed through larger spacing between droplets or the incorporation of wash droplets.

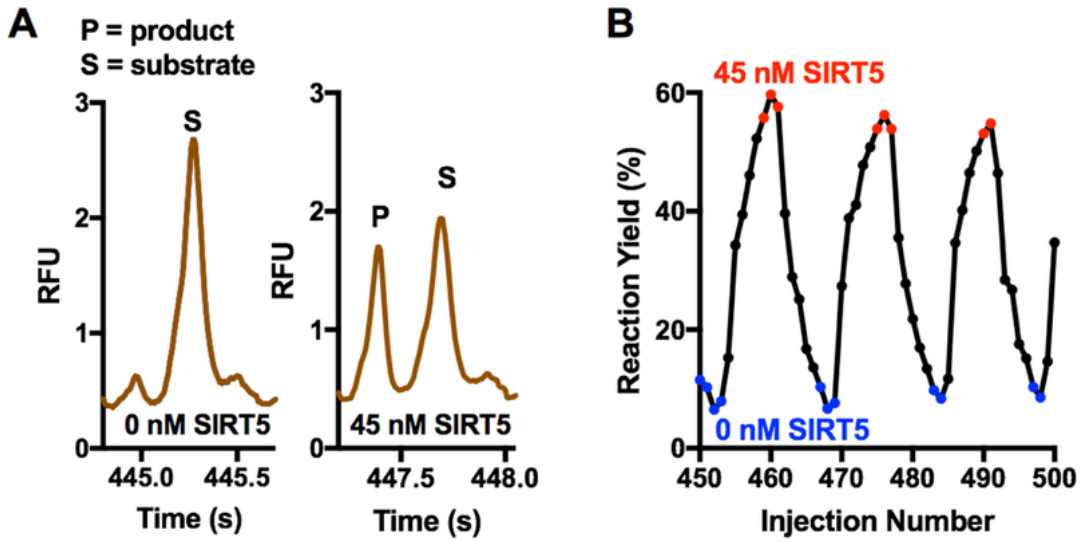

Figure 2-10. Performance of density-based oil drain for analysis of SIRT5 reaction samples by free-solution microchip capillary electrophoresis. Examples of raw traces from individual injections from samples with 0 nM SIRT5 and 45 nM SIRT5 (A). Selection of a series of yields from electropherograms highlighted in figure 2-9. Electropherograms from samples with 0 nM SIRT5, 45 nM SIRT5, and transitions between droplets are shown in blue, red, and black respectively.

Previous reports of SIRT5 screening by droplet-MCE achieved a throughput of 2 s/sample with the use of a hybrid PDMS-glass device, as compared to the 10 s/sample reported here.[33] Although there was a lower throughput and resolution, fabrication of the density-based device requires fewer steps and fewer connections, making setup and operation more accessible. Furthermore, the versatility of this device has been demonstrated with other applications such as capillary gel electrophoresis and the screening of protein-protein interactions. There is also the potential for coupling other microfluidic functions to this device, such as reagent addition, to further improve sample preparation and throughput. There are some limitations with this system regarding screening applications, considering that small molecules will freely diffuse through the low-density mineral oil that is used. As a result, reactions must be fully quenched prior to droplet formation and analysis, and only peptides or other larger molecules may be analyzed. Overall,

this design is a promising approach to monitoring enzymatic activity assays by MCE and droplet sample introduction.

2.4 Conclusions

In this work we improve on and build CE, MCE, and MS assays for the evaluation of SIRT5 enzymatic activity. A previously developed assay, based on a fluorescently labeled substrate peptide, was adapted to a commercial system by adjusting injection parameters and field strengths. Eight compounds were identified as novel SIRT5 inhibitors through dose-response analysis, and lead compounds will be explored further as potential therapeutic agents in treating metastatic melanomas. Additionally, we were able to increase the throughput of our MCE separations to 150 ms as compared to the 250 ms separation times previously reported. This fast, on-chip separation was coupled to a droplet sample introduction via a density-based oil drain. This device was used to screen over 160 samples with a throughput of 10 s/sample, using only 4 nL droplet volumes. Finally, we worked toward developing a droplet-MS assay with reagent addition to screen SIRT5 enzymatic activity in a label-free manner and further reduce enzyme consumption. We identified an MS compatible reaction buffer that preserved SIRT5 activity and monitored substrate peptide over 120 samples with successful reagent addition. Future work is focused on employing this microfluidic platform for screening a compound library against SIRT5 to identify novel inhibitors.

2.5 References

(1) Sauve, A. A.; Wolberger, C.; Schramm, V. L.; Boeke, J. D. The Biochemistry of Sirtuins. **2006**. https://doi.org/10.1146/annurev.biochem.74.082803.133500.

(2) Schiedel, M.; Robaa, D.; Rumpf, T.; Sippl, W.; Jung, M. The Current State of NAD +-Dependent Histone Deacetylases (Sirtuins) as Novel Therapeutic Targets. *C 2017 Wiley Period. Inc. Med. Res. Rev 38* (1). https://doi.org/10.1002/med.21436.

(3) Du, J.; Zhou, Y.; Su, X.; Yu, J. J.; Khan, S.; Jiang, H.; Kim, J.; Woo, J.; Kim, J. H.; Choi,

B. H.; He, B.; Chen, W.; Zhang, S.; Cerione, R. A.; Auwerx, J.; Hao, Q.; Lin, H. Sirt5 Is a NAD-Dependent Protein Lysine Demalonylase and Desuccinylase. *Science (80-.).* **2011**, *334* (6057), 806–809. https://doi.org/10.1126/SCIENCE.1207861.

(4) Peng, C.; Lu, Z.; Xie, Z.; Cheng, Z.; Chen, Y.; Tan, M.; Luo, H.; Zhang, Y.; He, W.; Yang, K.; Zwaans, B. M. M.; Tishkoff, D.; Ho, L.; Lombard, D.; He, T.-C.; Dai, J.; Verdin, E.; Ye, Y.; Zhao, Y. The First Identification of Lysine Malonylation Substrates and Its Regulatory Enzyme* □ S. *Mol. Cell. Proteomics* **2011**, *10*, M111.012658. https://doi.org/10.1074/mcp.M111.012658.

(5) Identification of 67 Histone Marks and Histone Lysine Crotonylation as a New Type of Histone Modification | Elsevier Enhanced Reader https://reader.elsevier.com/reader/sd/pii/S0092867411008919?token=CBE1013C238030888A34A199416D0816DCA2A79BB68B82C7D6C090880B369E9315685B4B0B9AEA2FDB17E6F3FE790F57&originRegion=us-east-1&originCreation=20220208135148 (accessed Feb 8, 2022).

(6) Herskovits, A. Z.; Guarente, L. Sirtuin Deacetylases in Neurodegenerative Diseases of Aging 746 Sirtuin Deacetylases in Neurodegenerative Diseases of Aging. *Rev. npg Cell Res.* **2013**, *23* (6), 746–758. https://doi.org/10.1038/cr.2013.70.

(7) Longo, V. D.; Kennedy, B. K. Sirtuins in Aging and Age-Related Disease. *Cell* **2006**, *126* (2), 257–268. https://doi.org/10.1016/J.CELL.2006.07.002.

(8) Li, Y.; Liu, T.; Liao, S.; Li, Y.; Lan, Y.; Wang, A.; Wang, Y.; He, B. A Mini-Review on Sirtuin Activity Assays. *Biochem. Biophys. Res. Commun.* **2015**, *467* (3), 459–466. https://doi.org/10.1016/J.BBRC.2015.09.172.

(9) Wegener, D.; Wirsching, F.; Riester, D.; Schwienhorst, A. A Fluorogenic Histone Deacetylase Assay Well Suited for High-Throughput Activity Screening. *Chem. Biol.* **2003**, *10* (1), 61–68. https://doi.org/10.1016/S1074-5521(02)00305-8.

(10) Milne, J. C.; Lambert, P. D.; Schenk, S.; Carney, D. P.; Smith, J. J.; Gagne, D. J.; Jin, L.; Boss, O.; Perni, R. B.; Vu, C. B.; Bemis, J. E.; Xie, R.; Disch, J. S.; Ng, P. Y.; Nunes, J. J.; Lynch, A. V; Yang, H.; Galonek, H.; Israelian, K.; Choy, W.; Iffland, A.; Lavu, S.; Medvedik, O.; Sinclair, D. A.; Olefsky, J. M.; Jirousek, M. R.; Elliott, P. J.; Westphal, C. H. Small Molecule Activators of SIRT1 as Therapeutics for the Treatment of Type 2 Diabetes. https://doi.org/10.1038/nature06261.

(11) Marcotte, P. A.; Richardson, P. R.; Guo, J.; Barrett, L. W.; Xu, N.; Gunasekera, A.; Glaser, K. B. Fluorescence Assay of SIRT Protein Deacetylases Using an Acetylated Peptide Substrate and a Secondary Trypsin Reaction. *Anal. Biochem.* **2004**, *332* (1), 90–99. https://doi.org/10.1016/J.AB.2004.05.039.

(12) Borra, M. T.; Smith, B. C.; Denu, J. M. Mechanism of Human SIRT1 Activation by Resveratrol. *J. Biol. Chem.* **2005**, *280* (17), 17187–17195. https://doi.org/10.1074/JBC.M501250200.

(13) Pacholec, M.; Bleasdale, J. E.; Chrunyk, B.; Cunningham, D.; Flynn, D.; Garofalo, R. S.; Griffith, D.; Griffor, M.; Loulakis, P.; Pabst, B.; Qiu, X.; Stockman, B.; Thanabal, V.;

Varghese, A.; Ward, J.; Withka, J.; Ahn, K. SRT1720, SRT2183, SRT1460, and Resveratrol Are Not Direct Activators of SIRT1. *J. Biol. Chem.* **2010**, *285* (11), 8340–8351. https://doi.org/10.1074/JBC.M109.088682.

(14) Smith, J. S.; Brachmann, C. B.; Celic, I.; Kenna, M. A.; Muhammad, S.; Starai, V. J.; Avalos, J. L.; Escalante-Semerena, J. C.; Grubmeyer, C.; Wolberger, C.; Boeke, J. D. A Phylogenetically Conserved NAD+-Dependent Protein Deacetylase Activity in the Sir2 Protein Family. *Proc. Natl. Acad. Sci. U. S. A.* **2000**, *97* (12), 6658–6663. https://doi.org/10.1073/pnas.97.12.6658.

(15) Huang, J.; Hilz, J.; Moazed, H.; Frye, D.; Landry, R. A.; Sutton, J.; Tafrov, A.; Heller, S. T.; Stebbins, R. C.; Pillus, J.; Sternglanz, L.; Smith, R.; Brach-Mann, J. S.; Celic, C. B.; Kenna, I.; Muhammad, M. A.; Starai, S.; Avalos, V. J.; Escalante-Semerena, J. L.; Grubmeyer, J. C.; Wolberger, C.; Boeke, C.; Imai, J. D.; Armstrong, S.; Kaeberlein, C. M.; Guarente, M. Silent Information Regulator 2 Family of NAD-Dependent Histoneprotein Deacetylases Generates a Unique Product, 1-O-Acetyl-ADP-Ribose. *Biochem. Biophys. Res. Commun* **1999**, *99*, 795.

(16) Cai, L.-F.; Zhu, Y.; Du, G.-S.; Fang, Q. Droplet-Based Microfluidic Flow Injection System with Large-Scale Concentration Gradient by a Single Nanoliter-Scale Injection for Enzyme Inhibition Assay. **2011**. https://doi.org/10.1021/ac2029198.

(17) Liu, W. wen; Zhu, Y. "Development and Application of Analytical Detection Techniques for Droplet-Based Microfluidics"-A Review. *Anal. Chim. Acta* **2020**, *1113*, 66–84. https://doi.org/10.1016/J.ACA.2020.03.011.

(18) Guetschow, E. D.; Kumar, S.; Lombard, D. B.; Kennedy, R. T. Identification of Sirtuin 5 Inhibitors by Ultrafast Microchip Electrophoresis Using Nanoliter Volume Samples. https://doi.org/10.1007/s00216-015-9206-0.

(19) An Integrated On-Chip Sirtuin Assay. https://doi.org/10.1002/elps.201000220.

(20) Development of a Capillary Electrophoresis-Based Assay of Sirtuin Enzymes. https://doi.org/10.1002/elps.200800361.

(21) Sun, S.; Buer, B. C.; Neil, E.; Marsh, G.; Kennedy, R. T. A Label-Free Sirtuin 1 Assay Based on Droplet-Electrospray Ionization Mass Spectrometry. **2016**. https://doi.org/10.1039/c6ay00698a.

(22) Kumar, S.; Lombard, D. B. Generation and Purification of Catalytically Active Recombinant Sirtuin5 (SIRT5) Protein. In *Histone Deacetylases: Methods and Protocols*; Sarkar, S., Ed.; Springer New York: New York, NY, 2016; pp 241–257. https://doi.org/10.1007/978-1-4939-3667-0_16.

(23) Shackman, J. G.; Watson, C. J.; Kennedy, R. T. High-Throughput Automated Post-Processing of Separation Data. *J. Chromatogr. A* **2004**, *1040* (2), 273–282. https://doi.org/10.1016/J.CHROMA.2004.04.004.

(24) Harrison, D. J.; Fluri, K.; Seiler, K.; Fan, Z.; Effenhauser, C. S.; Manz, A. Micromachining a Miniaturized Capillary Electrophoresis-Based Chemical Analysis System on a Chip. *Science (80-.).* **1993**, *261* (5123), 895–897. https://doi.org/10.1126/science.261.5123.895.

(25) Roper, M. G.; Shackman, J. G.; Dahlgren, G. M.; Kennedy, R. T. Microfluidic Chip for Continuous Monitoring of Hormone Secretion from Live Cells Using an Electrophoresis-Based Immunoassay. *Anal. Chem.* **2003**, *75* (18), 4711–4717. https://doi.org/10.1021/ac0346813.

(26) Simpson, P. C.; Roach, D.; Woolley, A. T.; Thorsen, T.; Johnston, R.; Sensabaugh, G. F.; Mathies, R. A. *High-Throughput Genetic Analysis Using Microfabricated 96-Sample Capillary Array Electrophoresis Microplates*; 1998; Vol. 95.

(27) Guetschow, E. D.; Steyer, D. J.; Kennedy, R. T. Subsecond Electrophoretic Separations from Droplet Samples for Screening of Enzyme Modulators. **2014**. https://doi.org/10.1021/ac502758h.

(28) Chabert, M.; Dorfman, K. D.; De Cremoux, P.; Roeraade, J.; Viovy, J.-L. Automated Microdroplet Platform for Sample Manipulation and Polymerase Chain Reaction. **2006**. https://doi.org/10.1021/ac061205e.

(29) Inglese, J.; Johnson, R. L.; Simeonov, A.; Xia, M.; Zheng, W.; Austin, C. P.; Auld, D. S. High-Throughput Screening Assays for the Identification of Chemical Probes. https://doi.org/10.1038/nchembio.2007.17.

(30) Von Ahsen, O.; Bçmer, U. High-Throughput Screening for Kinase Inhibitors. https://doi.org/10.1002/cbic.200400211.

(31) Schuetz, A.; Min, J.; Antoshenko, T.; Wang, C. L.; Allali-Hassani, A.; Dong, A.; Loppnau, P.; Vedadi, M.; Bochkarev, A.; Sternglanz, R.; Plotnikov, A. N. Structural Basis of Inhibition of the Human NAD+-Dependent Deacetylase SIRT5 by Suramin. *Structure* **2007**, *15* (3), 377–389. https://doi.org/10.1016/J.STR.2007.02.002.

Chapter 3: Ion Mobility-Mass Spectrometry Coupled to Droplet Microfluidics for Rapid Protein Structure Analysis and Drug Discovery

3.1 Introduction

Structural biology is critical for modern drug discovery, revealing key details that can lead to compounds of high clinical efficacy; however, target structure assessments are often left to the later stages of drug discovery and development. This time lag is often due to limitations associated with high-resolution structural biology techniques with respect to sample purity and throughput[1–4]. In addition, such approaches are not always amenable to protein targets that are difficult to express or challenging to capture in a functional, ligand-bound state. Calorimetric assays, such as differential scanning calorimetry (DSC) and isothermal titration calorimetry (ITC), can detect global changes in protein structure in a more robust and higher-throughput manner than their atomic-resolution counterparts[5–7]. Despite this, calorimetric technologies reveal little to no information regarding ligand binding location or binding stoichiometry and lack the throughput necessary for deployment in many drug discovery applications.

Over the last few decades, mass spectrometry (MS) has emerged as a promising approach for the characterization of interactions between proteins and drug-like small molecules[8]. MS technologies can evaluate low volume samples, are compatible with a relatively wide range of solution conditions, provide universal detection of ligand biding events, and provide the ability to make measurements within complex mixtures[9]. In particular, native MS has become an important addition to the biophysical characterization toolbox. Under native MS conditions, non-covalent

interactions within and between biomolecules can be preserved for direct interrogation by MS, thus providing ligand binding stoichiometry and dissociation constant (K_D) information [10–12].

MS and native MS can be coupled to ion mobility (IM-MS) to provide greater insight into the impact of ligand binding on protein structure and dynamics, further aiding drug discovery and development. IM-MS separates proteins and protein-ligand complexes based on their shape and charge, and can be used to differentiate conformational dynamics upon ligand binding while preserving information about stoichiometry and binding kinetics[13]. For a deeper understanding of protein stability and the conformational changes induced by ligand binding, collision induced unfolding (CIU) can be employed[14]. In such experiments proteins or protein-ligand complexes are accelerated through a neutral gas prior to IM separation, causing the protein to undergo partial unfolding. The magnitude of the activation experienced by gas-phase proteins can be gradually increased and plotted against the changes in IM drift time observed in what is called a CIU fingerprint and can be used to assess changes in protein-stability upon ligand binding, as well as identify conformational intermediates and transition regions[14]. CIU fingerprinting has been applied to several protein-ligand systems of pharmaceutical interest including: protein kinases, membrane proteins, and metalloproteases[15–17]. The dynamic information gained from CIU often compliments high-resolution approaches such as X-ray crystallography.

Because IM-MS and CIU occur in the gas phase, structural interrogation based on these techniques is typically much faster than other biophysical approaches typically deployed within drug discovery and development workflows. Acquisition of a single CIU fingerprint typically requires ~5 min; however recent advances in software development and post-acquisition analysis have reduced this data collection time to less than 30 seconds[18]. The main bottleneck in implementing CIU in a high-throughput screening manner lies in manner in which samples are

introduced to MS. Despite technical challenges, there has been a push to develop high-throughput sample introduction platforms for MS. Commercial systems such as the Agilent Rapidfire or Advion Nanomate can achieve automated sample introduction at rates of 0.14 Hz and 0.02 Hz respectively.[19] Although these systems can achieve fast and automated sample introduction, they both have high consumables costs and require microliter amounts of sample.[19] There has also been recent advances in acoustic mist ionization (AMI-MS) technologies, where ultrasonic pulses inject a mist of sample droplets into the MS from a well plate.[20] For these technologies, sample introduction rates of up to 0.33 Hz have been achieved using picoliter amounts of sample[20]. This technology, however, is not widely available and its compatibility with nMS and IM-MS is currently unknown.

Microfluidics, particularly droplet-microfluidics where sample plugs are separated by an immiscible carrier phase, coupled to mass spectrometry is an attractive approach for high throughput screening[21]. These sample plugs can range from femtoliter to nanoliter in volume, where each droplet can be manipulated and treated like an individual microreactor. Droplet-MS provides a robust way to introduce hundreds or even thousands of picoliter to nanoliter samples into MS in a semi-automated fashion[22,23]. While this type of screening platform has been primarily used for small molecule analysis, prior work has shown that droplet-MS can be used for intact protein analysis and that such technologies can be coupled directly to IM-MS [24,25].

Here we develop a microfluidic platform coupled to rapid CIU data acquisition to explore the potential of CIU fingerprinting for high-throughput biophysical analysis of protein-ligand interactions for the first time. We also examine the impact that the droplet microenvironment has on global protein structure and demonstrate the first example of non-covalent complexes preserved during the droplet-nESI process. Finally, we apply our droplet-CIU method to screen a library of

96 small molecules against the silent mating type information regulation 2 homolog 5(Sirtuin 5, or SIRT5), a protein-target of pharmaceutical interest. Our CIU data identifies many novel binders and quantifies their impact on overall SIRT5 stability. The low sample consumption and relatively high throughput of our approach suggests its potential for use in future drug discovery efforts where protein stability shift information needs to be accessed early on in order to evaluate the potential efficacies of candidate compounds.

3.2 Methods

Chemicals and Materials

All reagents were purchased from Sigma-Aldrich (St. Louis, MO) unless otherwise noted. SIRT5 was expressed and purified in house as previously described[26]. Test compounds were synthesized by the Neamati Group (University of Michigan, Ann Arbor, MI). Prior to all native MS experiments, protein samples were buffer exchanged into 100 mM Ammonium Acetate, pH 7.0 using Micro Biospin 30 columns (Bio-Rad, Hercules, CA) and diluted to a 10 uM working concentration.

Droplet Generation

Droplets were generated from 384-microwell plates as previously described[27], with modifications. Samples were drawn into 150 µm i.d. x 360 µm o.d. PFA tubing (IDEX Health and Science, Oak Harbor, WA) using a fusion 400 syringe pump (Chemyx, Strafford, TX) operated in withdrawal mode. The tubing was directed by an xyz-micropositioner, alternating between microwells containing sample and the perfluorodecalin (PFD) carrier phase. 2% (v/v) 008-flurosurfactant (RAN Biotechnologies, Beverly, MA) was added to the carrier phase to stabilize sample droplets during generation and infusion. Droplets were generated at a rate of 200 nL/min to prevent air from entering the PFA tubing when moving between adjacent microwells.

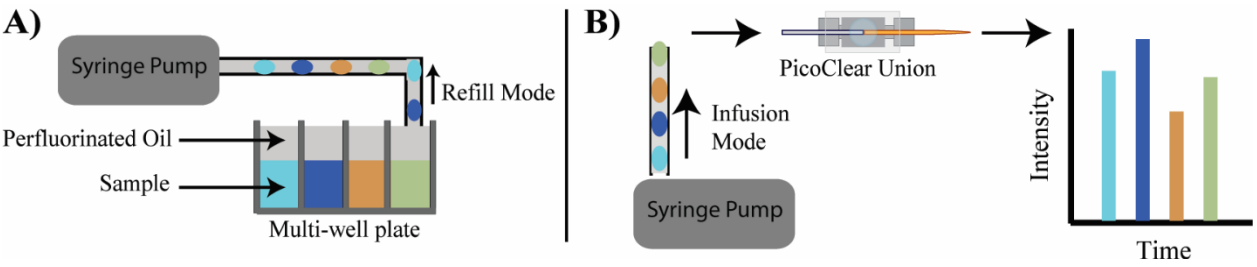

Figure 3-1. Illustration of droplet generation and introduction into the MS. Droplets are formed in a capillary tube using a syringe pump in refill mode, with a perfluorinated carrier phase separating aqueous sample plugs. The resulting sample array is pumped into a nESI emitter through a zero dead volume union. Discrete signals can be observed for each droplet in the total ion chromatogram (TIC).

Ion Mobility – Mass Spectrometry

All native MS experiments were performed on a Synapt G2 quadrupole–ion mobility–time-of-flight mass spectrometer (Q–IM–ToF MS) instrument (Waters Corp., Milford, MA). For direct infusion experiments, samples were loaded into home pulled, gold-coated borosilicate needles. For droplet experiments, samples were transferred to 100 um 1D x 360 od fused-silica needles pulled to a 30 um diameter (New Objective, Woburn, MA) using a zero dead volume Picoclear union (New Objective, Woburn, MA). Prior to droplet transfer, fused silica needles were derivatized with 2% trichloro(1H,1H,2H,2H-perfluorooctyl) silane dissolved in PFD using previously described methods[27] to prevent adhesion of aqueous samples. The instrument was tuned to optimize the ion transmission of the most intense intact SIRT5 ions. The electrospray capillary was held at a voltage of 1.2 kV with the sampling cone set to 30 V. The backing pressure was set to 5 mbar for SIRT5 and myoglobin samples and 7 mbar for IgG samples. IMS wave height and wave velocity were 40 V and 300 m/s, respectively. The pressure in the trap collision cell was set to 2.9×10^{-2} mbar with argon gas, the helium cell set to 1.4×10^{3} mbar, the traveling-wave IM separator set to 2.5 mbar, and the ToF MS set to 1.5×10^{-6} mbar. The transfer cell was held to 30 V accelerating potential to reduce noise from surfactant clusters while maintaining

protein-ligand interactions during droplet-based experiments. A cartoon representation of droplet generation, transfer, and MS readout is shown in **Figure 3-1**.

Droplet CIU Data Acquisition and Analysis

SIRT5 was pre-incubated with test compounds in a 1:1 molar ratio for 15 minutes, prior to droplet generation. Sample droplets were perfused into the MS at 400 nL/min. CIU experiments were performed by ramping the trap cell collision voltage from 10 V to 90 V in 5V increments with a 2 s dwell time at each collision voltage. Instrument control methods for all CIU acquisitions were generated automatically using a Python program, available at https://github.com/RuotoloLab/MethodEditor. The program reads a user-generated template file that describes the desired acquisition settings (m/z ranges, CIU voltage ramp, time per CIU voltage, and general instrument tuning and calibration settings) and produces the corresponding MassLynx method files (.exp) and a sample list that can be imported into the MassLynx control software. The imported acquisition can then be run automatically in MassLynx, requiring only a start command from the user. For droplet CIU experiments, a time delay was added between the start of the method and data acquisition to allow sufficient time for the droplets to be started and synchronized with the start of data acquisition by the automated method. TWIMExtract[28] was used to extract raw drift time data for charge states of interest. This text-formatted data was then imported and analyzed in CIUSuite2[18]. Data processing included the use of on-board Gaussian Denoising, a 2x interpolation factor of the collision voltage axis, and two rounds of 2D Savitsky-Golay smoothing with a five-bin window. Median fingerprint feature values and feature transitions, or CIU50's, were fit post-processing. Features were defined with a minimum length of 2 collision voltage values and a maximum feature width of 1 ms.

3.3 Results and Discussion

Reducing CIU Fingerprint Acquisition Time:

Previous CIU data have been collected on timescales ranging from 5 to 40 min, limiting the ability to collect full fingerprint datasets for screening. New CIUSuite2 software, utilizing on-board smoothing and interpolation algorithms tailored for the CIU experiment, have made it possible to reduce fingerprint collection to the sub-minute timescale. The capabilities of fast CIU were investigated using myoglobin, a well-studied protein system by IM-MS and lower-throughput CIU[29–31]. Dwell times per collision voltage (CV) were reduced from 30 s/CV to 2 s/CV. Averaged fingerprints, after employing smoothing and interpolation, revealed the same features (**Figure 3-2A,C**) and transitions (**Figure 3-2B,D**) within error while requiring 15X less analysis time. Additionally, features and transitions were fit with a small margin of error for fast CIU experiments, once smoothing algorithms were applied (**Figure 3-2E,F**) Dwell times per CV could not be reduced below 2 s/CV due to limitations with instrument electronics.

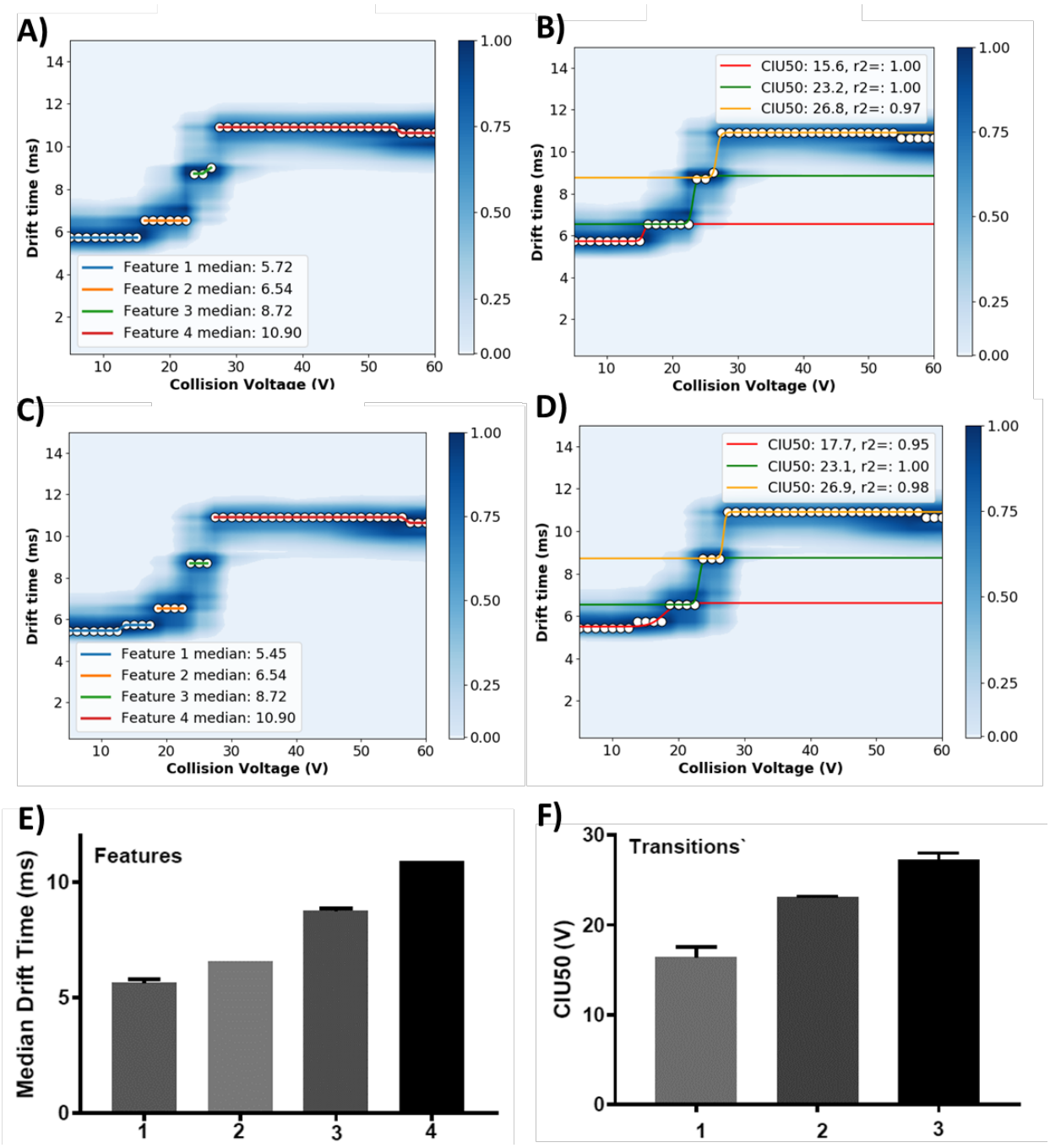

Figure 3-2. Increasing throughput of CIU fingerprints. CIU fingerprints of myoglobin collected with an acquisition rate of 30 s per collision voltage, fitted with features (A) and CIU50 transitions (B) n = 3. Fingerprints of albumin collected with an acquisition rate of 2s per collision voltage, fitted with features (A) and CIU50 transitions (B) n = 3. Fitting of both features (E) and transitions (F) for fast CIU data acquisition, with less than 3% and less than 6% error respectively. Both fell within error of features and CIU50 values obtained from CIU experiments with traditional acquisition rates.

Stable Generation and Transfer of Sample Droplets:

To match our new abilities to rapidly collect and interpret CIU data, we developed an automated sample introduction system for IM-MS. Droplet microfluidics was chosen as our sample introduction method for IM-MS because it provides low volumes match the requirements of nESI, and numerous tools have been developed to rapidly manipulate droplets.[21,22] Droplet encapsulated samples containing micromolar concentrations of native-like proteins presented unique challenges when designing our microfluidic sample delivery devices for downstream IM-MS and CIU assays. In early device prototypes, droplets were prone to shearing during flow (**Figure 3-3A**) and protein aggregation (**Figure 3-3B**), likely due to interactions with the protein analytes at the droplet surface. These aggregation events occurred both in the absence of a carrier phase surfactant and in the presence of three commonly used classes of fluorosurfactants: perfluorooctanol, Novec 7500, and FC-70, which have commonly been used to stabilize droplet[32]. To address these issues, nESI emitters were derivatized with 1H, 1H, 2H, 2H-Perfluorooctyltriethoxysilane to reduce surface interaction with the protein analytes. Additionally, 008-Fluorosurfactant (Ran-Biotechnologies), a surfactant used to stabilize droplets in microfluidic systems that undergo thermocycling, was used in the carrier phase. While the salinization of the

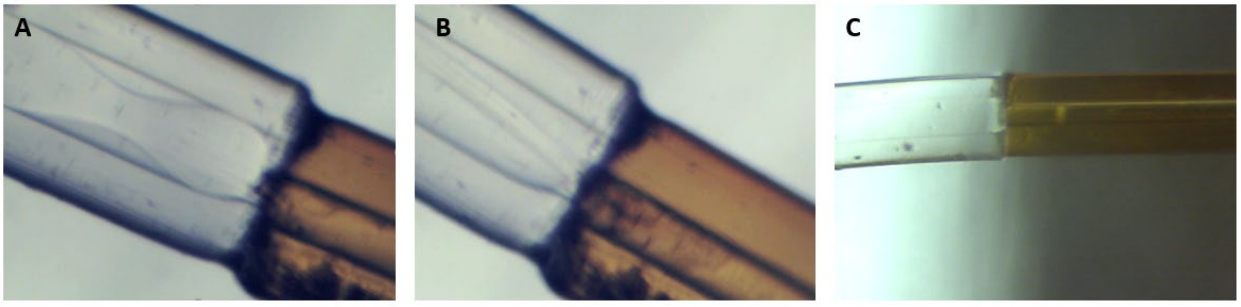

Figure 3-3. Droplet transfer to nESI fused silica emitter. 40 nL droplets containing 10 uM myoglobin in 100 mM ammonium acetate, pH 6.74 were generated in 150/360 ID/OD tubing and transferred to a 100 um ID nESI emitter. The carrier phase was PFD in all experiments. A representative image of droplet shearing in the absence of surfactant (A). A representative image of protein aggregation in-droplet, in the presence of Novec 7500 (B). Example of successful droplet transfer in the presence of 2% w/v 008 fluorosurfactant in the PFD carrier phase to a derivatized nESI emitter (C).

emitter helped prevent droplet shearing prior to infusion, it was found that the addition of the 008-fluorosurfactant was crucial for stable droplet formation. (**Figure 3-3C**).

Although droplets could be stably generated and transferred to IM-MS for analysis, there was a significant amount of carryover between sample droplets under these conditions. Myoglobin signal intensity increased 40-fold across 100 samples, indicating protein transfer between droplets during perfusion (**Figure 3-4A**). It was found that alternating protein-containing sample droplets with blank droplets (80% water, 20% methanol, 0.5% formic acid) was sufficient to reduce the averaged peak area variation in sample droplets to less than 5% (**Figure3-4B**). Denatured protein

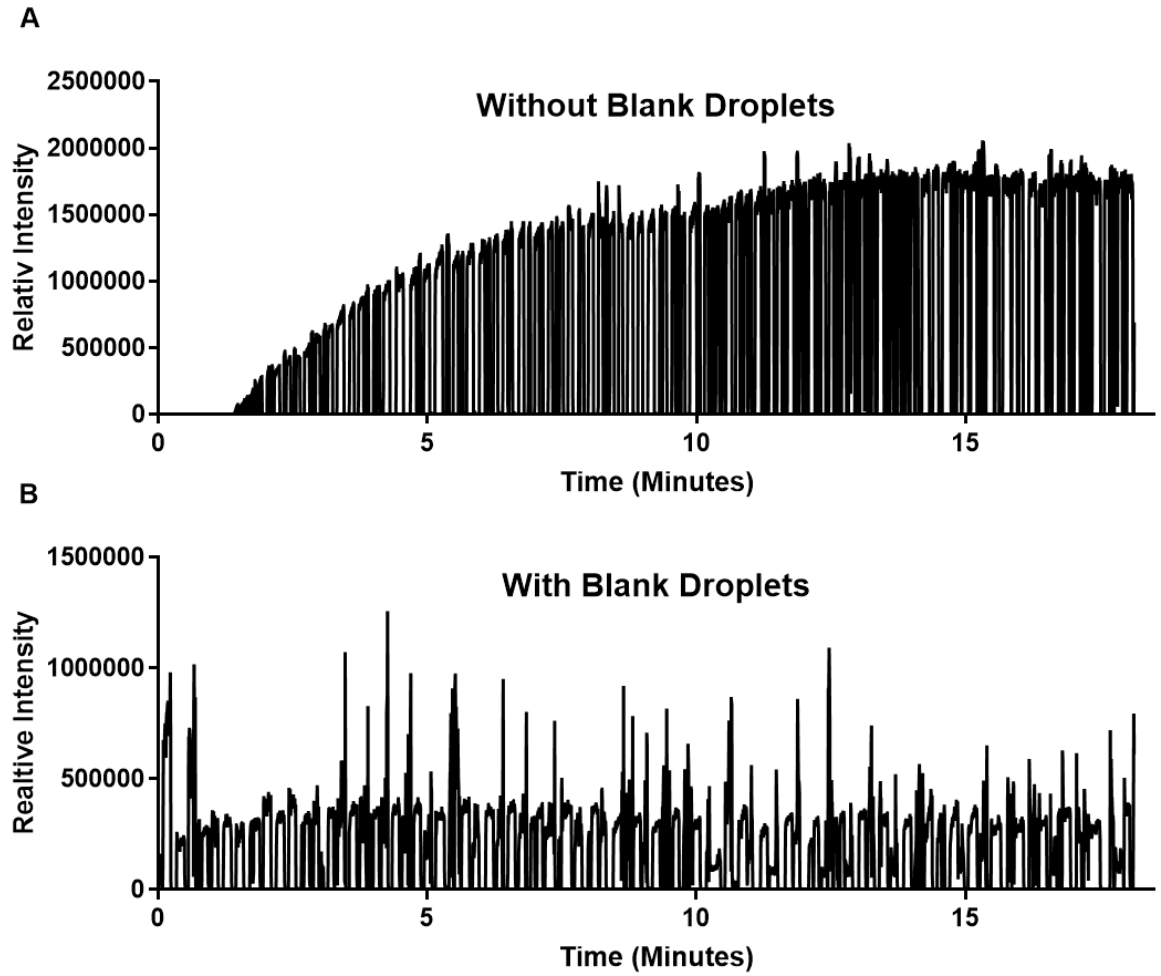

Figure 3-4. Demonstration of carryover during perfusion of droplet train. TIC of droplet train only containing sample plugs with 10 uM myoglobin in 100 uM ammonium acetate. (A). TIC of droplet train with sample plugs alternating between 10 uM myoglobin and blank droplets (80% water, 20% methanol, 0.5% formic acid) (B).

transferred between droplets accounts for the signal observed within the blank droplets. Spikes in protein signals can also be observed at the edges of the sample droplet distributions detected. We attribute this minor amount of protein denaturation to interactions between the protein and the aqueous-carrier phase interface.

Droplet CIU

We then explored using droplets as a sample introduction system for a CIU assay targeting SIRT5, a potential therapeutic target[33–35]. Droplets were generated from samples containing 10 uM SIRT5 co-incubated with a known small molecule inhibitor, 2,2'-((9H-fluorene-2,7-disulfonyl)bis(azanediyl))diacetic acid (fluorene compound).Like myoglobin, these sample droplets were stably perfused into the MS with less than 5% carryover between protein-containing droplets (**Figure 3-5A**). Additionally, it is possible to observe both apo- and fluorene-bound SIRT5 within a single droplet (**Figure 3-5B**), while only low intensity signals for denatured SIRT5 are seen in blank droplets (**Figure 3-5C**). Using our modified method editor (see Experimental Section for details), CIU fingerprints were collected over the course of two sample droplets and the IM-MS data was combined into a single contour plot with post-acquisition analysis in CIUSuite2 (**Figure 3-5D**). Our results demonstrate that it is possible to employ CIU to analyze inhibitor-protein complexes in a semi-automated fashion at a rate of 2 samples/min, consuming only 12.8 ng of protein per assay, while simultaneously determining protein-ligand binding stoichiometries. It is also important to note that is the first example of a non-covalent interaction observed by MS in an oil/water droplet microenvironment. This was achieved while simultaneously reducing typical CIU acquisition times by a factor of ten and reducing typical sample consumption by two orders of magnitude.

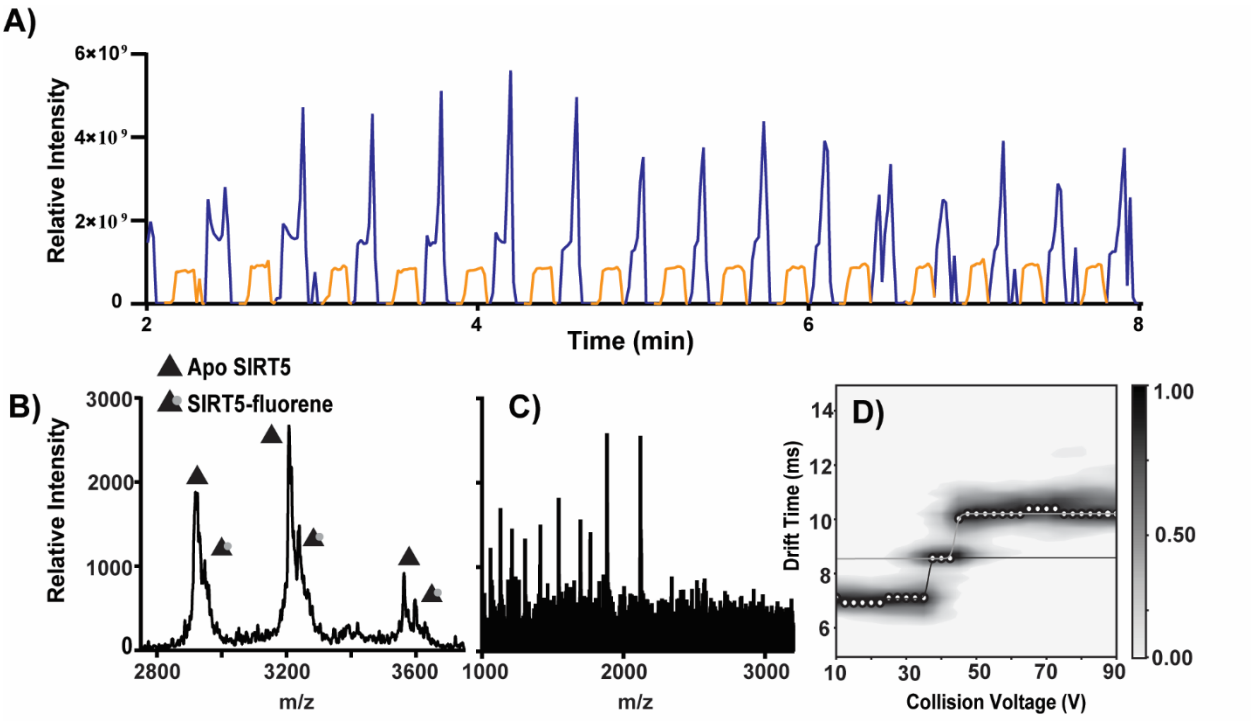

Figure 3-5. CIU of inhibitor-bound SIRT5 in droplets. TIC of incoming droplet train with sample containing and blank droplets colored in blue and orange, respectively (A). MS averaged over a single sample containing droplet (B). MS averaged over a single blank droplet (C). CIU fingerprint collected over the span of two sample droplets, merged into a single fingerprint with post-acquisition data processing (D).

It was essential to investigate the impact that the droplet microenvironment has on native-like protein structure. It has been shown that the presence of some surfactants can interact with and potentially alter protein conformation[36], and thus complicate the interpretation of CIU fingerprints. The arrival time distributions (ATDs) of the most intense charge states in three different proteins were compared between those perfused in droplets and those perfused by standard direct infusion (**Figure 3-6A-C**). Each of these proteins vary in size, domain number, and overall structure. Overall, we find no significant differences ATDs between droplet nESI and direct nESI samples. Additionally, we detect no significant differences in the CIU features or transitions recorded for SIRT5 ions collected from droplets (**Figure 3-6D**) versus those observed through direct infusion (**Figure 3-6E**). An RMSD comparison plot between the two sets of fingerprints highlights that most of the differences in the fingerprints can be attributed to low-

intensity noise that does not impact CIU feature finding or transition fitting (**Figure 3-6F**). Overall, our data suggests that the droplet microenvironment, including the added 008-fluorosurfactant, does not generally alter global protein structures.

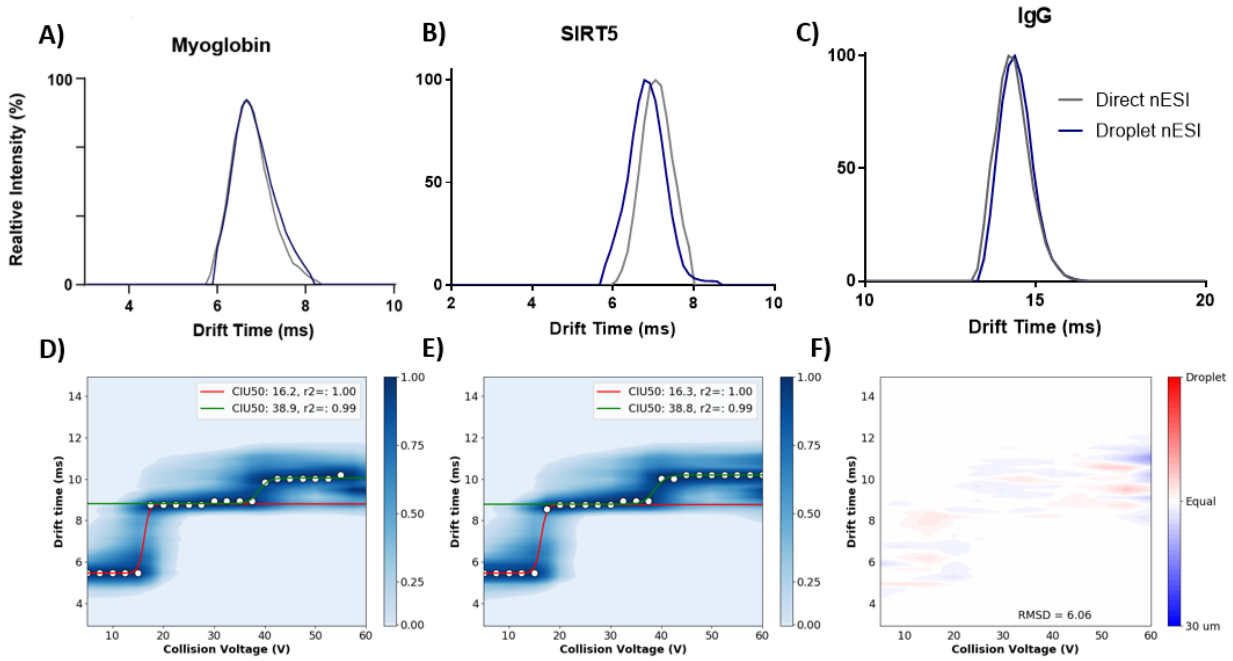

Figure 3-6. Comparison of protein structures infused from droplet versus non-droplet aqueous environments. ATD comparisons for myoglobin (A) SIRT5 (B) and IgG (C). ATDs averaged from samples introduced via droplets are shown in blue and ATDs averaged from samples introduced via direct infusion are shown in gray signal intensities in droplets versus direct infusion were normalized to their respective highest values. Averaged SIRT5 CIU fingerprints collected from droplets (D) and direct infusion (E) n=3. RMSD comparison between the two fingerprint sets (F).

While the presence of fluorosurfactant did not alter SIRT5 protein structure, we do observe a group of MS signal corresponding to surfactant clusters that overlap with our targeted SIRT5 signals in m/z. These signals impacted our early efforts at SIRT5 CIU feature and transition fitting. In an effort to overcome this chemical noise, we employed a voltage ramp from 0 V to 100 V in the transfer region of the MS to dissociate such surfactant cluster ions (**Figure 3-7A-C**). The MS signals for apo- and SIRT5-fluorene were simultaneously monitored (**Figure 3-7D**) during this process and a transfer energy of 30 V was chosen for all CIU experiments in order to maximize

signal for SIRT5-ligand complexes while suitably reducing surfactant signals for automated feature fitting in CIUSuite2.

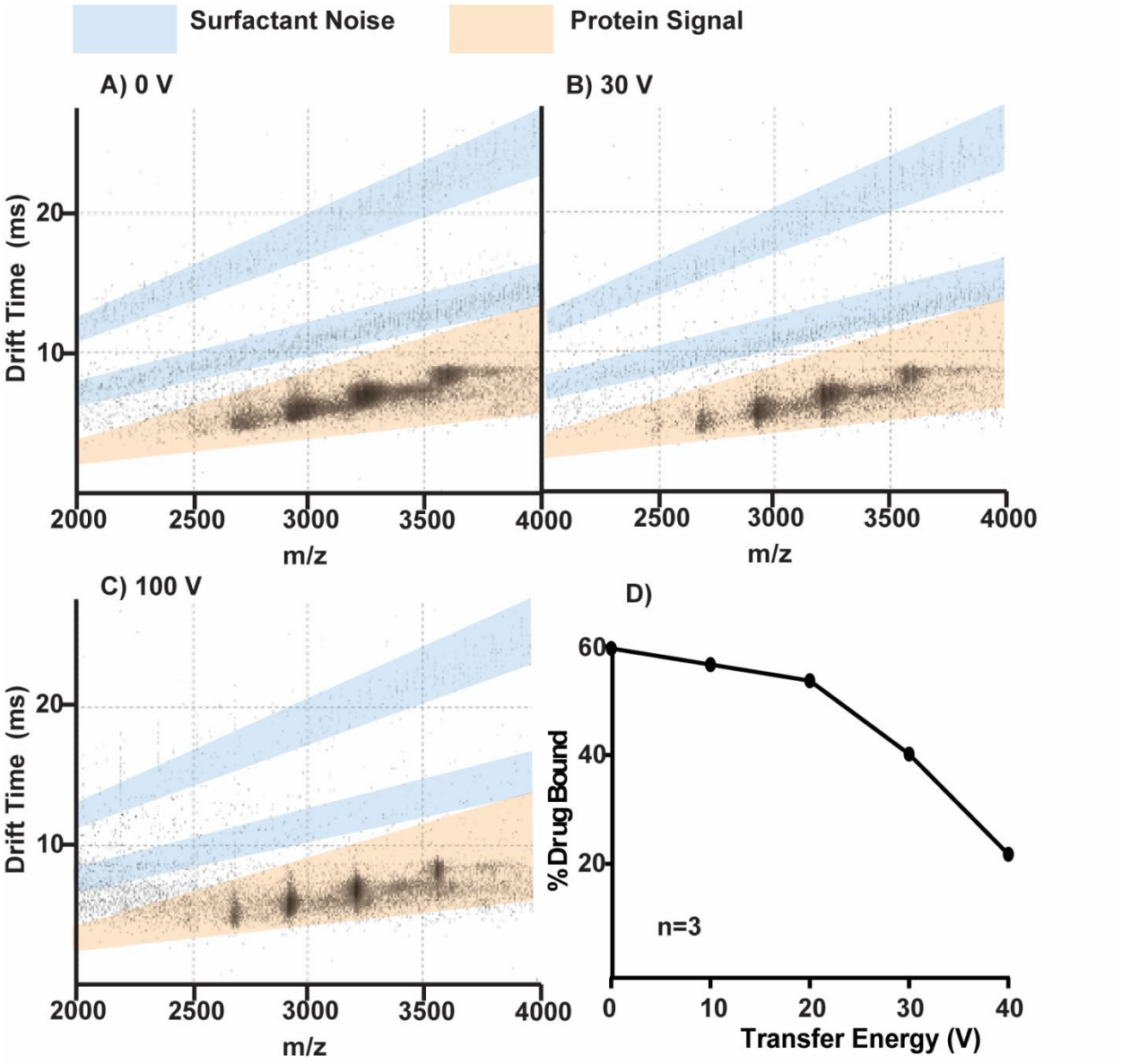

Figure 3-7. Reducing overlapping surfactant noise in droplet samples. IM-MS data for SIRT5-fluorene ionized from 2% surfactant stabilized droplets with the energy in the transfer region set to 0 V (A), 30 V (B), and 100 V (C). Percent ligand loss was monitored with increasing transfer energy (n=3)(D).

Application to SIRT5 Droplet-CIU Screen

The results described above indicate that it is possible to perform CIU assays of protein-ligand complexes from nanoliter droplet samples on the second timescale. In addition, while our data suggest that an entire CIU fingerprint can be collected for each protein-ligand complex detected, it is also possible to target the collection of CIU data to narrow regions of drift time/voltage space in order to increase throughput. In this way, it would be possible to identify inhibitors and determine their effect on protein stability, while minimizing acquisition times. To maximize our ultimate throughput, a pilot screen with known SIRT5 inhibitors was performed to

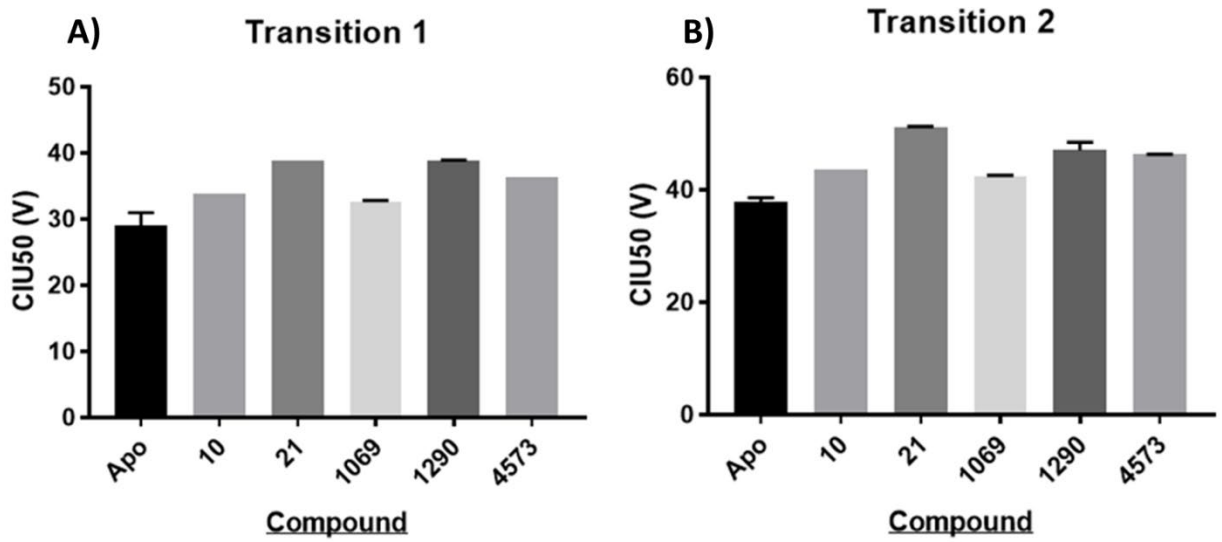

Figure 3-8. Comparison of CIU50 values between apo- and inhibitor-bound SIRT5. CIU fingerprints were scanned from 5V to 60V and averaged for each inhibitor. CIU50 values were obtained and plotted for the first (A) and second (B) transition regions between features.

identify the most differentiating regions of the CIU fingerprint and reduce the number of CVs scanned per sample. All SIRT5 CIU fingerprints exhibit three distinct features and two transition regions, correlated to a compact starting structure and two unfolded states accessed during CIU by the SIRT5 ions probed here (**Figure 3-5D).** Although inhibitor binding did not significantly impact the averaged median drift time for each CIU feature detected, compound binding did increase the collision energy needed to reach both the first and second CIU transitions recorded (**Figure 3-8**). This result indicates that the inhibitors screened against SIRT5 exhibit a stabilizing effect on the

protein structure, as expected. Not only does this information aid in identifying the likely mode of action for the SIRT5 inhibitors studied here, but differences in the CIU data recorded could be used in the future to identify separate classes of SIRT5 inhibitors based on their different interaction modes or locations on the protein surface.

To further validate the ability of CIU to differentiate SIRT5 inhibitors, a classification scheme was built in CIUSuite2 using the training set of compounds from above. Training data was sorted into two classes: apo-SIRT5 and inhibitor bound-SIRT5. Using this two-class classification scheme, each voltage was assessed, and scores were assigned based the ability of each voltage slice to differentiate between the two training classes (**Figure 3-9A**). The voltages 30 V and 37.5 V were automatically selected by the CIUSuite2 algorithm and an internal cross-validation of the resulting classifier reveals evidence of robust performance (**Figure 3-9B**). Interestingly, the voltages selected for our CIU classifier fall within the transition region of apo-SIRT5 CIU fingerprints. Based on the area under the corresponding receiver operating characteristic curve (AUC-ROC), our analysis shows a 0.96 maximum classification accuracy when CIU data acquired at 30 V and 37.5 volts are used. An external validation was performed using CIU fingerprint data from SIRT5 bound to compound 1290, which was excluded from the original training data used to build the classification scheme and treated as a unknown in the context of validation run. The results of this external validation were plotted using a linear discriminant analysis, and we observed a clear separation between apo- and bound-SIRT5 and SIRT5-1290 data (**Figure 3-9C**). The high probability of this classification scheme correctly identifying 1290-SIRT5 as a bound state is displayed in **Figure 3-9D**. Together the data from **Figure 3-8** and the analysis shown in **Figure 3-9** demonstrate that a limited voltage range,

encompassing the transition regions in the SIRT5 CIU fingerprint, can be used to robustly differentiate apo- versus inhibitor-bound states of SIRT5.

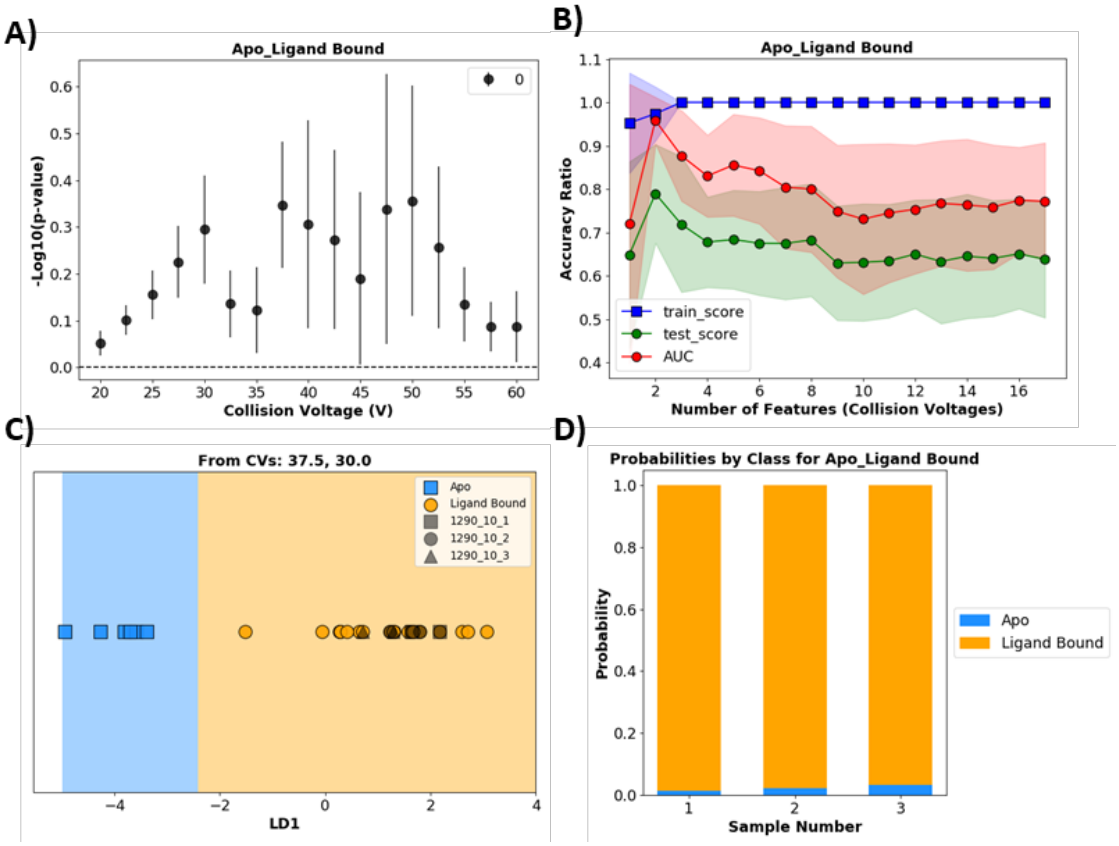

Figure 3-9. CIU-based classification of SIRT5 ligands. Each voltage was scored for its ability to differentiate inhibitors from apo-SIRT5 (n=3) (A). Voltages 30 and 37.5 were selected for an internal cross-validation test, where accuracy was tracked with the test data (green), the training data (blue), and the area under the ROC curve (red) versus the number of collision voltages included in the classification scheme (B). An external validation was run using compound 1290 (not included in the original classification scheme) and collision voltages 30 and 37.5. A linear discriminant plot shows the resulting classification and separation of apo- versus inhibitor-bound SIRT5 (C). A bar chart representing the probability of class assignments for compound 1290 for three replicates, using the classification engine built in panel A and B (D).

This CIU workflow was then used to screen 96 compounds against SIRT5 to identify potential binders and inhibitors. This small molecule library was based on the scaffolds of known SIRT5 inhibitors identified through biochemical assays and co-crystallization studies (unpublished, Neamati Group, University of Michigan). Reactions were prepared in 384-well

plates where SIRT5 was incubated with small-molecule compounds in a 1:1 molar ratio. Samples were introduced to the MS using the droplet generation and transfer method described above, and collision voltages were scanned from 30 V to 55 V for each sample droplet. Samples were run in batches of 48 and total analysis time was 70 min. Feature and transition regions were fit for each fingerprint and CIU50 values for each compound were derived and plotted versus the apo-SIRT5 CIU50 values for both the first and second transition (**Figure 3-10**). In this screen, 24 compounds exhibited increased CIU50 values for both their first and second CIU transitions and were confirmed as novel binders of SIRT5 through subsequently-collected MS data.

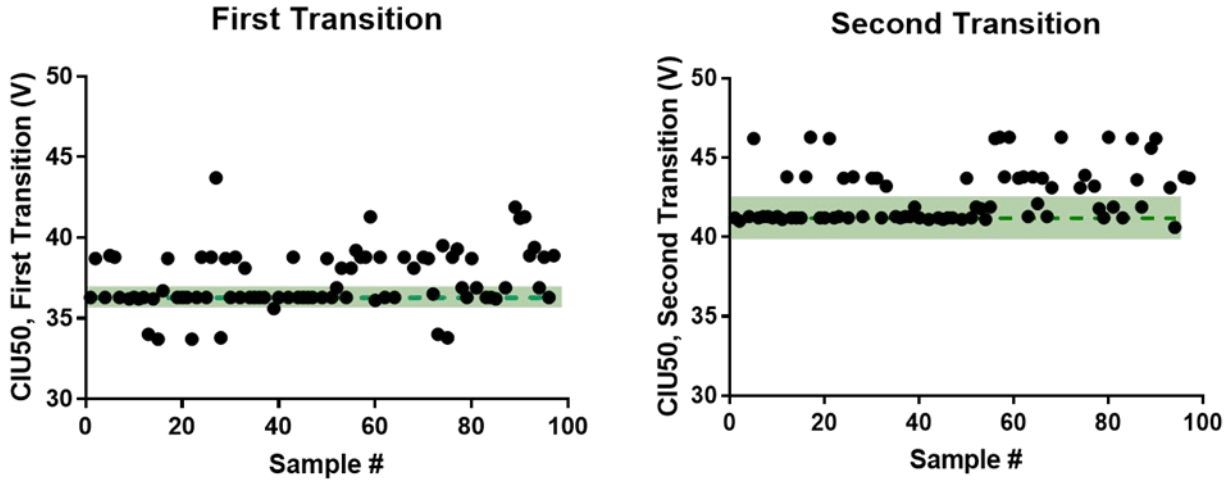

Figure 3-10. 96-compound screen for potential SIRT5 binders. CIU fingerprints from 30 V to 55 V for each compound. Transition regions were fit for every fingerprint, generating CIU50 values for the first (A) and second (B) transition regions. Each point represents a CIU50 value for an individual compound. The apo-SIRT5 CIU50 value for each respective transition is denoted by the dashed green line. The shaded region represents 3σ of the apo value.

Of the 96 compounds screened, 8 were selected to validate the results from the screen. SIRT5 was pre-incubated with the compounds in a 1:1 molar ratio and introduced to the MS with standard direct infusion. CIU fingerprints were collected over a range of 5 V to 60 V, a more comprehensive range than used for the droplet-based screen. These CIU fingerprints were collected in triplicate and averaged for each SIRT5-compound complex (**Figure 3-11**). Seven out

of the eight compounds assayed were consistent with the results from the higher-throughput CIU screen. The results for compound YH-162 did not agree with the initial results found in the screen; however, upon closer investigation poor spray stability and signal intensity for the corresponding sample droplet in the screen is likely the cause of this false positive. This contributed to poor feature and transition fitting and is likely to be responsible for the differences in the CIU50 values from the initial screen versus the CIU50 values represented in **Figure 3-11**. Overall, the values were consistent with the initial high-throughput CIU screen, demonstrating the potential utility of our approach for identifying potential inhibitors and their effect on overall protein structural stability.

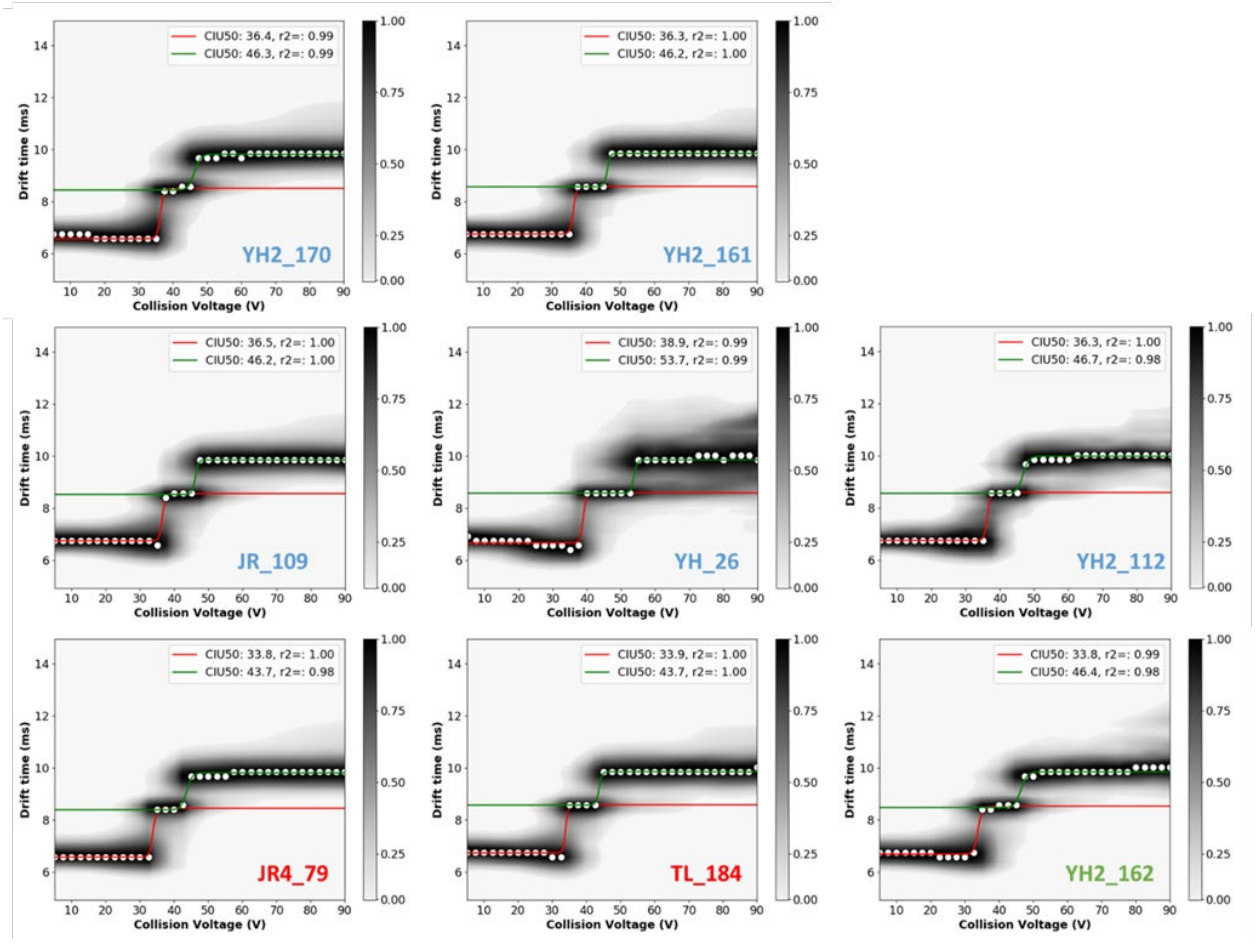

Figure 3-11. Validating results of CIU screen. CIU fingerprints of eight compounds incubated with SIRT5 with transition values that differed significantly from apo-SIRT5 (n=3). Compounds with names written in blue indicate a stabilization upon ligand binding and are consistent with the results from the initial screen (A-E). Compounds with names written in red indicate destabilization upon ligand binding are consistent with results from the initial screen (F-G). Compounds with names in green indicate ambiguous results where there was a destabilization of the first transition and stabilization of the second transition. These results are not consistent with the results from the screen (H).

Several similarities emerged between "hit" compound structures in our CIU screeen for SIRT5 inhibitors. All of the identified compounds had conjugated ring structures, resulting in fairly planar scaffolds. Additionally, almost every hit compound had a carboxylic acid end cap, an important electron donating functional group present in many drug molecules.[37] Compounds differed in the linker region between conjugated ring structures and fell into three common groups:

structures with thiourea linkers **(Figure 3-12A**), sulfonamide linkers (**Figure 3-12B**), anfd amide linkers (**Figure 3-12C**). There was no significance in structure stabilization observed based on CIU50 differences between the different compound classes. Nonetheless, these compounds represent the leading scaffolds that could be further developed and explored as SIRT5 inhibtors

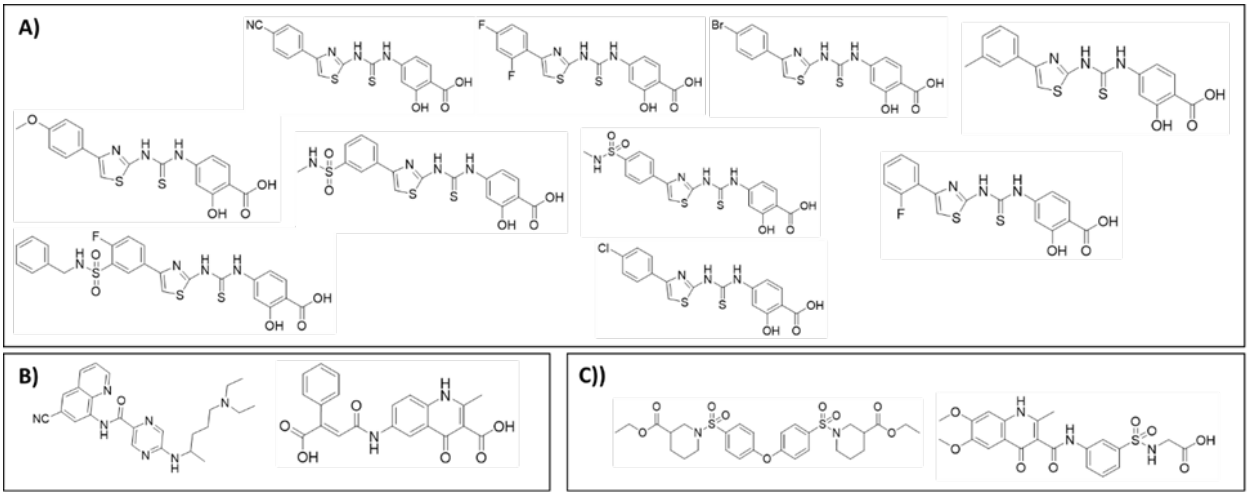

Figure 3-12. Hit compound structures. Compounds were separated into three groups based on similarities in molecular structure: Thiourea linker containing compounds (A), compounds with sulfonamide linkers (B), and compounds with amide linkers (C).

based on our data.

To gain further insight into the mechanisms of SIRT5 inhibition, the relationship between SIRT5-ligand complex structure and its enzymatic activity were investigated. IC50 values for known SIRT5 inhibitors were obtained using a previously established CE-based method[38] (**Figure 3-13**).

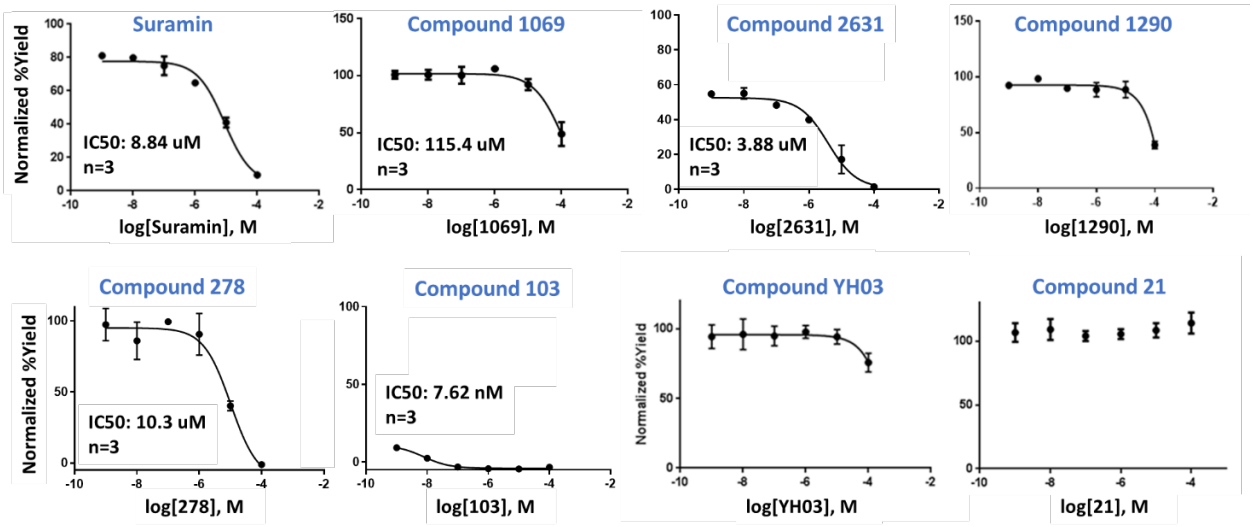

Figure 3-13. Dose-response analysis for known SIRT5 inhibitors. SIRT5 enzymatic activity was measured in the presence of 1 nM to 100 uM inhibitor. Normalized percent yields were based on the ratio of substrate peptide to product peptide signal. IC50 values were calculated from best fit curves, using a one site, nonlinear regression fit.

All SIRT5 inhibitors studied here exhibited a positive shift in CIU50 values for both the first and second CIU transitions. Inhibitors with the greatest potency towards SIRT5 activity also caused the largest shifts in CIU50 for the first transition, while the opposite trend is observed for the second transition (Figure 3-14). These inhibitors are known to bind in the ligand binding domain, and we hypothesize that the first transition region may represent the unfolding of this region of the protein, while the second transition region may relate to the unfolding of the zinc-binding domain within SIRT5. In the future, such information could be used to sort active site inhibitors from those that act allosterically. Although compound 103 does not align with this trend, it is possible that the IC50 recorded by our CE assay is an inaccurate due to lack of data points at higher concentrations (**Figure 3-13**). CIU50 values were unable to be obtained for suramin due to SIRT5 aggregation upon co-incubation at the micromolar concentrations necessary for native CIU experiments. Overall, CIU experiments have not only identified novel SIRT5 binders, but

have also provided more insight into the relationship between SIRT5 structure and its mechanisms of small-molecule enzymatic inhibition. These label-free, information rich unfolding assay has

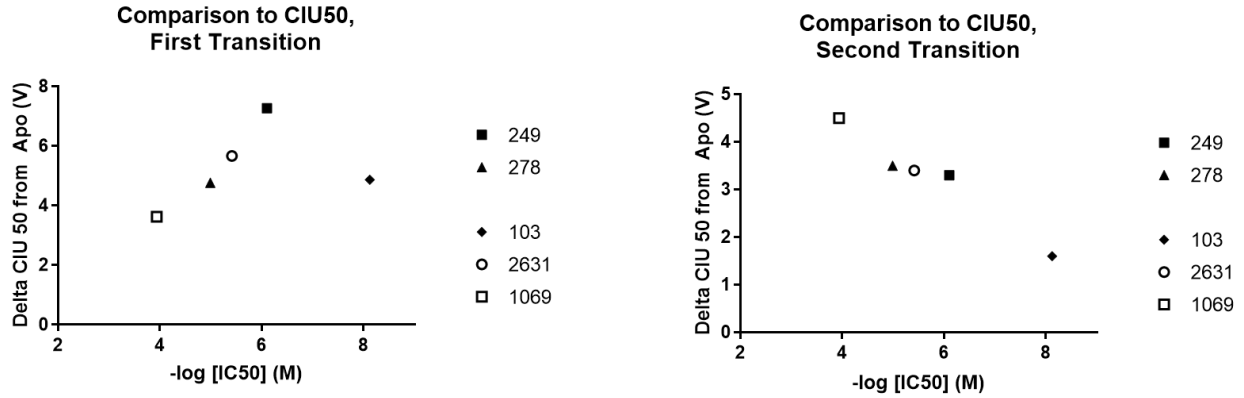

Figure 3-14. Comparison of CIU50 values to IC50 values (n=3) of known SIRT5 inhibitors for the first (A) and second (B) transitions. Delta CIU50 values were calculated by subtracting the average apo CIU50 from the CIU50 of each SIRT5-inhibitor complex. IC50 values were plotted on a log scale for comparative purposes.

the potential to compliment traditional enzymatic screening assays, and requires far less time and sample than calorimetric approaches.

3.4 Conclusions

In this work we describe a droplet-microfluidics sample introduction system for native IM-MS, demonstrate CIU data collection on the sub-minute timescale, and discuss semi-automated CIU data collection for high-throughput screening applications. Utilizing on-board smoothing and interpolation algorithms tailored for the CIU experiment, it was possible to reduce CIU fingerprint collection time by 10X when compared to typical CIU data collection schemes. A droplet-based sample introduction approach, suitable for samples with high protein concentrations, was developed and coupled to our fast CIU data acquisition. It was also shown that non-covalent complexes are preserved within droplets and that the droplet microenvironment does not significantly alter global protein structure in general. Furthermore, we were able to identify differentiating regions within a given SIRT5 CIU fingerprint and apply this droplet CIU workflow

to a 96-compound screen against SIRT5. Over 20 novel SIRT5 binders were identified in this screen. Additionally, we found that inhibitors stabilize particular SIRT5 conformations, and that this stabilization effect can be correlated with SIRT5 enzymatic activity. Overall, this work demonstrated that CIU can be employed as a screening tool that provides valuable insight into protein-ligand interactions. Future work will focus on improving automation of data acquisition and applications to other protein systems.

3.5 References

(1) Renaud, J.-P.; Chung, C.; Danielson, U. H.; Egner, U.; Hennig, M.; Hubbard, R. E.; Nar, H. Biophysics in Drug Discovery: Impact, Challenges and Opportunities. *Nat. Rev. Drug Discov. 2016 1510* **2016**, *15* (10), 679–698. https://doi.org/10.1038/nrd.2016.123.

(2) Maveyraud, L.; Mourey, L. Molecules Protein X-Ray Crystallography and Drug Discovery. https://doi.org/10.3390/molecules25051030.

(3) Renaud, J.-P.; Chari, A.; Ciferri, C.; Liu, W.; Rémigy, H.-W.; Stark, H.; Wiesmann, C. Cryo-EM in Drug Discovery: Achievements, Limitations and Prospects. *Nat. Rev. Drug Discov.* **2018**, *17* (7), 471–492. https://doi.org/10.1038/nrd.2018.77.

(4) Cala, O.; Guillière, F.; Krimm, I. NMR-Based Analysis of Protein-Ligand Interactions. https://doi.org/10.1007/s00216-013-6931-0.

(5) Weber, P. C.; Salemme, F. R. Applications of Calorimetric Methods to Drug Discovery and the Study of Protein Interactions. *Curr. Opin. Struct. Biol.* **2003**, *13* (1), 115–121. https://doi.org/10.1016/S0959-440X(03)00003-4.

(6) Leavitt, S.; Freire, E. Direct Measurement of Protein Binding Energetics by Isothermal Titration Calorimetry. *Curr. Opin. Struct. Biol.* **2001**, *11* (5), 560–566. https://doi.org/10.1016/S0959-440X(00)00248-7.

(7) Olsson, T. S. G.; Williams, M. A.; Pitt, W. R.; Ladbury, J. E. The Thermodynamics of Protein–Ligand Interaction and Solvation: Insights for Ligand Design. *J. Mol. Biol.* **2008**, *384* (4), 1002–1017. https://doi.org/10.1016/J.JMB.2008.09.073.

(8) Ishii, K.; Noda, M.; Uchiyama, S. Biophysics and Physicobiology Mass Spectrometric Analysis of Protein-Ligand Interactions. **2016**, *13*, 87–95. https://doi.org/10.2142/biophysico.13.0_87.

(9) Chen, G.; Fan, M.; Liu, Y.; Sun, B.; Liu, M.; Wu, J.; Li, N.; Guo, M. Advances in MS Based Strategies for Probing Ligand-Target Interactions: Focus on Soft Ionization Mass Spectrometric Techniques . *Frontiers in Chemistry* . 2019, p 703.

(10) Barth, M.; Schmidt, C. Native Mass Spectrometry-A Valuable Tool in Structural Biology.

2020. https://doi.org/10.1002/jms.4578.

(11) Cubrilovic, D.; Biela, A.; Sielaff, F.; Steinmetzer, T.; Klebe, G.; Zenobi, R. Quantifying Protein-Ligand Binding Constants Using Electrospray Ionization Mass Spectrometry: A Systematic Binding Affinity Study of a Series of Hydrophobically Modified Trypsin Inhibitors. *J. Am. Soc. Mass Spectrom* **2012**, *23*, 1768–1777. https://doi.org/10.1007/s13361-012-0451-6.

(12) Hopper, J. T. S.; Robinson, C. V. Mass Spectrometry Quantifies Protein Interactions--from Molecular Chaperones to Membrane Porins. *Angew. Chem. Int. Ed. Engl.* **2014**, *53* (51), 14002–14015. https://doi.org/10.1002/anie.201403741.

(13) Eyers, C. E.; Vonderach, M.; Ferries, S.; Jeacock, K.; Eyers, P. A. Understanding Protein–Drug Interactions Using Ion Mobility–Mass Spectrometry. *Curr. Opin. Chem. Biol.* **2018**, *42*, 167–176. https://doi.org/10.1016/J.CBPA.2017.12.013.

(14) Dixit, S. M.; Polasky, D. A.; Ruotolo, B. T. Collision Induced Unfolding of Isolated Proteins in the Gas Phase: Past, Present, and Future. *Curr. Opin. Chem. Biol.* **2018**, *42*, 93–100. https://doi.org/10.1016/J.CBPA.2017.11.010.

(15) N. Rabuck, J.; Hyung, S.-J.; S. Ko, K.; C. Fox, C.; B. Soellner, M.; T. Ruotolo, B. Activation State-Selective Kinase Inhibitor Assay Based on Ion Mobility-Mass Spectrometry. *Anal. Chem.* **2013**, *85* (15), 6995–7002. https://doi.org/10.1021/ac4012655.

(16) Allison, T. M.; Reading, E.; Liko, I.; Baldwin, A. J.; Laganowsky, A.; Robinson, C. V. ARTICLE Quantifying the Stabilizing Effects of Protein-Ligand Interactions in the Gas Phase. *Nat. Commun.* **2015**. https://doi.org/10.1038/ncomms9551.

(17) Mehmood, S.; Marcoux, J.; Gault, J.; Quigley, A.; Michaelis, S.; Young, S. G.; Carpenter, E. P.; Robinson, C. V. Mass Spectrometry Captures Off-Target Drug Binding and Provides Mechanistic Insights into the Human Metalloprotease ZMPSTE24. *Nat. Chem.* **2016**, *8* (12), 1152–1158. https://doi.org/10.1038/nchem.2591.

(18) Polasky, D. A.; M. Dixit, S.; M. Fantin, S.; T. Ruotolo, B. CIUSuite 2: Next-Generation Software for the Analysis of Gas-Phase Protein Unfolding Data. *Anal. Chem.* **2019**, *91* (4), 3147–3155. https://doi.org/10.1021/acs.analchem.8b05762.

(19) Kempa, E. E.; Hollywood, K. A.; Smith, C. A.; Barran, P. E. High Throughput Screening of Complex Biological Samples with Mass Spectrometry – from Bulk Measurements to Single Cell Analysis. *Analyst* **2019**, *144* (3), 872–891. https://doi.org/10.1039/C8AN01448E.

(20) Sinclair, I.; Bachman, M.; Addison, D.; Rohman, M.; C. Murray, D.; Davies, G.; Mouchet, E.; E. Tonge, M.; G. Stearns, R.; Ghislain, L.; S. Datwani, S.; Majlof, L.; Hall, E.; R. Jones, G.; Hoyes, E.; Olechno, J.; N. Ellson, R.; E. Barran, P.; D. Pringle, S.; R. Morris, M.; Wingfield, J. Acoustic Mist Ionization Platform for Direct and Contactless Ultrahigh-Throughput Mass Spectrometry Analysis of Liquid Samples. *Anal. Chem.* **2019**, *91* (6), 3790–3794. https://doi.org/10.1021/acs.analchem.9b00142.

(21) Zhu, Y.; Fang, Q. Analytical Detection Techniques for Droplet Microfluidics—A Review. *Anal. Chim. Acta* **2013**, *787*, 24–35. https://doi.org/10.1016/J.ACA.2013.04.064.

(22) Wang, X.; Yi, L.; Mukhitov, N.; Schrell, A. M.; Dhumpa, R.; Roper, M. G. Microfluidics-to-Mass Spectrometry: A Review of Coupling Methods and Applications. *J. Chromatogr. A* **2015**, *1382*, 98–116. https://doi.org/10.1016/J.CHROMA.2014.10.039.

(23) Payne, E. M.; Holland-Moritz, D. A.; Sun, S.; Kennedy, R. T. High-Throughput Screening by Droplet Microfluidics: Perspective into Key Challenges and Future Prospects. *Lab Chip* **2020**, *20*, 2247–2262. https://doi.org/10.1039/d0lc00347f.

(24) A. Smith, C.; Li, X.; H. Mize, T.; D. Sharpe, T.; I. Graziani, E.; Abell, C.; T. S. Huck, W. Sensitive, High Throughput Detection of Proteins in Individual, Surfactant-Stabilized Picoliter Droplets Using Nanoelectrospray Ionization Mass Spectrometry. *Anal. Chem.* **2013**, *85* (8), 3812–3816. https://doi.org/10.1021/ac400453t.

(25) Kempa, E. E.; Smith, C. A.; Li, X.; Bellina, B.; Richardson, K.; Pringle, S.; Galman, J. L.; Turner, N. J.; Barran, P. E. Coupling Droplet Microfluidics with Mass Spectrometry for Ultrahigh-Throughput Analysis of Complex Mixtures up to and above 30 Hz. *Anal. Chem.* **2020**, *92* (18), 12605–12612. https://doi.org/10.1021/acs.analchem.0c02632.

(26) Kumar, S.; Lombard, D. B. Generation and Purification of Catalytically Active Recombinant Sirtuin5 (SIRT5) Protein. In *Histone Deacetylases: Methods and Protocols*; Sarkar, S., Ed.; Springer New York: New York, NY, 2016; pp 241–257. https://doi.org/10.1007/978-1-4939-3667-0_16.

(27) Steyer, D. J.; Kennedy, R. T. High-Throughput Nanoelectrospray Ionization-Mass Spectrometry Analysis of Microfluidic Droplet Samples. *Anal. Chem.* **2019**. https://doi.org/10.1021/acs.analchem.9b00571.

(28) E. Haynes, S.; A. Polasky, D.; M. Dixit, S.; D. Majmudar, J.; Neeson, K.; T. Ruotolo, B.; R. Martin, B. Variable-Velocity Traveling-Wave Ion Mobility Separation Enhancing Peak Capacity for Data-Independent Acquisition Proteomics. *Anal. Chem.* **2017**, *89* (11), 5669–5672. https://doi.org/10.1021/acs.analchem.7b00112.

(29) May, J. C.; Jurneczko, E.; Stow, S. M.; Kratochvil, I.; Kalkhof, S.; McLean, J. A. Conformational Landscapes of Ubiquitin, Cytochrome c, and Myoglobin: Uniform Field Ion Mobility Measurements in Helium and Nitrogen Drift Gas. *Int. J. Mass Spectrom.* **2018**, *427*, 79–90. https://doi.org/10.1016/J.IJMS.2017.09.014.

(30) Katta, V.; T. Chait, B. Observation of the Heme-Globin Complex in Native Myoglobin by Electrospray-Ionization Mass Spectrometry. *J. Am. Chem. Soc.* **2002**, *113* (22), 8534–8535. https://doi.org/10.1021/ja00022a058.

(31) B. Shelimov, K.; F. Jarrold, M. Conformations, Unfolding, and Refolding of Apomyoglobin in Vacuum: An Activation Barrier for Gas-Phase Protein Folding. *J. Am. Chem. Soc.* **1997**, *119* (13), 2987–2994. https://doi.org/10.1021/ja962914k.

(32) Joensson, H. N.; Andersson Svahn, H. Droplet Microfluidics—A Tool for Single-Cell Analysis. *Angew. Chemie Int. Ed.* **2012**, *51* (49), 12176–12192. https://doi.org/https://doi.org/10.1002/anie.201200460.

(33) Lu, W.; Zuo, Y.; Feng, Y.; Zhang, M. SIRT5 Facilitates Cancer Cell Growth and Drug Resistance in Non-Small Cell Lung Cancer. https://doi.org/10.1007/s13277-014-2372-4.

(34) Kalbas, D.; Liebscher, S.; Nowak, T.; Meleshin, M.; Pannek, M.; Popp, C.; Alhalabi, Z.; Bordusa, F.; Sippl, W.; Steegborn, C.; Schutkowski, M. Potent and Selective Inhibitors of Human Sirtuin 5. *J. Med. Chem.* **2018**, *61* (6), 2460–2471. https://doi.org/10.1021/acs.jmedchem.7b01648.

(35) Abril, Y. L. N.; Fernandez, I. R.; Hong, J. Y.; Chiang, Y.-L.; Kutateladze, D. A.; Zhao, Q.; Yang, M.; Hu, J.; Sadhukhan, S.; Li, B.; He, B.; Remick, B.; Bai, J. J.; Mullmann, J.; Wang, F.; Maymi, V.; Dhawan, R.; Auwerx, J.; Southard, T.; Cerione, R. A.; Lin, H.; Weiss, R. S. Pharmacological and Genetic Perturbation Establish SIRT5 as a Promising Target in Breast Cancer. *Oncogene* **2021**, *40* (9), 1644–1658. https://doi.org/10.1038/s41388-020-01637-w.

(36) Baret, J.-C. Surfactants in Droplet-Based Microfluidics †. https://doi.org/10.1039/c1lc20582j.

(37) Ballatore, C.; Huryn, D. M.; Smith, A. B. Carboxylic Acid (Bio)Isosteres in Drug Design. *ChemMedChem* **2013**, *8* (3), 385–395. https://doi.org/10.1002/CMDC.201200585.

(38) Guetschow, E. D.; Kumar, S.; Lombard, D. B.; Kennedy, R. T. Identification of Sirtuin 5 Inhibitors by Ultrafast Microchip Electrophoresis Using Nanoliter Volume Samples. https://doi.org/10.1007/s00216-015-9206-0.

Chapter 4: Detection and Quantitation of Intact Monoclonal Anitbodies from Cell Expression Media

4.1 Introduction

Biotherapeutics based on monoclonal antibodies (mAbs) represent both a highly successful and a critically important class of treatments for diseases including cancers, autoimmune disorders and coronavirus infections.[1] The success of mAbs as biotherapeutics can be attributed to their higher specificity and affinity for target molecules when compared to their small-molecule counter parts, thus increasing their therapeutic window and reducing their potential side effects[2–6,] . Higher order structure (HOS), post-translational modifications (PTMs), and stability all contribute to mAb efficacy, and are all key aspects that must be evaluated during the drug discovery and development[7,8]. The structural complexity of mAbs that give rise to their success as therapeutic agents also creates many analytical challenges associated with evaluating their downstream efficacy and safety.

Immunoglobulin Gs, or IgGs, are the dominant mAb subclass used in the generation of biotherapeutics. Notably, IgGs generally produced through recombinant DNA technology within mammalian cells[9]. A key issue in biopharmaceutical development is identifying cell culture conditions that will maximize antibody production to improve efficiency[10]. Factors such as cell type, culture media components, temperature, and pH can all impact cell growth and IgG expression levels, potentially leading to thousands of potential growth conditions to evaluate[11]. Varying growth conditions also impacts normal cellular processes, including the post-translational modification of expressed proteins[11]. Glycosylation is a prominent PTM that can impact IgG

function and efficacy as well as formulation and storage requirements[7,12,13,14]. As such, there is a critical need for high-throughput technologies that can both quantify protein production from culture media, while simultaneously evaluating PTM profiles in the detected mAb populations.

Mass spectrometry (MS) is a widely used tool for intact mAb analysis. Analysis by MS is rapid, information rich, and suitable for complex mixtures[15,16,17]. In the past decade MS has been used for top-down mAb profiling, PTM identification, and the analysis of recombinant mAb mixtures[18,19]. In addition, native MS, which seeks to capture higher order structure information from mAbs and other biomolecular systems by preserving their native structures during ionization, has been used to probe the role of PTMs and stress conditions on mAb structures[19]. With advances in MS scan rates and resolving power, the potential exists to analyze thousands of mAb samples in a day on a single instrument, making MS well-suited for high-throughput applications associated with biotherapeutic discovery and development.[20]

While MS can rapidly detect intact mAbs, high-throughput sample introduction of protein analytes from complex matrices remains a challenge. Sample cleanup is necessary prior to electrospray (ESI) and nanoelectrospray (nESI) MS analysis, due to ionization suppression, overlapping background signal, and spray instability that can be caused by the matrix components associated with biotheraputic production (e.g., cell culture media)[21] and formulation. Chromatographic approaches, including hydrophobic interaction chromatography, reversed-phase chromatography, size exclusion chromatography, and affinity chromatography, are most commonly used for mAb purification[22,23]. While these methods are robust, they often require large amounts of sample and solvent. Additionally, the timescale of such sample preparation is typically on the order of minutes to hours and is thus not optimal for use in high-throughput analyses[22–26]

A wide range of high-throughput MS technologies have been developed for the analysis of mAbs. For instance, the use of surface modified magnetic beads has emerged as a batch purification and desalting method for small volume mAb samples prior to MS analysis.[27] Such technologies have been used in conjunction with robotic sampling to enable 0.03 Hz sample delivery for MS analysis, a 10-fold improvement over prior approaches[28]. Droplet-microfluidics coupled to nESI-MS is a promising workflow for high-throughput intact protein and mAb analysis[29–31]. For example, prior work has demonstrated that intact, native-like Trastuzumab can be detected within a single 408 pL droplet, at a droplet sampling rate of 10 Hz, producing a mass measurement that fell within error of MS data obtained using a conventional ESI emitter[30]. Additionally, the throughout limitations for intact protein analysis by droplet-MS have been explored. Sampling rates of up to 33 Hz have been achieved across three different MS instrument platforms[31]. The quantitative capabilities droplet-based MS methods, however, have not yet been explored and sample cleanup is still typically required prior to infusion into the MS detector.

Here we develop an MS-compatible Protein A-based cleanup protocol, coupled to microdroplet entrainment and analysis by native MS for screening of antibody production from different media. The droplet-MS sample introduction platform enables rapid and semi-automated quantitation of IgGs expressed under varying media conditions. We achieve intact mAb detection from a single droplet with an LOD of 0.15 mg/mL and an LOQ of 2.6 mg/mL, with a throughput of 0.04 Hz. We then use high-resolution native MS to characterize glycosylation profiles from productive media conditions. Protein A purification coupled to Droplet-MS analysis enables high-throughput quantification of mAbs from complex background matrices, along with supplemental glycan profiling, in a simple, fast, and label-free experiment.

4.2 Methods

Materials and Sample Preparation

All reagents were purchased from Sigma Aldrich (St. Louis, MO) unless otherwise noted. For MS tuning and initial droplet experiments, SiLuLite SigmaMab IgG1λ from human myeloma was used. Samples were reconstituted in Milli-Q water (Millipore) to a concentration of 1 mg/mL then buffer exchanged into 200 mM ammonium acetate using Micro Biopsin 30 columns (Bio-rad, Hercules, Ca). All mAb samples were provided by Bristol-Myers Squibb (New Brunswick, NJ). BMS mAb samples were stored in 20 mM histidine, 250 mM sucrose, 50 µM diethylenetriamiepentaacetic acid (DTPA), 0.05% polysorbate 80, pH 6.0 at a concentration of ~180 mg/mL. BMS mAb was buffer exchanged into 200 mM ammonium acetate using size exclusion chromatography. The size exclusion column (GE Superdex 200 Increase 10/300 GL) was pre-equilibrated with the ammonium acetate buffer, prior to sample loading. Fractions containing mAb were then pooled and stored at a concentration of 4 mg/mL.

Droplet Generation

Droplets were generated from 384-microwell plates as previously described[32], with modifications. Samples were drawn into 150 µm i.d. x 360 µm o.d. PFA tubing (IDEX Health and Science, Oak Harbor, WA) using a fusion 400 syringe pump (Chemyx, Strafford, TX) operated in withdrawal mode. The tubing was directed by an xyz-micropositioner, alternating between microwells containing sample and the perfluorodecalin (PFD) carrier phase. 2% (v/v) 008-flurosurfactant (RAN Biotechnologies, Beverly, MA) was added to the carrier phase to stabilize sample droplets during generation and infusion. Droplets were generated at a rate of 200 nL/min to prevent air from entering the PFA tubing when moving between adjacent microwells.

Droplet nESI Analysis

All droplet-MS experiments were performed on a Synapt G2 quadrupole–ion mobility–time-of-flight mass spectrometer (Q–IM–ToF MS) instrument (Waters Corp., Milford, MA). For continuous direct infusion experiments, samples were loaded into gold-coated, borosilicate needles, pulled to 7-9 um. For droplet experiments, samples were transferred to 100 um 1D x 360 od fused-silica needles pulled to a 30 um diameter (New Objective, Woburn, MA) using a zero dead volume Picoclear union (New Objective, Woburn, MA). Prior to droplet transfer, fused silica needles were derivatized with 2% trichloro(1H,1H,2H,2H-perfluorooctyl) silane dissolved in PFD using previously described methods[33] to prevent adhesion of aqueous samples. The MS was run in positive mode and the electrospray capillary was held at a voltage of 1.3 kV with the sampling cone set to 40 V. The backing pressure was set to 7 mbar for all mAb samples. The wave height and wave velocity were 10 V and 300 m/s within the IM traveling-wave ion guide, respectively. The pressure in the trap collision cell was set to 4.8×10^{-2} mbar with argon gas, the helium cell set to 1.4×10^{3} mbar, the traveling-wave IM separator set to 3.4 mbar, and the ToF MS set to 2.2×10^{-6} mbar. A scan rate of 0.5 scans per second was used to generate at least five points per droplet while maximizing signal to noise ratio.

Modified Protein A Purification

A schematic representation of the binding and elution protocol is shown in Figure 4-1. Magnetic beads modified with protein A were used for mAb capture (Dynabeads, Invitrogen, Waltham, MA). A 50 uL bead suspensions was placed in each sample well of a 384 well-plate, with a magnet placed below. Once beads were separated from solution, the supernatant was removed and discarded. Expression media containing mAb was diluted into 100 uL of PBS (10 mM phosphate, 2.7 mM potassium chloride, 137 mM sodium chloride, pH = 7.4) with 0.02% Tween-20 and mixed

with the plated beads by pipette until homogeneous. The samples were then incubated on rotation at room temperature for 20 minutes. The plate was then placed back on a magnet and the supernatant was removed. This was followed by three wash steps with 100 uL of Milli-Q water. A volume of 25 uL of 200 mM acetic acid was used for mAb elution from the beads. The plate was incubated on rotation at room temperature for 30 minutes. The plate was then placed on top of magnets to separate the beads from solution once more. Droplets were then generated from the top of each sample well.

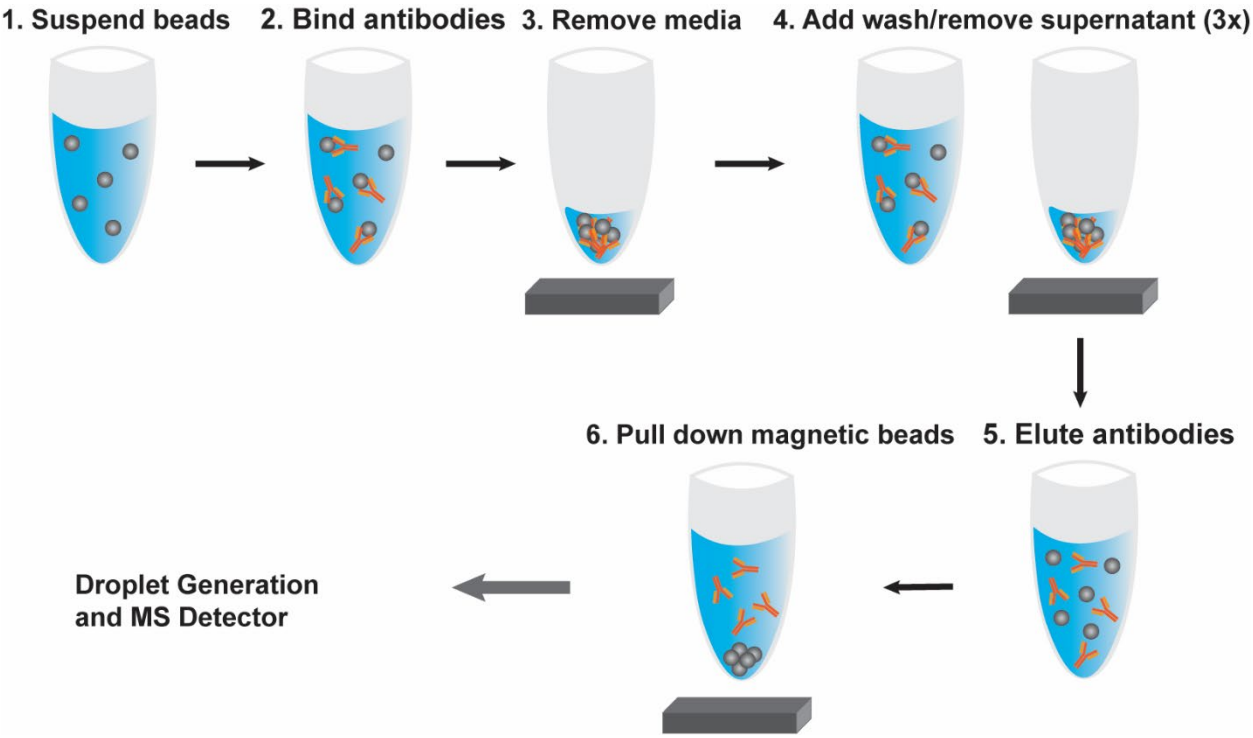

Figure 4-1. Illustration of Dynabead Protein A binding and elution protocol for mAb purification. Magnetic beads are represented as dark gray spheres and mAbs are shown in orange.

High-Resolution Mass Spectrometry for Glycan Profiling

Antibody samples were prepared using the protein A protocol described above. Glycan analysis was performed on intact antibodies using a Q Exactive UHMR hybrid quadrupole-orbitrap

mass spectrometer. (ThermoFisher, Waltham, MA). Samples were directly infused using 7-9 um gold-coated borosilicate emitters. The mAb samples were purified from cell culture media as described above. For all experiments on the Q Exactive the spray voltage was set to 1.3 kV and the capillary temperature was held at 275 ºC. The desolvation voltage was set to 100 V to remove salt adducts and improve resolution. Resulting mass spectra were deconvoluted using BioPharma Finder. The ReSpect (isotopically unresolved) deconvolution algorithm was applied with a deconvolution mass tolerance of 50 ppm. The input m/z range was confined from 3,000 to 8,000 with an output range of 10 kDa to 160 kDa.

4.3 Results and Discussion

Droplet Analysis of mAb Standards

Before quantifying IgGs present within a complex background matrix, such as cell culture media, we wanted to determine whether IgG would be stable within a droplet microenvironment. It has been shown that high concentrations of proteins or other biomolecules present within a droplet can disrupt the droplet-carrier interface through interactions with the carrier phase and adhesion to surfaces in the fluid path[34]. This behavior can lead to unstable droplet flow, as well as carryover from sample to sample. Additionally, it has been demonstrated that some surfactants used to stabilize droplets can interact with and potentially disrupt protein analytes[35].

To test if the selected carrier phase and surfactant were compatible with mAb samples, 40 nL droplets containing 1 mg/mL of Sigma IgG1 standard in 200 mM ammonium acetate were generated. These droplets were alternated with blank droplets containing methanol and water in a 1:1 ratio with 0.5% formic acid. Droplets were then pumped into the nESI source at 400 nL/min. Over the course of these experiments (100 sample droplets) we observed a consistent droplet size and spacing for both samples and blanks (< 5% RSD in volume), indicating stable droplet

interfaces and flow (**Figure 4-2A**). When the total ion current associated with the most intense IgG charge state was extracted, we observe uniform time dependent signals corresponding to each sample droplet (peak area RSD of 5.1%). Furthermore, we detect less than 3% protein signal in blank droplets when compared to sample containing droplets, demonstrating little to no sample carryover between droplets (**Figure 4-2B**). Averaged spectra across a single sample droplet revealed the same native-like charge state distribution typically observed for IgG under continuous direct infusion conditions (**Figure 4-2C**).[36] This result suggests that the droplet microenvironment is not significantly altering the HOS of the mAb of interest. The averaged spectra across the blank samples contain very little signal in the m/z range associated with native-like mAbs, again indicating a lack of carryover between individual droplet samples (**Figure 4-2D**). Taken together, these results illustrate the conditions used here enable native-like protein nESI-MS from droplet samples with no carry-over between samples.

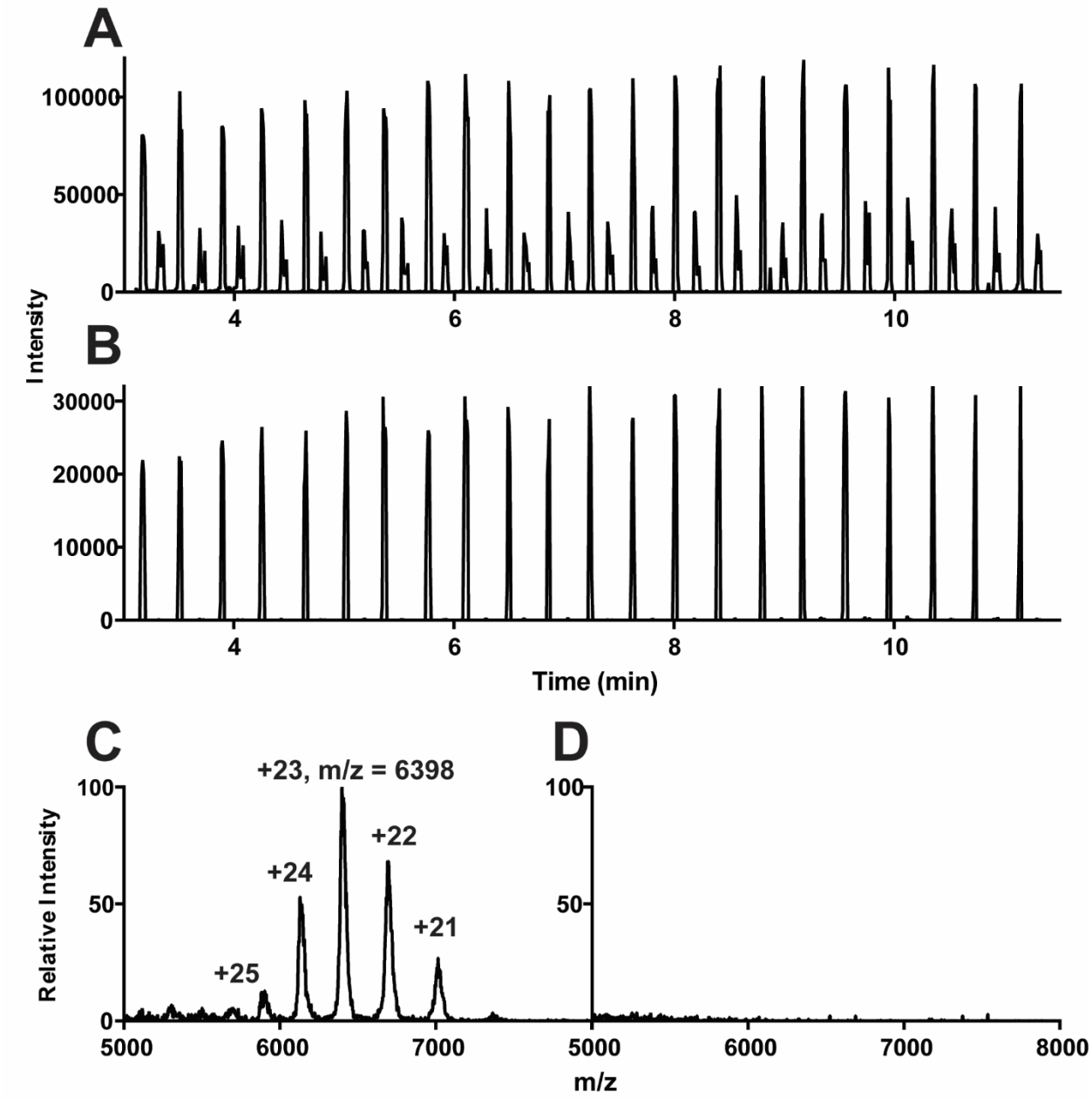

Figure 4-2. Example trace of Intact IgG infused to the MS via droplet nESI. Total ion chromatogram of incoming droplet train alternating between sample (1 mg/mL of IgG in 200 mM ammonium acetate) and blank (50:50 methanol:water, 0.5% formic acid) (A). Extracted ion chromatogram of most intense charge state, m/z = 6398 (B). Averaged mass spectra from a single sample droplet (C). Averaged mass spectra from a single blank droplet (D).

Selecting MS-Compatible Elution Buffers

Our primary interest for this work is the detection of mAbs that have been expressed in differing cell lines and growth conditions. While intact mAbs can be successfully analyzed via droplet-MS using standard native MS buffer conditions, the removal of salts and other cell-media components is necessary for mAb detection in our samples of interest. When purified mAb was spiked into clarified cell-culture media, we observe a loss of charge state resolution and unstable nESI currents in the MS data acquired **(Figure 4-3A)** as compared to MS data obtained from purified mAb samples housed in 200 mM ammonium acetate **(Figure 4-3B)**. Protein A affinity purification is a widely used method for the purification of IgG type antibodies[37]. The two most common elution buffers called for by protein A affinity protocols, citric acid and glycine, however, are not nESI-MS compatible. Citric acid is non-volatile and therefore resulted in poor ionization of our target mAb **(Figure 4-3C)**. Alternatively, glycine is readily ionizable, and thus causes ionization suppression of our analyte **(Figure 4-3D)**. We hypothesized that volatile, organic acids would be both MS appropriate and compatible with a protein A affinity purification approach. The target mAb was spiked into both 200 mM formic and acetic acid. Although improved spray stability was achieved and individual charge states were resolved in both buffers, acetic acid resulted in the best S/N and charge state resolution of the intact mAb (**Figure 4-4E,F**). In order to match our native MS control experiments described above, we maintained an ionic strength of 200 mM in our samples following protein A purification.

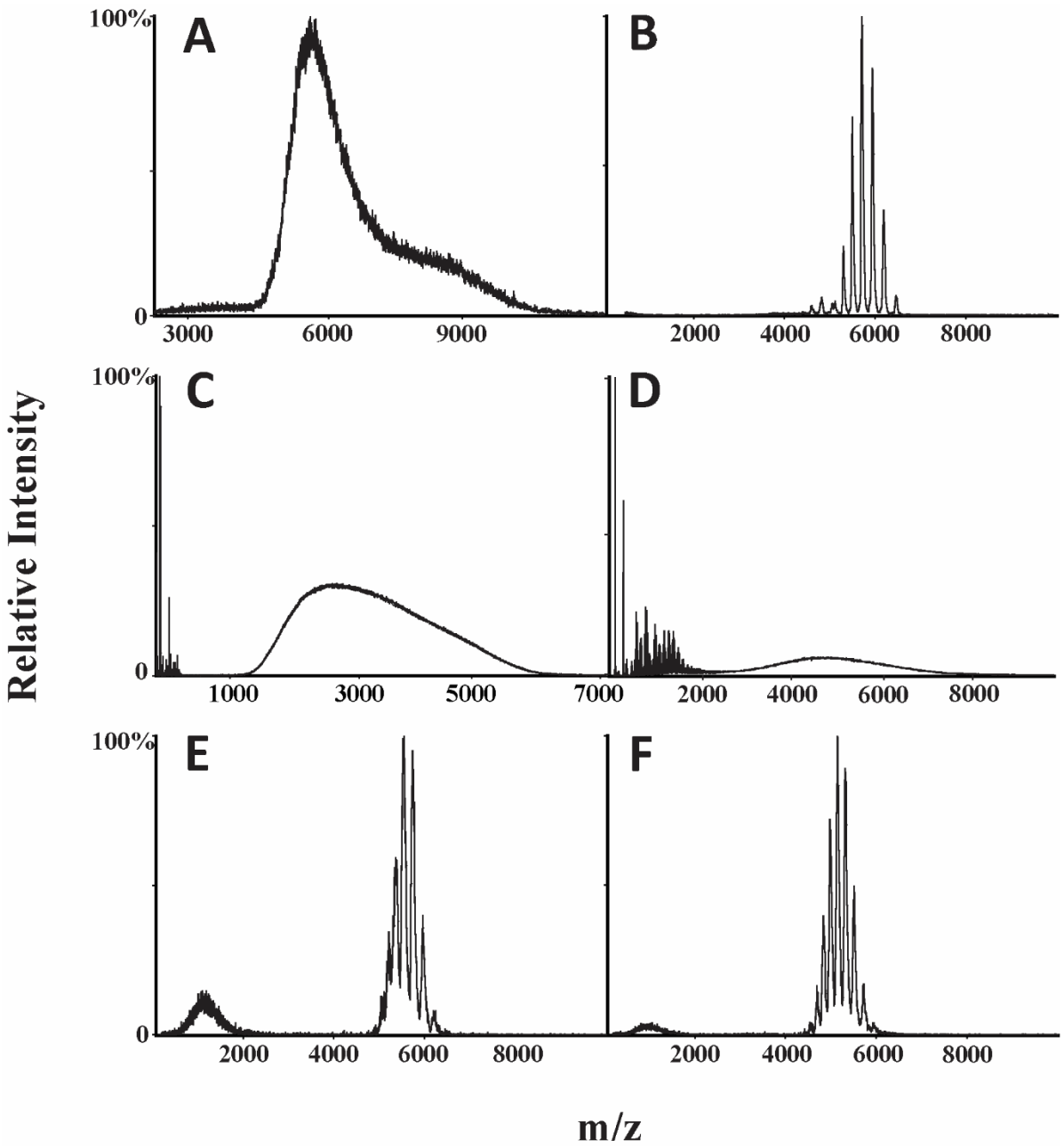

Figure 4-3. Comparison of mAb spectra in a selection of potential elution buffers for protein A affinity purification: 1 mg/mL purified mAb in clarified cell-expression media (A) 1 mg/mL purified mAb in 200 mM ammonium acetate (B) 1 mg/mL purified mAb in 200 mM (C) 1 mg/mL purified mAb in 200 mM glycine (D) 1mg/mL purified mAb in 200 mM formic acid (E) 1 mg/mL purified mAb in 200 mM acetic acid.

Optimization of Binding and Elution

Affinity purifications typically include an antibody binding step, wash step(s) to remove unwanted components from expression or storage matrices, and an elution step. To maximize recovery, we tested varying incubation durations for the binding step associated with our protein A purification. In order to mimic the matrix expected in cell culture samples, model mAbs were spiked into clarified cell-expression media then diluted 20-fold into 200 uL of PBS with 0.02% Tween-20 for a final concentration of 0.1 mg/mL. The samples were then co-incubated with protein A-modified magnetic beads, washed (3X), and eluted. Percent recovery was calculated by dividing the total mass loaded by the total mass recovered. Percent recovery plateaued at ~75% from a binding period of 20 min or longer **(Figure 4-4)**. A 20-min incubation period was chosen for all subsequent experiments, to maximize recovery while increasing the throughput of our sample cleanup.

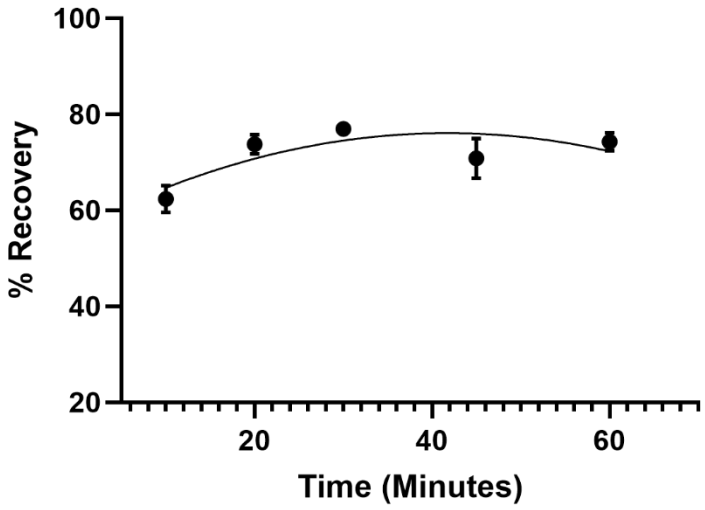

Figure 4-4. Percent recovery of mAb at different incubation periods during the Protein A binding step. Samples were diluted into PBS with 0.02% Tween-20 and loaded onto protein a-modified magnetic beads. Binding times ranged from 10 minutes to 60 minutes. Protein concentration in loaded and eluted samples was determined by A280 absorbance (n=3).

For compatibility with droplet generation from well-plates, it was necessary to reduce the volumes at each step in our protein A affinity purification method. A summary of the final protocol is shown below (**Table 4-1**). We observed no significant change in percent recovery upon reducing the volumes associated with our protein A purification strategy. Two wash steps were added to ensure thorough desalting, reduced adduction and optimized mass resolution. We did not detect any mAb sample loss during any of our wash steps.

Elution Step	Buffer	Volume (µL)	Time (min)
Binding	PBS, 0.02% Tween-20	100	20
Wash 1	DI Water	100	3
Wash 2	DI Water	100	3
Wash 3	DI Water	100	3
Elution	200 mM Acetic Acid	25	10

Table 4-1. Modified elution protocol for Dynabeads Protein A. Times represent the incubation period for each step.

In-Droplet Quantification

To use droplet MS to screen for cell culture conditions that produced the most recombinant mAb, it was necessary to evaluate if our native MS approach could provide quantitatively reliable data for such samples. In order to calibrate the MS intensity values recorded in our data against mAb concentrations in solution, our target mAb was spiked into clarified cell-expression media, then purified using our modified protein A protocol. Target mAb concentrations were measured pre- and post-purification using A280 absorbance as described above. Droplets were then generated and pumped into the MS for detection (**Figure 4-5A**).

The most intense charge state for our mAb of interest was the +25 charge state, at m/z = 5971 (**Figure 4-5B**). We found that using the height of this signal, rather than its area, or combined peak area and height values across all charge states, resulted in the best linearity (R^2 = 0.9922, LoD = 0.15 mg/mL, LoQ = 2.6 mg/mL) for our resulting calibration curves (**Figure 4-5C,D**). This

is likely because due to the challenges associated with distinguish protein signal from noise at lower mAb concentrations, leading to wider apparent peak widths for lower intensity charge states. Using total peak area to calculate mAb concentrations, however, had a better linear correspondence with results obtained by LC-MS,a widely accepted method for mAb quantification. (**Figure 4-7**).

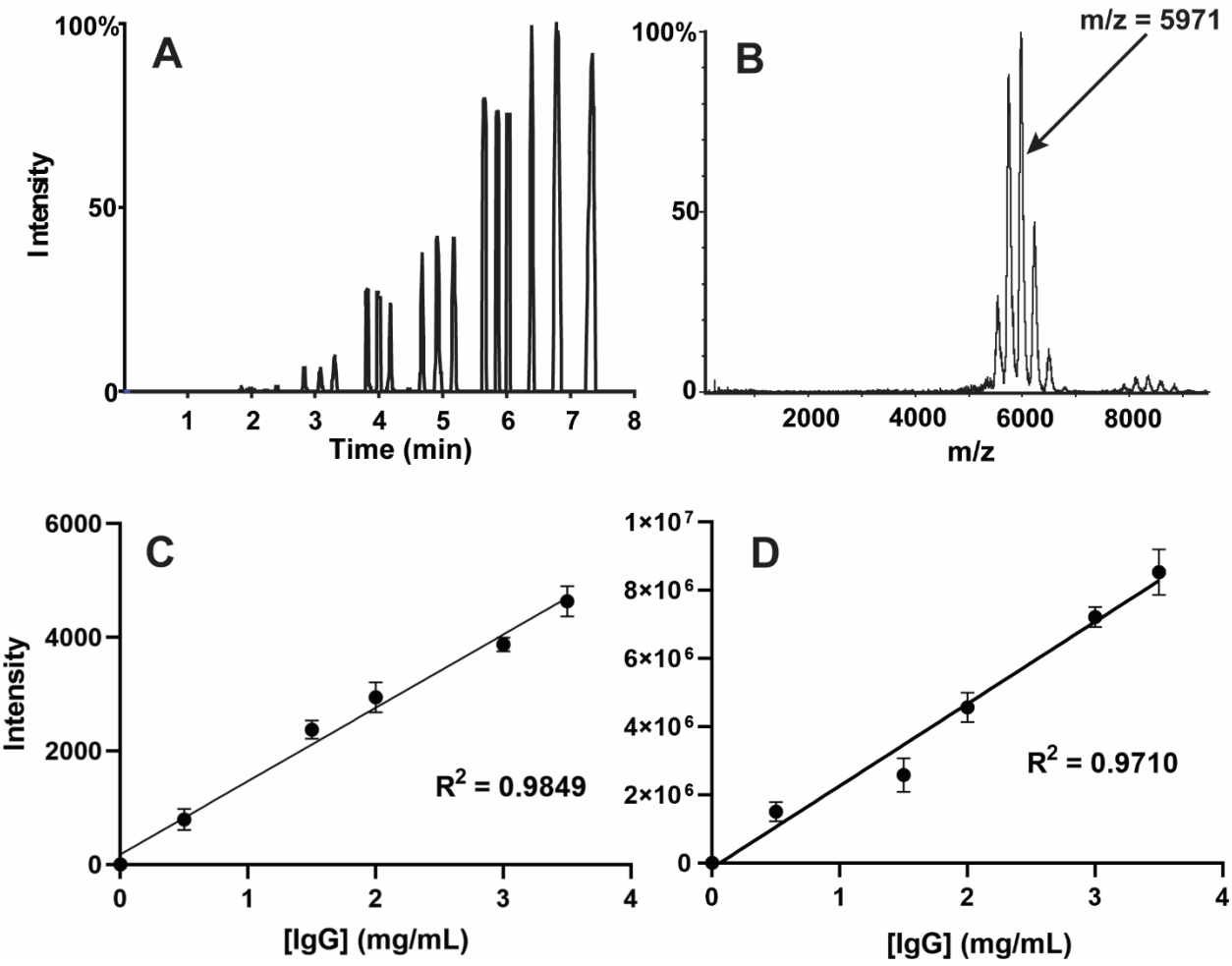

Figure 4-5. In-droplet calibration curve for mAb of interest. Extracted ion chromatogram of m/z = 5971 (A) Averaged spectra over a single droplet, highlighting the most intense charge state (B). Calibration curve generated using averaged peak height of m/z = 5971. Good linearity demonstrated from 0.1 mg/mL to 3.5 mg/mL (n=3) (C). Calibration curve generated using total peak area of all charge states from 0.1mg/mL to 3.5 mg/mL (n=3, from repeated in-droplet calibrations) (D).

Cell-Line Screen

We applied our droplet-MS method to 48 samples representing mAb expressed in Chinese Hampster Ovary (CHO) cells using different combinations of pH, temperature, and varying media components to determine which conditions promoted the largest amount of protein expression overall. Using the protein A purification method coupled to droplet sample introduction, as described above, these 48 samples were purified in 70 min and required a total MS analysis time of 20 min. Our MS data reveals differences in the intensities detected for the target mAb ions, indicating the presence of different mAb concentrations within each sample (**Figure 4-6**).

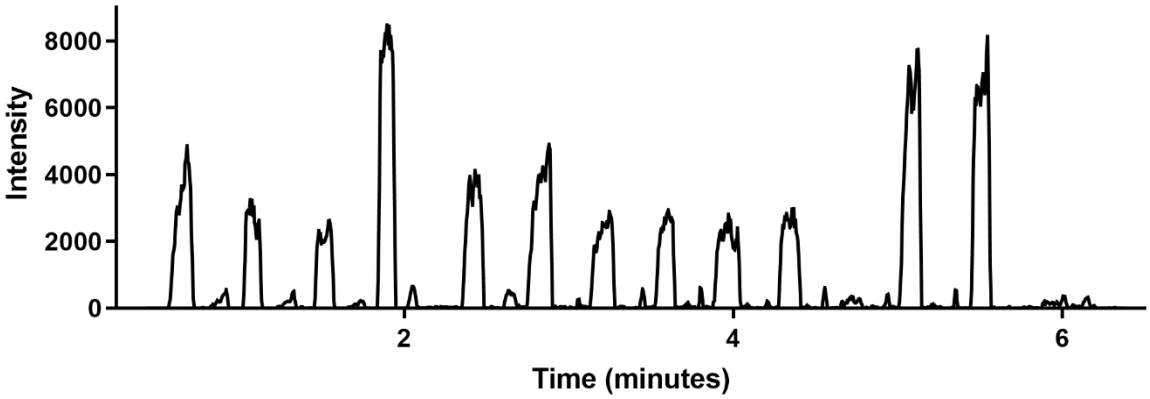

Figure 4-6. Segment of extracted ion chromatogram (m/z = 5791) of incoming droplet train. Differences in signal intensity can be observed between discrete sample droplets.

LC-MS methods are the gold-standard for mAb quantification; however, the typical affinity chromatography methods used for mAb purification and analysis take 10-20 min/sample. To evaluate the quantitative accuracy of our droplet-MS method we compared our results to measurements made by LC-MS (**Figure 4-7**). There was a good linear correlation between concentrations measured by LC-MS versus the droplet-MS method. Notably, both methods agreed on which expression conditions produced the most mAb and the droplet-MS method successfully identified all 8 blank samples (containing only expression media). Importantly, our droplet-MS

reduces the analysis time for a single sample by an order of magnitude, as compared to typical afiinity-based chromatographic chromatographic methods.[38,39] At 0.04 Hz, droplet-MS is on par with the fastest reported methods for mAb quantification from complex background matrices (0.03 Hz), without requiring the use of expensive robotics. There is potential for droplet-MS mAb quantification to reach even higher throughputs by increasing flow rates and decreasing droplet

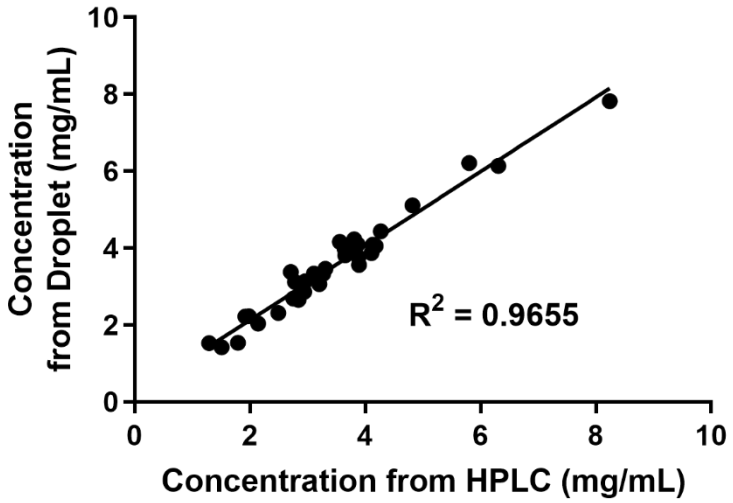

Figure 4-7. Relative quantitation of mAb in 48 different cell culture conditions. Concentration of mAb in 48 samples in cell culture media as measured by LC-MS versus concentration measured from droplet-MS assay following protein A purification. Droplet-MS values based on calibration curve derived from total peak area. A linear trendline demonstrates the correlation between the two methods.

size; however, this would likely be at the cost of sensitivity.

To further assess the accuracy and differentiating power of our droplet-MS method, we carried out a Bland-Altman analysis to quantitatively compare the two methods (**Figure 4-8**).[40,41] In the Bland Altman Analysis, the difference between the concentrations determined by each method are plotted against the average concentration determined by each method. The calculated bias is derived from the average of differences between the methods. The low bias, 0.08 ± 0.26, indicated no systematic error between the LC-MS and droplet-MS methods. The calculated confidence interval (95%) was sufficient for our purposes since the mean absolute error of our

measurements was 0.52 mg/mL. While the droplet-MS method would not be able to statistically differentiate between a sample that contained a concentration of 3 mg/mL mAb from one with 3.5 mg/mL, we can confidently identify the top 20% most concentrated mAb samples from our screen, thus enabling the identification of the most productive media conditions for mAb production.

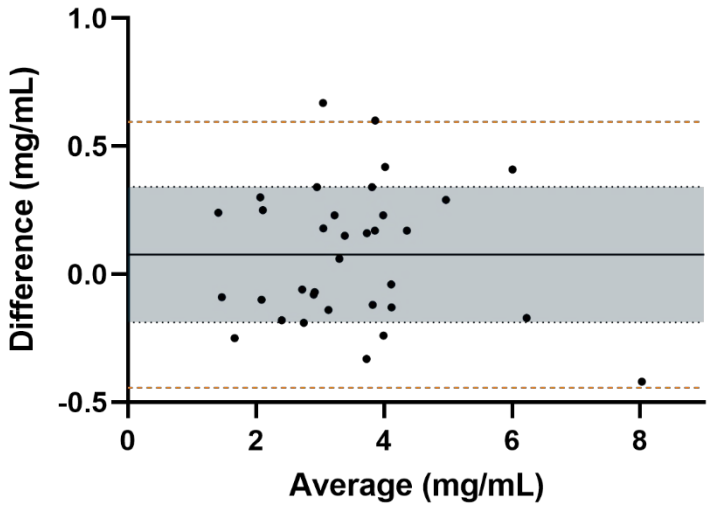

Figure 4-8. A Bland-Altman plot comparing the mAb concentration for each expression condition by LC-MS and droplet-MS. Bias with standard error (0.08 ± 0.26) is shown. The limits of agreement (or 95% confidence interval) is shown as calculated by bias ± 1.96*standard deviation of the differences between the two methods.

PTM Analysis

Understanding the PTM profiles of therapeutic mAbs is critical, as PTM modification can greatly affect the potency and efficacy of these biotherpeutics.[42] To supplement our work in identifying the most productive media conditions, we investigated the effect of expression conditions on the PTM profile of target mAb produced across three of the most productive cell culture conditions identified in the droplet-MS screen. High resolution MS was implemented, in tandem with the modified protein A cleanup protocol, for glycoform analysis. The high resolution MS data reveals evidence for a range of glycoforms associated with the intact mAb (**Figure 4-9B**).

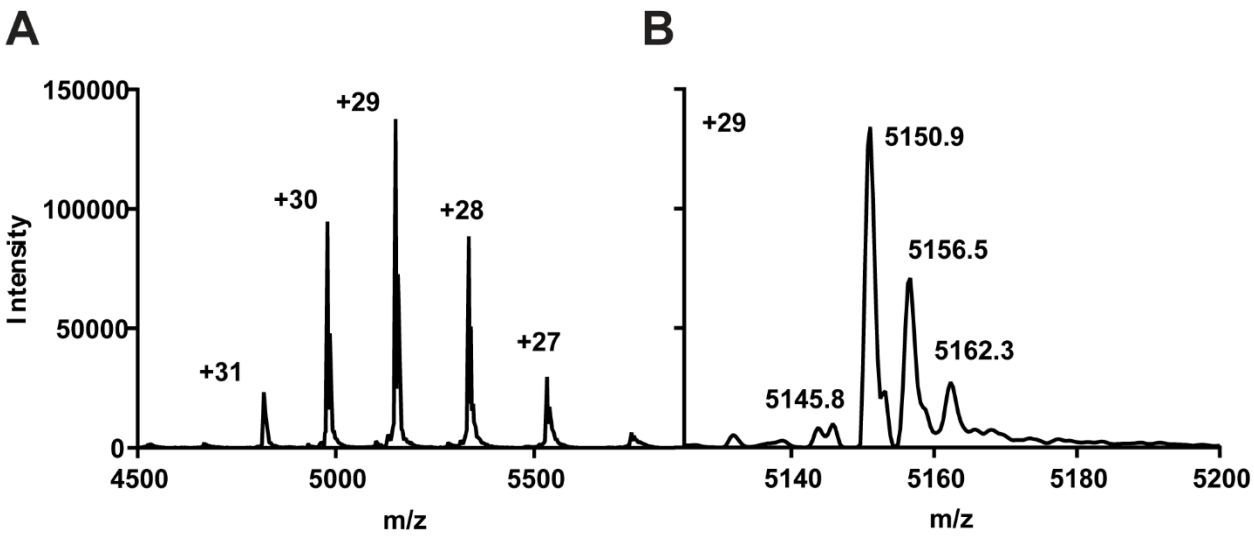

Figure 4-9. Example UHMR data for mAb purified from cell culture media. Full spectra for mAb of interest with bassline resolution of charge states (A). Zoomed-in view of the +29 charge state, where multiple modifications are resolved (B).

Mass deconvolution was employed to determine the molecular weight and possible identities of the modified mAb species present under different expression conditions (**Table 4-2**). While our data indicates that the most abundant glycoform detected shares the same molecular weight in each of the samples tested, we observe variations in relative intensities observed across the less abundant glycoforms detected, in some cases varying by as much as 40% in relative abundance. Additionally, there appears to be no obvious correlation between mAb expression levels and the glycoforms detected by native MS. Overall, our analysis demonstrates that PTM profiling of intact mAbs with direct infusion is possible with the use of the protein A cleanup and high-resolution MS, without the need for lengthier chromatographic approaches. Additionally, future droplet experiments coupled to high resolution MS could be prosecuted for direct, high throughput glycoform characterization and identification.

Sample	Average Mass (Da)	Relative Abundance (%)	Delta Mass (Da)
C4			
	149513.06	100	0.00
	149352.41	99.64	-160.66
	149680.28	56.59	167.22
	149558.64	34.75	45.58
	149375.50	31.91	-136.56
	149144.83	24.54	-368
	149788.88	23.24	275.81
	149849.27	22.08	336.20
	1496188.14	20.15	105.08
	149715.25	18.64	202.19
D6			
	149508.98	100.00	0.00
	149675.64	97.68	166.66
	149351.28	93.22	-157.70
	150055.69	58.08	546.70
	149738.25	52.57	229.27
	149974.41	47.26	465.42
	145081.63	44.94	-4427.36
	149870.58	44.90	361.59
	149408.36	41.84	-100.63
	149581.00	39.95	72.02
E6			
	149511.78	100.00	0.00
	149680.98	66.44	169.20
	149891.03	45.85	379.25
	149654.59	44.31	142.81
	149787.86	43.91	276.08
	150055.19	43.09	543.41
	149729.42	41.78	217.64
	150165.11	39.71	653.33
	149958.23	39.07	446.45
	149828.16	36.07	316.38

Table 4-2. Most abundant species in three different mAb expression conditions. The top ten masses derived from the deconvoluted spectrum are listed with their corresponding relative abundance and delta mass from the most abundant species present.

4.4 Conclusions

In this work we present a novel, MS-compatible protein A purification for mAbs coupled to a droplet microfluidic sample introduction format. It was determined that acetic acid can be used as a suitable elution buffer for protein A based purification, with good percent recovery (~75%). In-droplet calibration curves showed linearity over the concentration range of interest, producing an ultimate LOD of 0.15 mg/ml and LOQ of 2.6 mg/mL. This method was applied to a screen of 48 cell expression conditions, where we were able to determine relative differences in mAb production with increased throughput as compared to traditional chromatographic approaches. Additionally, the throughput of droplet-MS is on par with the fastest reports for mAb quantification from expression media, without necessitating the use of specialized robotic systems. Miniaturized protein A purification coupled to Droplet-MS could be readily implemented as a first-pass screening strategy for the production of many antibody-based therapeutics, although the sensitivity and quantitative capabilities of LC-MS are superior. Improvements to the droplet-MS system could be made by increasing sample recovery and the addition of an internal standard. Future work is aimed at coupling droplet sample introduction to high resolution MS for rapid glycan profiling. The ultimate goal would be to couple high resolution droplet-MS to an on-line, on-chip sample preparation for high-throughput PTM analysis.

4.5 References

(1) Urquhart, Li. Top Drugs and Companies by Sales in 2018. *Nat. Rev. Drug Discov.* **2019**, *18* (245).

(2) Weiner, G. J. Building Better Monoclonal Antibody-Based Therapeutics. *Nat. Publ. Gr.* **2015**. https://doi.org/10.1038/nrc3930.

(3) Cruz, E.; Kayser, V. Monoclonal Antibody Therapy of Solid Tumors: Clinical Limitations and Novel Strategies to Enhance Treatment Efficacy. *Biol. Targets Ther.* **2019**, *13*, 33–51. https://doi.org/10.2147/BTT.S166310.

(4) Shefet-Carasso, L.; Benhar, I. Antibody-Targeted Drugs and Drug Resistance—Challenges and Solutions. *Drug Resist. Updat.* **2015**, *18*, 36–46.

https://doi.org/10.1016/J.DRUP.2014.11.001.
(5) Glassman, P. M.; Balthasar, J. P. Mechanistic Considerations for the Use of Monoclonal Antibodies for Cancer Therapy. *Cancer Biol. Med.* **2014**, *11* (1), 20–33. https://doi.org/10.7497/j.issn.2095-3941.2014.01.002.
(6) Hafeez, U.; Gan, H. K.; Scott, A. M. Monoclonal Antibodies as Immunomodulatory Therapy against Cancer and Autoimmune Diseases. *Curr. Opin. Pharmacol.* **2018**, *41*, 114–121. https://doi.org/10.1016/J.COPH.2018.05.010.
(7) Jefferis, R. Glycosylation as a Strategy to Improve Antibody-Based Therapeutics. *Nat. Rev. Drug Discov.* **2009**, *8* (3), 226–234. https://doi.org/10.1038/nrd2804.
(8) Chiu, M. L.; Goulet, D. R.; Teplyakov, A.; Gilliland, G. L. Antibody Structure and Function: The Basis for Engineering Therapeutics. *Antibodies* **2019**, *8* (4), 55. https://doi.org/10.3390/antib8040055.
(9) Rodrigues, M. E.; Costa, A. R.; Henriques, M.; Azeredo, J.; Oliveira, R. Technological Progresses in Monoclonal Antibody Production Systems. *Biotechnol. Prog.* **2010**, *26* (2), 332–351. https://doi.org/10.1002/btpr.348.
(10) Rathore, A. S. Follow-on Protein Products: Scientific Issues, Developments and Challenges. *Trends Biotechnol.* **2009**, *27* (12), 698–705. https://doi.org/10.1016/J.TIBTECH.2009.09.004.
(11) Wang, Y.; Li, X.; Liu, Y. H.; Richardson, D.; Li, H.; Shameem, M.; Yang, X. Simultaneous Monitoring of Oxidation, Deamidation, Isomerization, and Glycosylation of Monoclonal Antibodies by Liquid Chromatography-Mass Spectrometry Method with Ultrafast Tryptic Digestion. *MAbs* **2016**, *8* (8), 1477–1486. https://doi.org/10.1080/19420862.2016.1226715.
(12) Alam, M. E.; Slaney, T. R.; Wu, L.; Das, T. K.; Kar, S.; Barnett, G. V.; Leone, A.; Tessier, P. M. Unique Impacts of Methionine Oxidation, Tryptophan Oxidation, and Asparagine Deamidation on Antibody Stability and Aggregation. *J. Pharm. Sci.* **2020**, *109* (1), 656–669. https://doi.org/10.1016/J.XPHS.2019.10.051.
(13) Schmid, I.; Bonnington, L.; Gerl, M.; Bomans, K.; Thaller, A. L.; Wagner, K.; Schlothauer, T.; Falkenstein, R.; Zimmermann, B.; Kopitz, J.; Hasmann, M.; Bauss, F.; Haberger, M.; Reusch, D.; Bulau, P. Assessment of Susceptible Chemical Modification Sites of Trastuzumab and Endogenous Human Immunoglobulins at Physiological Conditions. *Commun. Biol.* **2018**, *1* (1). https://doi.org/10.1038/s42003-018-0032-8.
(14) Moritz, B.; Stracke, J. O. Assessment of Disulfide and Hinge Modifications in Monoclonal Antibodies. *Electrophoresis* **2017**, *38*, 769–785. https://doi.org/10.1002/elps.201600425.
(15) Thompson, N. J.; Rosati, S.; Rose, R. J.; Heck, A. J. R. The Impact of Mass Spectrometry on the Study of Intact Antibodies: From Post-Translational Modifications to Structural Analysis. *Chem. Commun* **2013**, *49*, 538. https://doi.org/10.1039/c2cc36755f.
(16) Zhang, Z.; Pan, H.; Chen, X. Mass Spectrometry for Structural Characterization of Therapeutic Antibodies. *Mass Spectrom. Rev.* **2009**, *28* (1), 147–176. https://doi.org/10.1002/mas.20190.
(17) Tian, Y.; Ruotolo, B. T. Analyst CRITICAL REVIEW The Growing Role of Structural Mass Spectrometry in the Discovery and Development of Therapeutic Antibodies. *Cite this Anal.* **2018**, *143*, 2459. https://doi.org/10.1039/c8an00295a.
(18) Lanucara, F.; Eyers, C. E. Top-down Mass Spectrometry for the Analysis of Combinatorial Post-Translational Modifications. *Mass Spectrom. Rev.* **2013**, *32* (1), 27–42. https://doi.org/10.1002/mas.21348.
(19) Rosati, S.; Yang, Y.; Barendregt, A.; R Heck, A. J. Detailed Mass Analysis of Structural

Heterogeneity in Monoclonal Antibodies Using Native Mass Spectrometry. *Nat. Protoc.* **2014**. https://doi.org/10.1038/nprot.2014.057.

(20) Lermyte, F. Chapter 1 Modern Mass Spectrometry and Advanced Fragmentation Methods. In *Advanced Fragmentation Methods in Biomolecular Mass Spectrometry: Probing Primary and Higher Order Structure with Electrons, Photons and Surfaces*; The Royal Society of Chemistry, 2021; pp 1–14. https://doi.org/10.1039/9781839161056-00001.

(21) Tubaon, R. M.; Haddad, P. R.; Quirino, J. P. Sample Clean-up Strategies for ESI Mass Spectrometry Applications in Bottom-up Proteomics: Trends from 2012 to 2016. *Proteomics* **2017**, *17* (20). https://doi.org/10.1002/pmic.201700011.

(22) Donnelly, D. P.; Rawlins, C. M.; Dehart, C. J.; Fornelli, L.; Schachner, L. F.; Lin, Z.; Lippens, J. L.; Aluri, K. C.; Sarin, R.; Chen, B.; Lantz, C.; Jung, W.; Johnson, K. R.; Koller, A.; Wolff, J. J.; Campuzano, I. D. G.; Auclair, J. R.; Ivanov, A. R.; Whitelegge, J. P.; Paša-Tolić, L.; Chamot-Rooke, J.; Danis, P. O.; Smith, L. M.; Tsybin, Y. O.; Loo, J. A.; Ge, Y.; Kelleher, N. L.; Agar, J. N. Best Practices and Benchmarks for Intact Protein Analysis for Top-down Mass Spectrometry. *Nat. Methods*. https://doi.org/10.1038/s41592-019-0457-0.

(23) Dillon, T. M.; Bondarenko, P. V.; Speed Ricci, M. Development of an Analytical Reversed-Phase High-Performance Liquid Chromatography–Electrospray Ionization Mass Spectrometry Method for Characterization of Recombinant Antibodies. *J. Chromatogr. A* **2004**, *1053* (1–2), 299–305. https://doi.org/10.1016/J.CHROMA.2004.08.058.

(24) Kükrer, B.; Filipe, V.; Van Duijn, E.; Kasper, P. T.; Vreeken, R. J.; Heck, A. J. R.; Jiskoot, W. Mass Spectrometric Analysis of Intact Human Monoclonal Antibody Aggregates Fractionated by Size-Exclusion Chromatography. *Pharm. Res.* **2010**, *27* (10), 2197–2204. https://doi.org/10.1007/s11095-010-0224-5.

(25) Tassi, M.; De Vos, J.; Chatterjee, S.; Sobott, F.; Bones, J.; Eeltink, S. Advances in Native High-Performance Liquid Chromatography and Intact Mass Spectrometry for the Characterization of Biopharmaceutical Products. *J. Sep. Sci.* **2018**, *41* (1), 125–144. https://doi.org/10.1002/jssc.201700988.

(26) Chen, B.; Lin, Z.; J. Alpert, A.; Fu, C.; Zhang, Q.; A. Pritts, W.; Ge, Y. Online Hydrophobic Interaction Chromatography–Mass Spectrometry for the Analysis of Intact Monoclonal Antibodies. *Anal. Chem.* **2018**, *90* (12), 7135–7138. https://doi.org/10.1021/acs.analchem.8b01865.

(27) Ka, M.; Ghorasaini, M.; Hartmann, R.; Lehmann, F.; Bergquist, J.; Kovac, L.; Bergstro, S. Magnetic Beads for Desalting of Monoclonal Antibodies and Antibody−Drug Conjugates. *Anal. Chem* **2020**, *92*, 2. https://doi.org/10.1021/acs.analchem.0c01106.

(28) Sawyer, W. S.; Srikumar, N.; Carver, J.; Chu, P. Y.; Shen, A.; Xu, A.; Williams, A. J.; Spiess, C.; Wu, C.; Liu, Y.; Tran, J. C. High-Throughput Antibody Screening from Complex Matrices Using Intact Protein Electrospray Mass Spectrometry. *Proc. Natl. Acad. Sci. U. S. A.* **2020**, *117* (18), 9851–9856. https://doi.org/10.1073/pnas.1917383117.

(29) Pedde, R. D.; Li, H.; Borchers, C. H.; Akbari, M. Microfluidic-Mass Spectrometry Interfaces for Translational Proteomics. *Trends Biotechnol.* **2017**, *35* (10), 954–970. https://doi.org/10.1016/J.TIBTECH.2017.06.006.

(30) A. Smith, C.; Li, X.; H. Mize, T.; D. Sharpe, T.; I. Graziani, E.; Abell, C.; T. S. Huck, W. Sensitive, High Throughput Detection of Proteins in Individual, Surfactant-Stabilized Picoliter Droplets Using Nanoelectrospray Ionization Mass Spectrometry. *Anal. Chem.* **2013**, *85* (8), 3812–3816. https://doi.org/10.1021/ac400453t.

(31) Kempa, E. E.; Smith, C. A.; Li, X.; Bellina, B.; Richardson, K.; Pringle, S.; Galman, J. L.;

Turner, N. J.; Barran, P. E. Coupling Droplet Microfluidics with Mass Spectrometry for Ultrahigh-Throughput Analysis of Complex Mixtures up to and above 30 Hz. *Anal. Chem.* **2020**, *92* (18), 12605–12612. https://doi.org/10.1021/acs.analchem.0c02632.

(32) Sun, S.; Slaney, T. R.; Kennedy, R. T. Label Free Screening of Enzyme Inhibitors at Femtomole Scale Using Segmented Flow Electrospray Ionization Mass Spectrometry. *Anal. Chem.* **2012**, *84* (13), 5794–5800. https://doi.org/10.1021/ac3011389.

(33) Steyer, D. J.; T. Kennedy, R. High-Throughput Nanoelectrospray Ionization-Mass Spectrometry Analysis of Microfluidic Droplet Samples. *Anal. Chem.* **2019**, *91* (10), 6645–6651. https://doi.org/10.1021/acs.analchem.9b00571.

(34) Spencer Roach, L.; Song, H.; Ismagilov, R. F. Controlling Nonspecific Protein Adsorption in a Plug-Based Microfluidic System by Controlling Interfacial Chemistry Using Fluorous-Phase Surfactants. *J. Colloid Interface Sci* **2003**, *42* (2), 5. https://doi.org/10.1021/ac049061w.

(35) Turner, S. R.; Litt, M.; Lynn, W. S. Protein Adsorption to Teflon: Effect on Apparent Molecular Area of Dipalmitoyl Lecithin. *J. Colloid Interface Sci.* **1974**, *48* (1), 100–104. https://doi.org/10.1016/0021-9797(74)90331-2.

(36) Campuzano, I. D. G.; Netirojjanakul, C.; Nshanian, M.; Lippens, J. L.; Kilgour, D. P. A.; Van Orden, S.; Loo, J. A. Native-MS Analysis of Monoclonal Antibody Conjugates by Fourier Transform Ion Cyclotron Resonance Mass Spectrometry. *Anal. Chem.* **2018**, *90* (1), 745–751. https://doi.org/10.1021/ACS.ANALCHEM.7B03021/SUPPL_FILE/AC7B03021_SI_001.PDF.

(37) Arora, S.; Saxena, V.; Ayyar, B. V. Affinity Chromatography: A Versatile Technique for Antibody Purification. *Methods* **2017**, *116*, 84–94. https://doi.org/10.1016/J.YMETH.2016.12.010.

(38) Grom, M.; Kozorog, M.; Caserman, S.; Pohar, A.; Likozar, B. Protein A Affinity Chromatography of Chinese Hamster Ovary (CHO) Cell Culture Broths Containing Biopharmaceutical Monoclonal Antibody (MAb): Experiments and Mechanistic Transport, Binding and Equilibrium Modeling. *J. Chromatogr. B* **2018**, *1083*, 44–56. https://doi.org/10.1016/J.JCHROMB.2018.02.032.

(39) Farid, S. S. Process Economics of Industrial Monoclonal Antibody Manufacture. *J. Chromatogr. B* **2007**, *848* (1), 8–18. https://doi.org/10.1016/J.JCHROMB.2006.07.037.

(40) Martin Bland, J.; Altman, D. STATISTICAL METHODS FOR ASSESSING AGREEMENT BETWEEN TWO METHODS OF CLINICAL MEASUREMENT. *Lancet* **1986**, *327* (8476), 307–310. https://doi.org/https://doi.org/10.1016/S0140-6736(86)90837-8.

(41) Bland, J. M.; Altman, D. G. Measuring Agreement in Method Comparison Studies. *Stat. Methods Med. Res.* **1999**, *8* (2), 135–160. https://doi.org/10.1177/096228029900800204.

(42) Walsh, G.; Jefferis, R. Post-Translational Modifications in the Context of Therapeutic Proteins. *Nat. Biotechnol.* **2006**, *24* (10), 1241–1252. https://doi.org/10.1038/nbt1252.

Chapter 5: Conclusions and Future Directions

5.1 Conclusions

This thesis has described novel approaches of coupling droplet microfluidics to capillary electrophoresis (CE) and mass spectrometry (MS) for the study of intact proteins and protein-ligand interactions.

In Chapter 2, improvements were made to previous microchip capillary electrophoresis (MCE) separation for the monitoring of Sirtuin-5 (SIRT5) enzymatic turnover, reducing separation times from 250 ms to 150 ms while preserving analyte signal and resolution. Droplet sample loading on-chip was achieved using a density-based oil drain, and over 160 SIRT5 samples were screened at a throughput of 10s/sample. This work demonstrated that droplet-CE could be implemented as a high-throughput screening tool in the greater drug discovery process, although there are some limitations that must be considered. As with other chip-based methods, the MCE device is sensitive to matrix effects, limiting the number of samples that can be analyzed in a single experiment. Furthermore, the enzymatic reaction in each sample must be fully quenched prior to droplet formation. This is because small molecule compounds can easily diffuse through the low density oil, affecting enzymatic turnover in adjacent droplets. Despite these challenges, droplet-MCE is an attractive HTS approach for protein families that are prone to high false positive rates in traditional optical assays.

Rapid collision induced unfolding (CIU) data acquisition was coupled to droplet microfluidics to achieve high-throughput biophysical analysis of protein-ligand interactions in **Chapter 3**. Fingerprint acquisition time was reduced 10-fold and an overall throughput of 30

s/sample was achieved. This platform was applied to a 96- compound screen against SIRT5, where over 20 novel SIRT5 binders were identified. It was also shown that non-covalent complexes are preserved in the droplet microenvironment and that identified inhibitors stabilize select SIRT5 conformations in the gas phase, providing mechanistic insight into small molecule modulation of SIRT5 activity. In the grater discovery process droplet-CIU could function as a complimentary screening approach to standard optical activity assays, potentially replacing the slower and laborious calorimetry platforms. The binding information provided by rapid CIU workflows could help streamline lead development by providing important biophysical data earlier on in the drug development pipeline.

In **Chapter 4**, an MS-compatible sample cleanup method was developed and coupled to droplet-nESI for screening antibody production in different media conditions. Detection of monoclonal antibody (mAb) in a single droplet was achieved with an LOD and LOQ of 0.15 mg/mL and 2.6 mg/mL respectively. This method was applied to a panel of IgGs expressed in 48 different media samples to determine the most productive media conditions and was complemented with high-resolution MS for glycan profiling. Quantification of mAbs by droplet-MS was on par with the fastest reported methods for mAb screening from culture media, while reducing sample consumption and eliminating the need for specialized robotics. Although the droplet method was 10X faster than standard chromatographic methods, LC-MS is superior in terms of sensitivity and quantitative capabilities. Improvements in the protein A/droplet-MS screening should focus on increasing recovery and improving spray stability. Nonetheless, droplet MS provides a rapid way to identify the most fruitful conditions for mAb production. This workflow could be used to media conditions for an array of mAb-based biotherapeutics on a previously unattainable scale.

5.2 Future Directions

Improving Throughput, Data Acquisition, and Data Analysis of Droplet-CIU Assay

As demonstrated in Chapter 3, fast CIU coupled droplet sample introduction is a promising approach for providing insight into protein-ligand interaction, with higher throughput than traditional biophysical methods. An immediate way to improve upon this method would be to increase the throughput of both sample introduction and data acquisition. Increasing the rate of sample introduction would be relatively straightforward through the reduction of sample volumes and increase in flow rates, although there are limitations on max flow rate compatibility with the 30 μm emitters used in the droplet-CIU experiments.[1] Larger emitters could be used with some sacrifice in sensitivity.[2]

The primary limitation in the throughput of our data acquisition was the effective scanning rate, set at 300 ms. This is due to an internal averaging of MS scans into what is termed "spectral bins" by the software. Faster scan rates or smaller collision voltage dwell times resulted in electronic breakdown and an inability to generate CIU fingerprints. To circumvent this, a variant of the Waters SONAR faster scanning acquisition mode could be installed on the instrument.[3] The use of this software in conjunction with droplet sample instruction has been demonstrated, with an acquisition rate equivalent to 200 spectra/s and a 5-fold increase in sampling points.[4] Additionally, further improvements could be made with the automation of the data acquisition. In the current workflow instrument control methods for CIU acquisitions were generated automatically, but the actual start of the data collection was performed manually and had to be timed with each droplet sample. MS-signal dependent data acquisition would streamline fast CIU process, where collision voltages would be ramped once a set analyte signal is detected. Such MS-signal dependent

softwares have been integrated with both droplet-ms and acoustic ionization-MS to trigger processes such as sample sorting, data collection, and signal averaging from individual samples.[3,5]

The greatest challenge in implementing droplet-CIU as a truly high-throughput screening method lies in the data analysis process. CIU experiments generate complex and information rich data sets that can be challenging to evaluate, despite advances in data analysis software. For example, it took ~ 1 week to analayze the 96 compounds screened against SIRT5 in **Chapter 2**. Such long analysis times render CIU impractical for large-scale screening endeavors. Future work should focus on developing machine learning algorithms to automatically generate, fit, and differentiate fingerprints, streamlining data processing.

Application of Droplet-CIU Workflow to Other Protein Systems of Interest

The utility of CIU for drug discovery has demonstrated but has not been employed in larger scale screening efforts due previous limitations in throughput and sample requirements.[6] One example is the use of CIU to distinguish between ATP-competitive and allosteric ligand binders of the Abelson protein tyrosine kinase (Abl).[7] Abl forms an oncogenic chimeric protein and is an important pharmacological target for the treatment of chronic myeloid leukemia.[8] While there are a number of FDA approved kinase inhibitors that target the ATP-binding domain, Abl commonly has mutations that will prevent these inhibitors from binding. As a result, there is interest in identifying inhibitors that bind at allosteric sites.[9,10]

It was found that there were dramatic differences in the CIU fingerprints of ATP-binding vs allosteric protein-inhibitor complexes, with a highly differentiating region in the 39-40V range (**Figure 5-1**).[7] With relatively low throughput (10 min/sample) and the need for manual introduction, this study was limited to nine compounds. The droplet-CIU platform and fast data

acquisition developed in Chapter 3 could readily be applied to a Abl kinase screen for the identification of allosteric inhibitors, with a focus on the differentiating voltages.

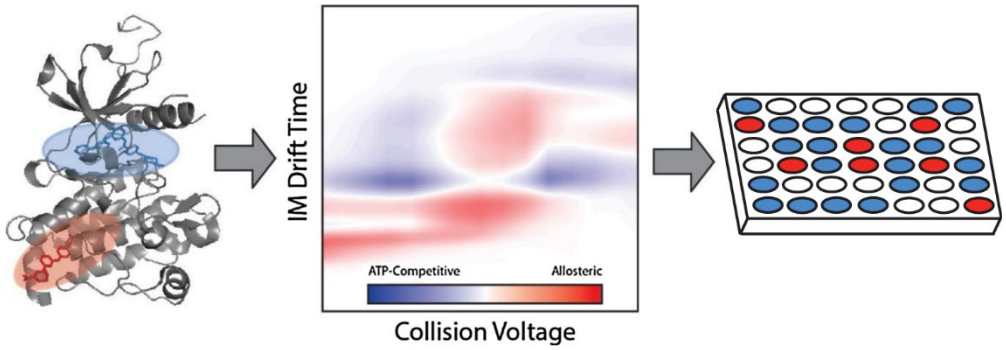

Figure 5-1. Schematic illustrating identification of allosteric Abl binders by CIU. Crystal structure of Abl kinase depicting binding locations of ATP-competitive (blue) and allosteric (red) inhibitors. Representative RMSD analysis highlighting differences in fingerprints generated from Abl-ligand complexes with ATP-competitive vs allosteric inhibitors (B). Data generated from a high-throughput CIU screen could be correlated back to their respective samples and used to distinguish inhibitors with different binding mechanisms (C). Adapted from Rabuck-Gibbons, 2018.

Beyond the study of protein-ligand interactions, CIU assays have been applied to biotherapeutics, such as mAbs. Extensive characterization of mAbs is critical for determining their stability and efficacy as a biopharmaceutical. CIU fingerprinting has been shown to be sensitive towards differences in glycosylation patterns, disulfide bridges, and small molecule conjugation, and biosimilars[11–15]. The droplet-based platform developed in Chapter 3 could be applied to classifying a broader range of mAbs, due to the high-throughput capabilities and lower sample requirements. This workflow could also be combined with the sample preparation methods described in Chapter 4 to investigate the effects of differing media conditions on mAb stability. The data generated from such experiments would also prove instrumental in constructing an antibody CIU fingerprint database for better classification of these biotherapeutics.

Interfacing Droplet Microfluidics with High-Resolution MS for PTM Profiling

Post translational modifications (PTMs), such as glycosylation, can significantly alter the stability and functionality of therapeutic mAbs.[16,17] Glycosylation patterns can be difficult to analyze due to the high heterogeneity in a given mAb population; however, high-resolution MS has proven to be a powerful tool for PTM characterization.[18] As with other MS-based screening approaches, the bottleneck for analysis throughput is sample introduction. There is a precedent for coupling droplet microfluidics for the detection of intact proteins by high-resolution MS, although this has not been demonstrated with mAbs.[4] Preliminary work has been done to couple our protein-A sample prep and droplet method to a UHMR Orbitrap MS (**Figure 5-2A**). Low signal intensity, likely due to the slow scanning rate and interfering surfactant noise, precluded the detection of discrete glycosylation states within a single droplet (**Figure 5-2B**). Future work

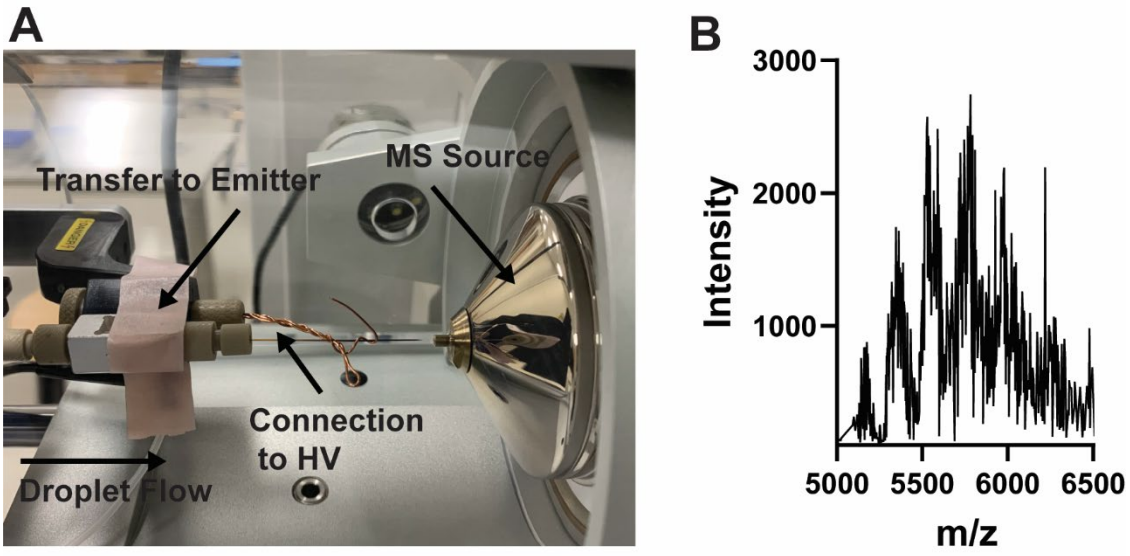

Figure 5-2. Interfacing droplet microfluidics with high-resolution MS for intact mAb detection. Image of droplet sample introduction coupled to a UHMR Orbitrap (A). Sample flow is driven by syringe pump and transferred to the nESI emitter via a zero dead volume PicoClear union. The union is secured to the xyz-stage and a copper wire is used to directly connect the emitter tip to the high voltage (HV) source. The emitter tip is then aligned with the instrument source. MS signal of a mAb averaged across a single 20 nL droplet (B).

should focus on optimizing ion transmission to increase mAb signal and decrease background surfactant noise to enable PTM characterization with intact protein samples.

Finally, droplet microfluidics could be coupled with an on-line, in-droplet trypsin digest for rapid mAb sequencing and PTM profiling. It has been shown a 1 ms protein digestion time can be achieved through the use of nESI and an accompanying sheath flow of nitrogen gas.[19] By coupling this digestion to a high-resolution MS, 100% sequence coverage for the light chains and 85% sequence coverage for the heavy chains of the therapeutic traztuzumab was achieved. This platform could readily be adapted to droplet flow, using the proposed design in **Figure 5-3**.

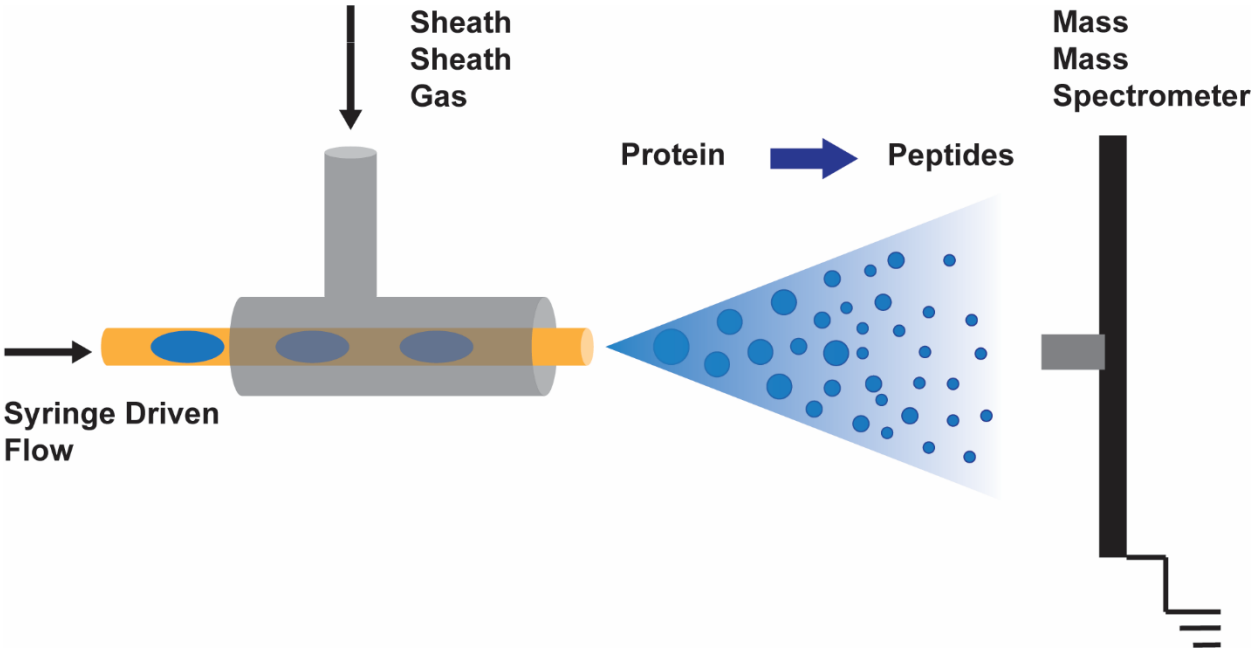

Figure 5-3. Proposed design for pairing droplet nESI with a rapid trypsin digest for high-throughput protein sequencing.

In this setup, droplets are generated from a well plate containing mAb samples with trypsin. Droplet samples are then flowed toward the nESI emitter and desolvation is aided using a sheath gas. The trypsin digest is accelerated in the plume of microdroplets formed. The greatest challenge would arise with the large amounts of data generated and a need for automated data analysis,

nevertheless combining droplet microfluidics with online trypsin digestion would enable rapid sequencing and provide information about PTM localization in a high-throughput fashion.

The ultimate goal would be the coupling of an on-line microfluidic sample preparation system to high resolution droplet-MS for intact protein and PTM analyses. A proposed microfluidic system is illustrated in **Figure 5-4** where a Coalesce-Attract-Resegment Wash" (CAR-Wash) approach would be used to remove cell media or storage buffer.[20] Protein samples would then need to be eluted prior to introduction into the MS. As with other structural MS approaches, this workflow would benefit from automated data analysis tools that could extract data from individual droplet traces, deconvolute spectra, and provide general PTM assignments. High-

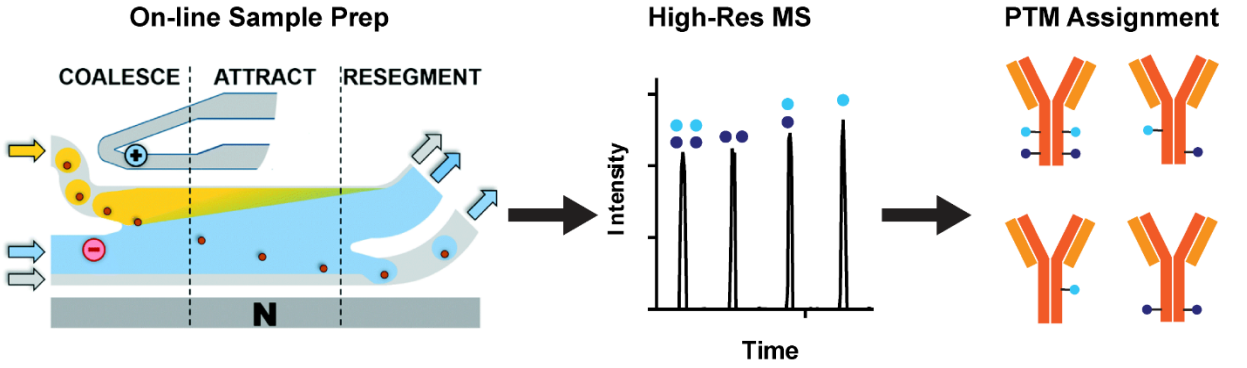

Figure 5-4. Proposed design for pairing CAR-wash approach with high resolution mass spectrometry for PTM profiling. Antibodies are loaded onto magnetic beads and washed through electrocoalescing. Droplets are then pumped into the mass spectrometer and subsequently analyzed for glycans and other modifications. Modified in part from Doonan, 2019.

throughput PTM analysis would have applications in several biomedical fields beyond biotherapeutic characterization, such as biomarker analysis and identification. The key challenges that remain are building robust microfluidic systems and developing data analysis tools to handle the vast amounts of chemical information generated.

5.3 References

(1) Steyer, D. J.; Kennedy, R. T. High-Throughput Nanoelectrospray Ionization-Mass Spectrometry Analysis of Microfluidic Droplet Samples. *Anal. Chem.* **2019**. https://doi.org/10.1021/acs.analchem.9b00571.

(2) Gibson, G. T. T.; Mugo, S. M.; Oleschuk, R. D. Nanoelectrospray Emitters: Trends and Perspective. *Mass Spectrom. Rev.* **2009**, *28* (6), 918–936. https://doi.org/10.1002/MAS.20248.

(3) Sinclair, I.; Bachman, M.; Addison, D.; Rohman, M.; C. Murray, D.; Davies, G.; Mouchet, E.; E. Tonge, M.; G. Stearns, R.; Ghislain, L.; S. Datwani, S.; Majlof, L.; Hall, E.; R. Jones, G.; Hoyes, E.; Olechno, J.; N. Ellson, R.; E. Barran, P.; D. Pringle, S.; R. Morris, M.; Wingfield, J. Acoustic Mist Ionization Platform for Direct and Contactless Ultrahigh-Throughput Mass Spectrometry Analysis of Liquid Samples. *Anal. Chem.* **2019**, *91* (6), 3790–3794. https://doi.org/10.1021/acs.analchem.9b00142.

(4) Kempa, E. E.; Smith, C. A.; Li, X.; Bellina, B.; Richardson, K.; Pringle, S.; Galman, J. L.; Turner, N. J.; Barran, P. E. Coupling Droplet Microfluidics with Mass Spectrometry for Ultrahigh-Throughput Analysis of Complex Mixtures up to and above 30 Hz. *Anal. Chem.* **2020**, *92* (18), 12605–12612. https://doi.org/10.1021/acs.analchem.0c02632.

(5) Holland-Moritz, D. A.; Wismer, M. K.; Mann, B. F.; Farasat, I.; Devine, P.; Guetschow, E. D.; Mangion, I.; Welch, C. J.; Moore, J. C.; Sun, S.; Kennedy, R. T. High-Throughput Screening Hot Paper Mass Activated Droplet Sorting (MADS) Enables High-Throughput Screening of Enzymatic Reactions at Nanoliter Scale. https://doi.org/10.1002/ange.201913203.

(6) Eschweiler, J. D.; Kerr, R.; Rabuck-Gibbons, J.; Ruotolo, B. T. Sizing Up Protein-Ligand Complexes: The Rise of Structural Mass Spectrometry Approaches in the Pharmaceutical Sciences. *Annu. Rev. Anal. Chem* **2017**, *10*, 25–44. https://doi.org/10.1146/annurev-anchem.

(7) Rabuck-Gibbons, J. N.; Keating, J. E.; Ruotolo, B. T. Collision Induced Unfolding and Dissociation Differentiates ATP-Competitive from Allosteric Protein Tyrosine Kinase Inhibitors. *Int. J. Mass Spectrom.* **2018**, *427*, 151–156. https://doi.org/10.1016/J.IJMS.2017.12.002.

(8) Deininger, M. W. N.; Goldman, J. M.; Melo, J. V. The Molecular Biology of Chronic Myeloid Leukemia. *Blood* **2000**, *96* (10), 3343–3356. https://doi.org/10.1182/BLOOD.V96.10.3343.

(9) Wu, P.; Nielsen, T. E.; Clausen, M. H. Small-Molecule Kinase Inhibitors: An Analysis of FDA-Approved Drugs. *Drug Discov. Today* **2016**, *21* (1), 5–10. https://doi.org/10.1016/J.DRUDIS.2015.07.008.

(10) Kuwano, M.; Sonoda, K.; Murakami, Y.; Watari, K.; Ono, M. Overcoming Drug Resistance to Receptor Tyrosine Kinase Inhibitors: Learning from Lung Cancer. *Pharmacol. Ther.* **2016**, *161*, 97–110. https://doi.org/10.1016/J.PHARMTHERA.2016.03.002.

(11) Beck, A.; Debaene, F.; Diemer, H.; Wagner-Rousset, E.; Colas, O.; Dorsselaer, A. Van; Cianférani, S. Cutting-Edge Mass Spectrometry Characterization of Originator, Biosimilar and Biobetter Antibodies. **2015**. https://doi.org/10.1002/jms.3554.

(12) Pisupati, K.; Benet, A.; Tian, Y.; Okbazghi, S.; Kang, J.; Ford, M.; Saveliev, S.; Sen, K. I.; Carlson, E.; Tolbert, T. J.; Ruotolo, B. T.; Schwendeman, S. P.; Schwendeman, A. MAbs Biosimilarity under Stress: A Forced Degradation Study of Remicade® and Remsima™ Biosimilarity under Stress: A Forced Degradation Study of Remicade Ò and Remsima TM. **2017**. https://doi.org/10.1080/19420862.2017.1347741.

(13) Tian, Y.; Ruotolo, B. T. Collision Induced Unfolding Detects Subtle Differences in Intact Antibody Glycoforms and Associated Fragments. *Int. J. Mass Spectrom.* **2018**, *425*, 1–9. https://doi.org/10.1016/J.IJMS.2017.12.005.

(14) Bagal, D.; F. Valliere-Douglass, J.; Balland, A.; D. Schnier, P. Resolving Disulfide Structural Isoforms of IgG2 Monoclonal Antibodies by Ion Mobility Mass Spectrometry. *Anal. Chem.* **2010**, *82* (16), 6751–6755. https://doi.org/10.1021/ac1013139.

(15) Tian, Y.; Han, L.; C. Buckner, A.; T. Ruotolo, B. Collision Induced Unfolding of Intact Antibodies: Rapid Characterization of Disulfide Bonding Patterns, Glycosylation, and Structures. *Anal. Chem.* **2015**, *87* (22), 11509–11515. https://doi.org/10.1021/acs.analchem.5b03291.

(16) Zheng, K.; Bantog, C.; Bayer, R. MAbs The Impact of Glycosylation on Monoclonal Antibody Conformation and Stability. **2011**. https://doi.org/10.4161/mabs.3.6.17922.

(17) Cymer, F.; Beck, H.; Rohde, A.; Reusch, D. Therapeutic Monoclonal Antibody N-Glycosylation – Structure, Function and Therapeutic Potential. *Biologicals* **2018**, *52*, 1–11. https://doi.org/10.1016/J.BIOLOGICALS.2017.11.001.

(18) Tian, Y.; Ruotolo, B. T. Analyst CRITICAL REVIEW The Growing Role of Structural Mass Spectrometry in the Discovery and Development of Therapeutic Antibodies. *Cite this Anal.* **2018**, *143*, 2459. https://doi.org/10.1039/c8an00295a.

(19) Zhong, X.; Chen, H.; Zare, R. N. Ultrafast Enzymatic Digestion of Proteins by Microdroplet Mass Spectrometry. https://doi.org/10.1038/s41467-020-14877-x.

(20) Doonan, S. R.; Lin, M.; Bailey, R. C. Droplet CAR-Wash: Continuous Picoliter-Scale Immunocapture and Washing. *Lab Chip* **2019**, *19* (9), 1589–1598. https://doi.org/10.1039/C9LC00125E.

Appendix

Supporting information for Chapter 2: Working towards a label-free, droplet-MS assay for the analysis of Sirtuin-5 enzymatic activity.

Label-Free MS Assay with Online Reagent Addition

While we were able to develop a high throughput droplet-MCE method for screening SIRT5 activity, we wanted to develop a label free assay that could also be coupled to online reagent addition. MS represents a powerful method for label-free screening of enzymatic turnover. Because MS measures the mass to charge ratio of an analyte, there is no need to label the substrate, limiting possible non-specific interactions. Additionally, coupling droplet microfluidics to MS is simpler than coupling droplet sample introduction to CE or MCE because the carrier phase does not need to be removed prior to infusion to the mass spectrometer. We developed a microfluidic system screening SIRT5 inhibitors including reagent addition, in-droplet incubation, followed by

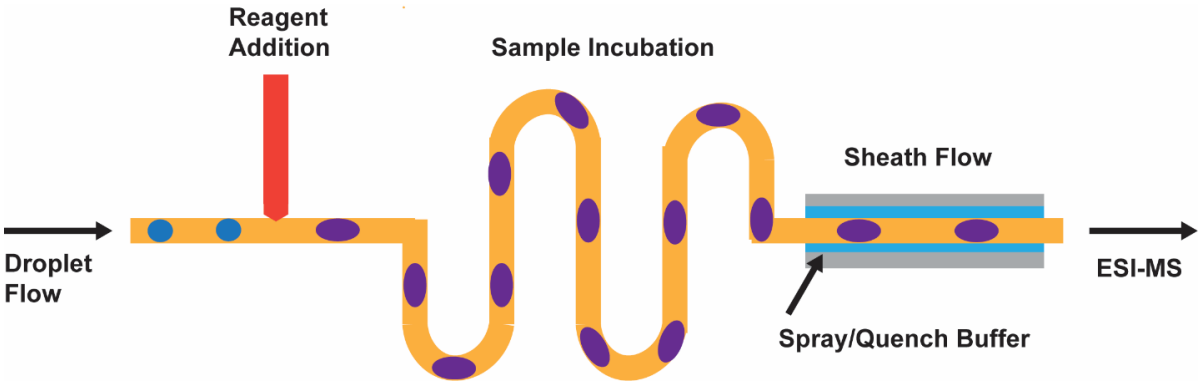

Figure I-1. Illustration of microfluidic platform for SIRT5 inhibitor screening. Droplets containing inhibitor, 1µM peptide substrate, 1 µM internal standard are flowed through using syringe driven flow. Reagent stream containing 45 nM SIRT5 is added to droplets. Droplets are then incubated and finally quenched with 80% acetonitrile (ACN), 20% water, and 0.1% formic acid prior to infusion into the MS.

reaction quenching and direct infusion into the mass spectrometer via a sheath flow source (**Figure I-1**).

Before coupling droplet-sample introduction to MS, it was necessary to find MS compatible buffers for the SIRT5 reaction. Use of the typical reaction buffer in SIRT5 activity assays (1 mM 1,4-dithiothreitol, 0.5 mM NAD^+, 4.5% (v/v) glycerol, 30 mM NaCl, and 2 mM sodium phosphate) caused ionization suppression of the analytes, resulting in no observable signal for the substrate or product peptides (**Figure I-2A**). Ammonium bicarbonate has been shown to

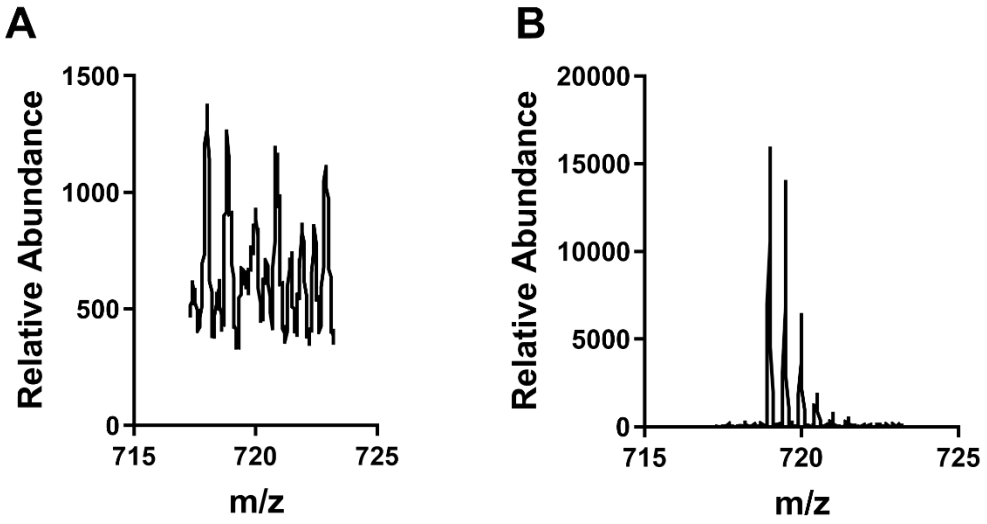

Figure I-2. Spectra of +2 charge state for SIRT5 substrate peptide. No peptide signal is observed when sample is infused from traditional SIRT5 buffer (A). Clear peptide signal observed when sample is infused from ammonium bicarbonate buffer (B). Substrate peptide concentration was held at 1 μM.

be a MS compatible buffer that also preserves enzymatic function. Substrate signal was observable with good S/N at the expected mass when infused from ammonium bicarbonate, with no other salts present (**Figure I-2B**). To test the activity of SIRT5 in ammonium bicarbonate, reaction progress was monitored from 5 min to 30 min. It was found that reaction yield still proceeded to 100% in ammonium bicarbonate, with the linear range up to 15 min (**Figure I-3**).

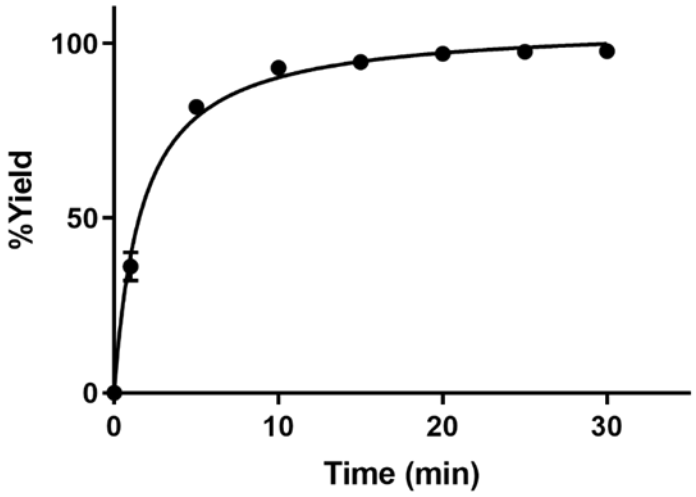

Figure I-4. Reaction progress of SIRT5 in ammonium bicarbonate. Samples contained 1 µM substrate and 45 nM SIRT5 and were quenched with 80% acetonitrile (ACN), 20% water, and 0.1% formic acid (n=3).

After verifying SIRT5 enzymatic activity in ammonium bicarbonate, it was important to test the stability of droplet infusion into the MS. A total of 120 droplets containing 1 µM substrate were perfused into the MS over the course of 20 min (**Figure I-4**). Droplet peak area across the entire time course was 6.8 %, indicating stable droplet flow and sample introduction. Stable device function is critical in HTS applications where there may be hundreds or thousands of samples to screen.

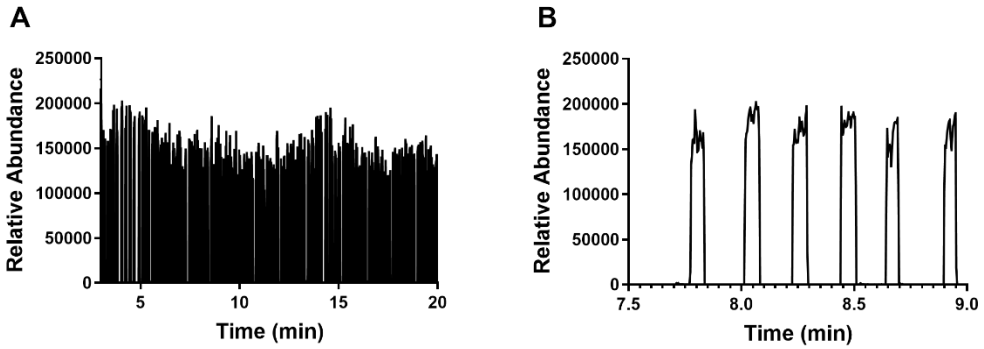

Figure I-3. Continuous droplet infusion into MS. Extracted ion chromatogram of 120 droplets containing 1 µM peptide directly infused into the MS over 20 min (A). Zoomed-in view from 7.5 min to 6 min reveals 6 individual droplet traces (B).

Although reactions in droplets occur at the low nL scale, reagent usage is determined by the amount of material plated in the multi-well plate for droplet generation. To further reduce the

consumption of valuable reagents (e.g., SIRT5 enzyme), we wanted to integrate a microfluidic reagent addition device to our droplet-based method. In this microfluidic setup, less than 1.2 µg of SIRT5 would be consumed for 100 reactions. PDMS devices were fabricated where teflon tubing containing droplet trains could be directly inserted (**Figure I-5**). After receiving reagent from the orthogonal reagent stream, droplets could be directly exported off the PDMS chip via teflon tubing for ESI-MS analysis. Because droplets were stabilized with 0.5 % PFO in the PFD carrier phase, it was necessary to use electrodes to disrupt droplet surface tension at the junction with the reagent stream and ensure merging. With a droplet flow rate of 800 nL/min and a reagent flow rate of 200 nL/min, it was demonstrated that droplets doubled in volume to 8 nL with consistent addition of reagent (**Figure I-5B**). Stock solutions containing 90 nM of SIRT5 were used for further experiments to ensure a 45 nM concertation of enzyme in each reaction droplet.

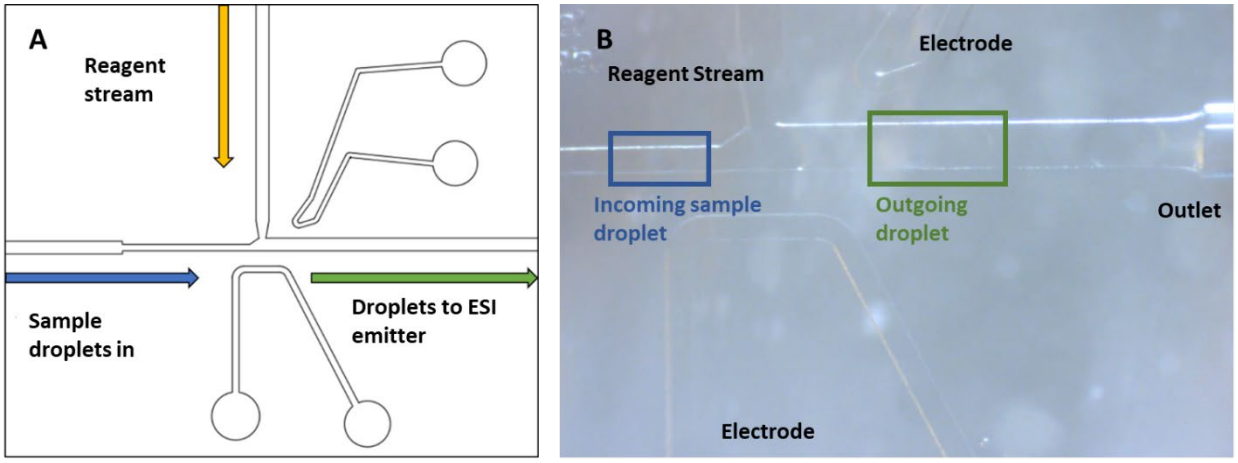

Figure I-5. Reagent addition device operation. Illustration of device showing direction and geometry of reagent and droplet flow. Electrodes were used to facilitate merging with the reagent stream (A). Samples contained 1 µM substrate peptide in ammonium bicarbonate. Incoming droplets were 4 nL in volume with 12 nL oil spacing and droplet flow was 800 nL/min. Reagent stream was continuous and flowed at 200 nL/min. Outgoing droplets were found to be increase 100% ± 7% in volume following reagent addition (B) (n=30).

To test the ability of our MS assay to quantify SIRT5 enzymatic turnover, an in-droplet calibration curve was performed **(Figure I-6)**. Sample droplets were generated from wells containing known amounts of substrate peptide and flowed through the reagent addition device. The reagent addition stream contained reaction buffer with no enzyme. Ten droplets were generated for each concentration and peak heights were averaged across the four middle droplets from each sample. >50% RSD in signal variation can be observed in the blank droplets in the total ion chromatogram; however, this is likely attributed to flow instability and background noise for the sheath flow prior to being fully equilibrated. The extracted ion chromatogram shows no significant peptide signal in the blank droplets. Good linearity was achieved from 0 nM to 1 µM, the working concentration range for our SIRT5 assay. Overall, this microfluidic setup is a potential first-step towards screening against SIRT5 activity in a high-throughput, label-free manner. With long-term operation of reagent addition and droplet sample introduction to MS, future work is focused on screening a larger (>1000 compounds) library against SIRT5 to identify new inhibitors.

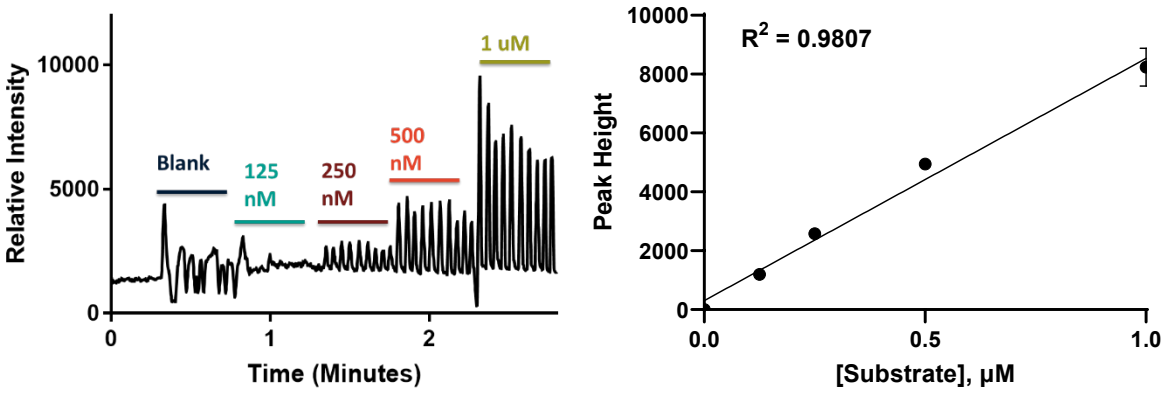

Figure I-6. In-droplet calibration curve with reagent addition. Total ion chromatogram for droplet calibration curve. Droplets contained substrate ranging from 0 nM to 1000 nM, with ten droplets at each concentration (A). A calibration curve generated using peak height from the extracted ion chromatogram of the substrate peptide. Peak heights from the four middle droplets at each concentration were used. The calibration curve was fit with a linear regression (B) (n=4).